Molecular mechanisms of mechanotransduction: functional analysis of the role of STOML3

Dissertation

zur Erlangung des akademischen Grades

doctor rerum naturalium

(Dr. rer. nat.)

eingereicht im Fachbereich Biologie, Chemie, Pharmazie

der Freien Universtität Berlin

von
Liudmila Lapatsina
aus Minsk

angefertigt in der Forschungsgruppe Molecular Physiology of Somatic Sensation
des Max-Delbrück Centrums für Molekulare Medizin unter der Leitung von
Professor Dr. Gary R. Lewin

Berlin, Mai 2011

This work was carried out in the period of Sep. 2006 to May 2011 under the supervision of Prof. Dr. Gary Lewin and Prof. Dr. Volker Haucke (FU) at the Max Delbrück Centrum für Molekulare Medizin (MDC) Berlin.

1st Reviewer: Prof. Dr. Volker Haucke
2nd Reviewer: Prof. Dr. Gary Lewin

date of defence: 31.08.2011

Aequam memento rebus in arduis servare mentem

Horace

Abstract.

The ability of complex vertebrate organisms to perceive various mechanical stimuli through sensory neurons innervating skin is crucial for interaction with the physical world. Mechanotransduction is the conversion of a mechanical stimulus into a biological response. The molecular basis of the mechanical transduction machinery is formed by specialized ion channels, which can form large multiprotein complexes together with different accessory proteins (Delmas et al, 2011; Ernstrom & Chalfie, 2002; Gillespie & Walker, 2001)

This work is focused on characterisation of STOML-3 protein, which is a member of the large protein family characterised by the presence of a stomatin domain. Functionally, STOML-3 was first described by us in connection with loss of mechanosensitivity in *stoml-3* null mice (Wetzel et al, 2007). A pronounced effect on mechanosensation in this mouse and the homology of STOML-3 with the MEC-2 protein, one of the main components of mechanotransducing machinery in *C.elegans,* allows us to hypothesise that STOML-3 is an essential component of mammalian mechanotransducing complex. Thus, I take an advantage of cell biology techniques in combination with gene engineering methods in order to verify this hypothesis, to elucidate possible molecular mechanisms by which STOML-3 functions and to identify STOML-3 interacting proteins as putative components of mammalian mechanotransducing machinery.

In the first part of my dissertation I present data regarding STOML-3 cell biology and dynamics, *in vitro* molecular interactions and a novel approach for purification of endogenous protein complexes from animal tissues. I also describe a novel STOML-3 positive vesicular pool, which we term the *transducosome*, and believe it is important for STOML3-mediated processes. The second part of this work is focused on characterisation of STOML-3 expression pattern in the mouse, using two transgenic mouse lines that were created in the course of this project and which are also described here. I describe STOML-3 expression pattern within previously reported tissues, as well as report about additional tissues and cellular types in which STOML-3 was detected using these transgenic mice. In conclusion, I discuss potential mechanisms of STOML-3 function, based on our recent results and results presented in this work.

The apparent role of STOML-3 in mechanotransduction in mammals makes this protein an important object of further studies and a potential pharmacological target. I demonstrate that

STOML-3 is located in a dynamic vesicular pool and possibly can change characteristics of the plasma membrane upon incorporation. Additionally, I show that STOML-3 expression is not restricted to neuronal tissues, but also present in cells from additional tissues that are reported to be able to detect and react on mechanical stimulation (e.g. olfactory epithelium and bone tissues). Thereby, the role of STOML3 in mechanosensation may be more general in character, than previously thought.

Zusammenfassung.

Die Fähigkeit von Vertebraten verschiedene mechanische Reize durch in der Haut eingebettete sensorische Neurone wahrzunehmen, ist essentiell für die Interaktion mit der Umwelt. Mechanotransduktion ist die Umwandlung eines mechanischen Reizes in eine zelluläre Antwort. Spezialisierte Ionenkanäle, die große Multiproteinkomplexe mit verschiedenen akzessorischen Proteinen formen können, bilden die molekulare Grundlage der Wahrnehmung mechanischer Kräfte (Delmas et al., 2011; Ernstrom & Chalfie, 2002; Gillespie & Walker, 2011).

Ziel der vorliegenden Arbeit ist die Charakterisierung von STOML-3, einem Mitglied der großen, durch die Anwesenheit einer Stomatin-Domäne charakterisierten Proteinfamilie. STOML-3 wurde in unserem Labor erstmals funktionell in Verbindung mit einem Teilverlust der Mechanosensitivität in *stoml3*-defizienten Mäusen beschrieben (Wetzel et al., 2007). Aufgrund des Effekt von STOML-3 auf die Mechanosensitivität der Maus und der Homologie von STOML-3 und MEC-2, einer der Hauptkomponenten der Mechanotransduktionsmaschinerie in C. elegans, ist anzunehmen, dass STOML-3 ein essentieller Bestandteil des mammalischen Mechanotransduktionskomplexes ist. Mittels zellbiologischer und gentechnischer Methoden wird versucht diese Hypothese zu verifizieren sowie mögliche der Funktion von STOML-3 zugrunde liegende molekulare Mechanismen aufzuklären. Darüber hinaus werden Interaktionspartner von STOML-3 als putative Komponenten der mammalischen Mechanotransduktionsmaschinerie identifiziert.

Der erste Teil der Dissertation thematisiert die zellbiologische Charakterisierung und die Dynamik von STOML-3. Außerdem werden *in vitro* molekulare Interaktionen von STOML-3 studiert und neue Ansätze zur Aufreinigung endogener Proteinkomplexe der Maus aufgezeigt. Darüber hinaus beschreibe ich einen STOML-3 positiven Vesikelpool, Transducosome getauft, der als für STOML-3 vermittelte Prozesse notwendig erachtet wird. Der zweite Teil der Arbeit ist auf die Charakterisierung der Expression von STOML-3 in zwei transgenen Mauslinien, die im Rahmen des Projekts generiert wurden, fokussiert. Die Expressionmuster von STOML3 werden in bereits dokumentierten Geweben analysiert. Zusätzlich detektiere ich STOML-3 in bisher nicht dokumentierten Geweben und Zelltypen. Schließlich diskutiere ich unter Berücksichtigung jüngster Ergebnisse unseres Labors und der in der vorliegenden Arbeit beschriebenen Ergebnisse einen potentiellen, der Funktion von STOML-3 zugrunde liegenden Mechanismus.

Die beschriebene Rolle von STOML-3 in der Mechanotransduktion der Säugetiere macht dieses Protein zu einem wichtigen Objekt weiterführender Studien und zeichnet es als potentielles pharmakologisches Ziel aus. STOML-3 ist in einem dynamischen Vesikelpool lokalisiert und übt nach Inkorporation in die Plasmamembran charakteristische Effekte auf diese aus. Darüber hinaus lokalisiere ich STOML-3 nicht nur in neuronalem Gewebe, sondern auch in Zellen nicht-neuronalen Gewebes (z.B. olfaktorisches Gewebe, Knochengewebe), die ebenfalls mechanische Reize detektieren und auf diese reagieren können. Unter Berücksichtigung der beschriebenen Erkenntnisse ist anzunehmen, dass die Funktion von STOML-3 in der Mechanosensation weitreichender als bisher angenommen ist.

Contents.

1. Introduction.

1.1. Somatosensory mechanotransduction.

To survive in a constantly changing environment every living organism has to be able to detect these changes and develop an appropriate response. Thus, during evolution specialised sensory systems have developed, which receive information from the environment through peripheral receptors and transmit this information to the central nervous system (Smith & Lewin, 2009). The somatosensory system is a distinct from all the other sensory systems in two main ways. First of all, the receptors of the system are distributed throughout the whole organism in contrast to the olfactory, auditory and the visual systems, where specialised receptors are restricted to distinct sensory regions or tissues. The second distinctive feature of the somatosensory system is the ability to detect and process stimuli of different modalities: mechanical, proprioceptive, thermal sensations and mediate the sense of pain.

The basic component of the mammalian somatosensory system, are specialised pseudo-unipolar sensory neurones that innervate the skin. Cell bodies of these neurons are located in the dorsal root ganglia (DRG) while a single axon bifurcates, forming a peripheral branch, that innervates skin and is sensitive to stimulus energy, and a central branch, that extends to the central nervous system. DRG cell bodies originated from neuronal-cell precursors, varying in their diameter size. A small cell diameter is characteristic for nociceptors, while mechano- and proprioceptors have predominantly large and intermediate sizes. Functionally, DRG neurons are also heterogeneous and represent nociceptors (including high-threshold mechanoreceptors), thermoreceptors, and low-threshold mechanoreceptors. This functional difference is partially reflected in morphological differences between DRG neurons (Lumpkin & Caterina, 2007; Lewin & Moshourab, 2004; Tsunozaki & Bautista, 2009). Virtually all mechanoreceptors have specialised endings that are involved in shaping dynamic response of the neuron to stimuli.

1.2 Cutaneous mechanoreceptors.

The skin of mammals is a specialised structure with a complex architecture and multiple functions. There are three types of skin that can be distinguished based on their primary characteristics: glabrous, hairy and mucocutaneous and the innervation pattern of these three skin types by cutaneous mechanoreceptors is distinct. A primary mechanoreceptor-end organ

of the hairy skin is the hair follicle receptor. In some species several distinct classes of hair follicle receptor can be assigned (Brown & Iggo, 1967). Glabrous skin contains two main types of mechanoreceptors: Meissner's corpuscle (rapidly adapting mechanoreceptor) and Merkel's receptor (slowly adapting mechanoreceptor). The dermal layer of the hairy and glabrous skin contains two more types of mechanoreceptors: the pacinian corpuscle, a rapidly-adapting receptor, and the Ruffini's corpuscle, a slowly adapting-receptor (**Figure 1**). Functionally, mechanoreceptors that mediate the sense of touch can be divided into two major groups according to their responses to constant and enduring stimuli. The response of slowly-adapting mechanoreceptors is continuous to a sustained stimulus, whereas rapidly-adapting group responds only during the on- and offset of the stimulus.
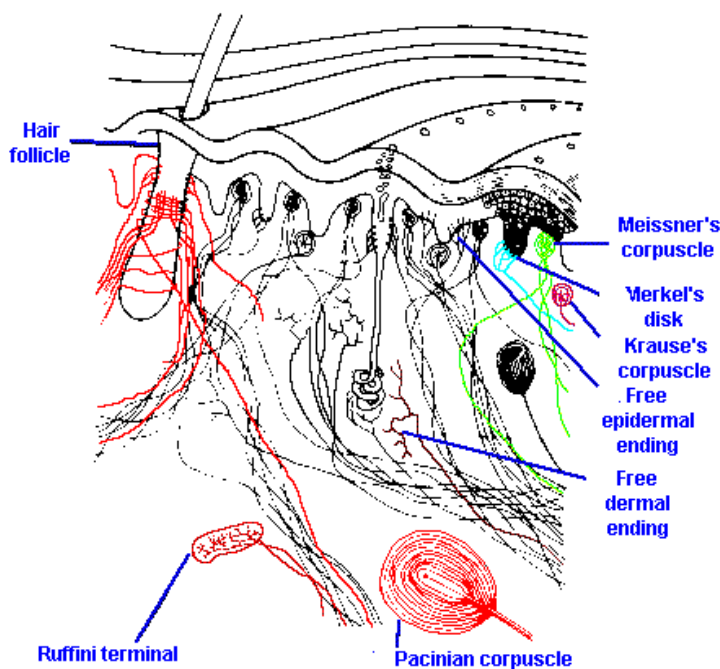
(Warwick R and Williams PL [ed]: Gray's Anatomy, 35th ed. Philadelphia, WB Saunders, 1973).

Figure 1. A section through a transitional region between glabrous and hairy skin showing the locations and arrangements of various dermal and epidermal receptors.

1.3   Understanding   mechanotransduction   in   somatosensory neurons.

Due to the heterogeneity of mechanosensory receptors and their distribution throughout the periphery with relatively low density, the study of mammalian mechanosensation has been slow in comparison with that of other sensory systems. Another problem has been the absence of clear genetic mutations in mammals, which lead to touch impairment. This fact might be explained by the importance of the somatosensory system and thus, redundancy of genes

involved in the detection of mechanical stimuli. Thereby use of a direct analysis of disease conditions and molecular-biological approaches in order to determine the key components of mammalian mechanotransducer, have not been successful. To overcome this problem and identify possible candidate molecules for the mammalian mechanotransducer a number of model organisms, such as the nematode *Caenorhabditis elegans* and the fruit fly *Drosophila melanogaster*, which have a short life-span and can be easily manipulated genetically, have been used by the researchers. Work on one of such model organisms, the nematode *Caenorhabditis elegans,* led to the discovery of a number of genes, mutations in which lead to abnormality in touch sensation. These genes were called *mecs* (from <u>mec</u>hanosensory abnormal) and corresponding protein products, were accordingly named MECs (Chalfie & Sulston, 1981a; Chalfie & Au, 1989).

1.3.1 Role of *C. elegans* in dissection of somatosensory system.

The nematode, *C. elegans*, is an extensively studied organism displaying well-defined behaviours to mechanical stimulation of the body (Chalfie & Sulston, 1981). Thus, gentle stimulation with an eyebrow hair causes worm to move away from the mechanical stimulus. Experiments, where a group of neurones with a characteristic set of 15 protofilament microtubules were ablated with a focused laser beam, showed that these non-ciliated touch responsive neurones (TRNs) are responsible for gentle body-touch sensation (Chalfie & Sulston, 1981b). Later, two additional groups of neurones, responsive to mechanical stimuli, were described: PVD neurones, which mediate harsh body-touch sensation and polymodal ciliated neurones, that are responsive to nose-touch, noxious chemicals and osmolarity (Bargmann et al, 1990; Kaplan & Horvitz, 1993; Way & Chalfie, 1989).

1.3.2 Genes involved in touch.

Mutagenesis and selection of mutant worms that failed to respond to gentle mechanical stimulation of the body identified about 15 genes involved in gentle body touch sensation (Chalfie & Au, 1989). The genes were called *mec*, and their protein products MEC. Functionally *mec* genes can be subdivided into those that are required for normal development and differentiation of TRN neurones, and those that do not disrupt normal development and rather belong to functional components of mechanotransduction machinery. The second group of *mec* genes include components of the cytoskeleton (*mec- 7, mec-12*), proteins of

extracellular matrix (*mec-1, mec-5, mec-9*), α-tubulin acetyltransferase (*mec-17*), membrane associated protein (*mec-2*) and members of the Deg/ENaC ion channel family (*mec-4* and *mec-10),* the functions of a few more *mec* genes are still unknown. Extensive studies carried out in heterologous systems like *Xenopus laevis* oocytes and *in-vivo* slit-worm preparation, confirmed a direct involvement of these proteins in mechanosensation (Brown et al, 2008; Goodman et al, 1998; O'Hagan et al, 2005). Based on substantial data obtained from these experiments, the following model of multimolecular mechanosensitive complex has been proposed (**Figure 2a**). The core component of the complex is a mechanically-gated ion channel, which opens in direct response to physical displacement of the transduction machinery. Two additional proteins, intracellular membrane-associated MEC-2 and MEC-6, were shown to interact with the degenerin channel (MEC-4/MEC-10) and modulate its properties, thus forming an essential core of mechanotransduction complex in the worm. Co-expression of these proteins with MEC-4/MEC-10 channel in *X. laevis* oocytes leads to approximately 40-fold increase in the channel current (Brown et al, 2008; Goodman et al, 2002). A search for orthologs of the *mec* genes in rodents revealed a number of proteins with a high level of homology, which might reflect a functional conservation. Thus, the next putative model of mammalian mechanotransducer was proposed (**Figure 2b**). This new model predicted that the mechanosensitive ion channel might belong to the acid-sensing ion channel (ASIC) family. The mammalian homolog of MEC-2 belongs to the stomatin family of proteins; four from five known members of this family are found to be expressed in mouse sensory neurones (Lapatsina et al, 2011). The nature of the mammalian MEC-6 homolog is less clear, though it has a certain level of homology with mammalian serum paraoxonase (Brown et al, 2008). Surprisingly, analysis of mouse mutants of ASICs revealed only moderate alteration in mechanosensation (Roza et al, 2004; Price et al, 2001; Page et al, 2004). In addition, ASICs do not appear to form a part of the central mechanosensitive channel (Lechner et al, 2009). At the same time, analyses of stoml-3-/- mice demonstrated that STOML-3 is indeed functionally orthologous to the MEC-2 protein (Wetzel et al, 2007).
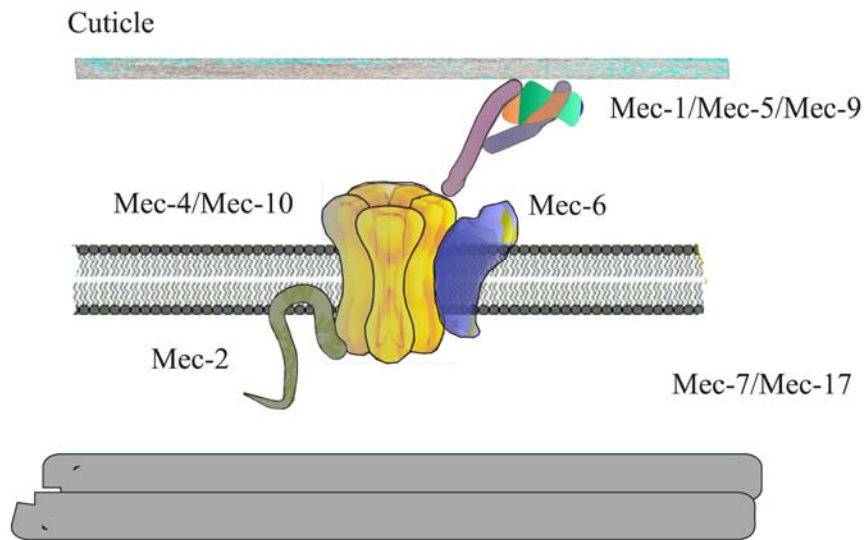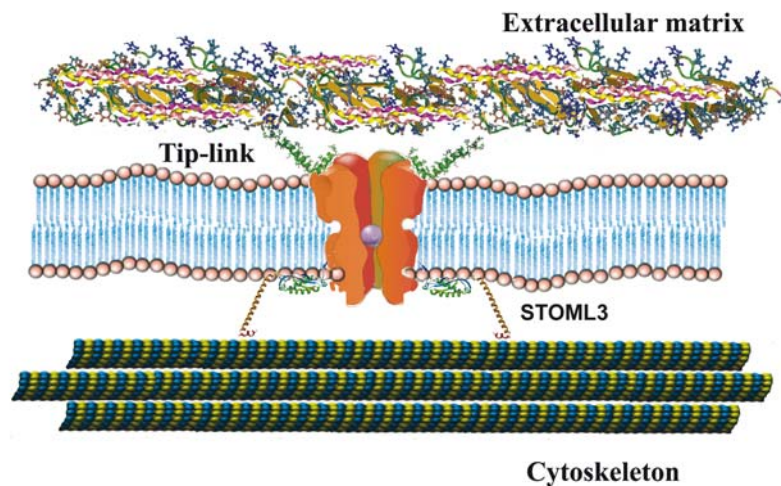
Figure 2. Molecular model of mechanotransduction in C.elegans (top) and in mammals (bottom).

(a) A scheme of C. elegans mechanotransducing multiprotein complex, formed by MEC proteins. The core component of the complex is a mechanically-gated ion channel, which is formed by MEC4/MEC10 proteins. MEC2 is a membrane-associated intracellular protein, which was thought to interact with MEC-7 and MEC-12, encoding microtubule proteins. Nevertheless, Cueva et al. has shown that there is no direst association of MEC-2 with distal endpoints of 15-protofilament microtubules in *C.elegans* (Cueva et al, 2007). MEC5 and MEC9, components of extracellular matrix, directly or indirectly interact with extracellular parts of the mechanosensitive ion channel.

(b) A scheme of the mechanotransduction machinery in mammals based on homology of several mammalian proteins to the MEC proteins of *C.elegans*. The immediate role in mechanotransduction was demonstrated only for STOML-3 protein, which shows high sequence homology to MEC-2.

1.3.3 Stomatin family of proteins.

Stomatins are a large family of proteins defined by the presence of a characteristic central domain as one of structural components (Tavernarakis et al, 1999). This domain shares a high level of similarity with the prohibitin, flotillin and HflK/HflC bacterial proteins and was named the SPHF domain after initials of the included protein families. The SPHF family defines a large group of proteins with more than 1300 predicted members; over 360 of these proteins have been identified to date (Morrow & Parton, 2005). Protein members of the family are widely distributed among all domains of life including *Archaea* (Green & Young, 2008; Rivera-Milla et al, 2006). In spite of a great phylogenetic distance between mammals, plants and bacteria the amino-acid sequence of the stomatin domain remains remarkably conserved (Green & Young, 2008).

1.3.4 Domain organisation and structure of stomatins.

Stomatin, stomatin-like protein-1 (STOML-1), stomatin-like protein-2 (STOML-2), stomatin-like protein-3 (STOML-3) and podocin are the mammalian members of the stomatin family of proteins. These proteins share 40 to 84% sequence similarity in the stomatin-domain and have similar membrane topology and primary domain organisation (**Figure 3**), with the notable exception of STOML-2, which has no a hydrophobic domain and most closely resembles bacterial stomatins in its organisation (Green & Young, 2008).
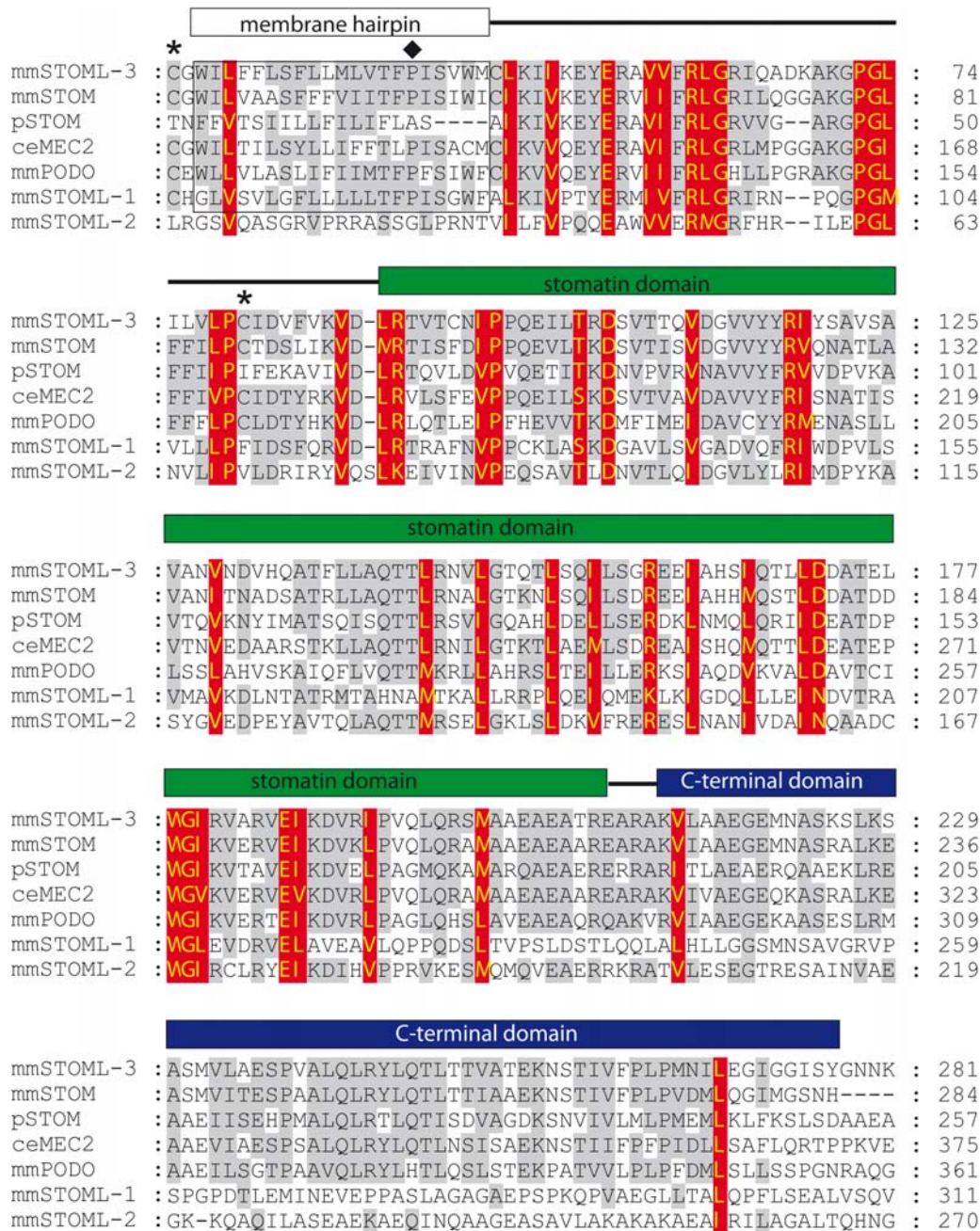
from Lapatsina et al., European Journal of Cell Biology. 2011

Figure 3. Sequence alignment of stomatin family members.
The alignment includes protein sequences starting from the membrane hydrophobic domain (boxed) to the C-terminal domain of stomatin. The proline residue required for hairpin formation within a transmembrane domain is indicated by ♦, palmitoylated cystein residues are indicated by *
mmSTOML-3, mmSTOM (stomatin), phSTOM (stomatin from *Pyrococcus horikoshii*), ceMEC2, mmPODO (podocin), mmSTOM-1, mmSTOM-2. **(mm- *Mus musculus*, ph - *Pyrococcus horikoshii*, ce - *C. elegans*.).**

A typical stomatin-domain protein is an integral membrane protein with a single, relatively short hydrophobic membrane insertion domain, followed by the core stomatin domain. A single conserved proline residue, known to be a potent helix breaker, (Nilsson et al, 1998; Alías et al, 2010; Yun et al, 1991) in the hydrophobic region forms a hairpin structure which

is required for the association with the plasma membrane (**Figure 4a**). Both N- and C- termini of the protein are intracellular and unique for every protein (Salzer et al, 1993; Snyers et al, 1998; Seidel & Prohaska, 1998; Boute et al, 2000a; Owczarek et al, 2001). Accordingly, different properties of stomatins, like cytoskeleton binding and homo-oligomerisation, have been shown to depend, in some cases, on these non-conserved regions. An atomic resolution structure of the mammalian stomatin-domain proteins has not been described to date; however, the recently solved crystal structure of the archaebacterial stomatin core domain (Yokoyama et al, 2008) from *Pyrococcus horikoshii* (p-stomatin) has greatly helped to predict topological and structural characteristics of the stomatin family proteins. It was shown that the core stomatin-domain is by itself able to oligomerise and form stable trimers. In addition, α-helical extensions at the C-terminus which are not involved in core-domain oligomerisation, were suggested to participate in membrane bending (**Figure 4b**) (Yokoyama et al, 2008).

from Lapatsina et al.,
European Journal of Cell Biology. 2011
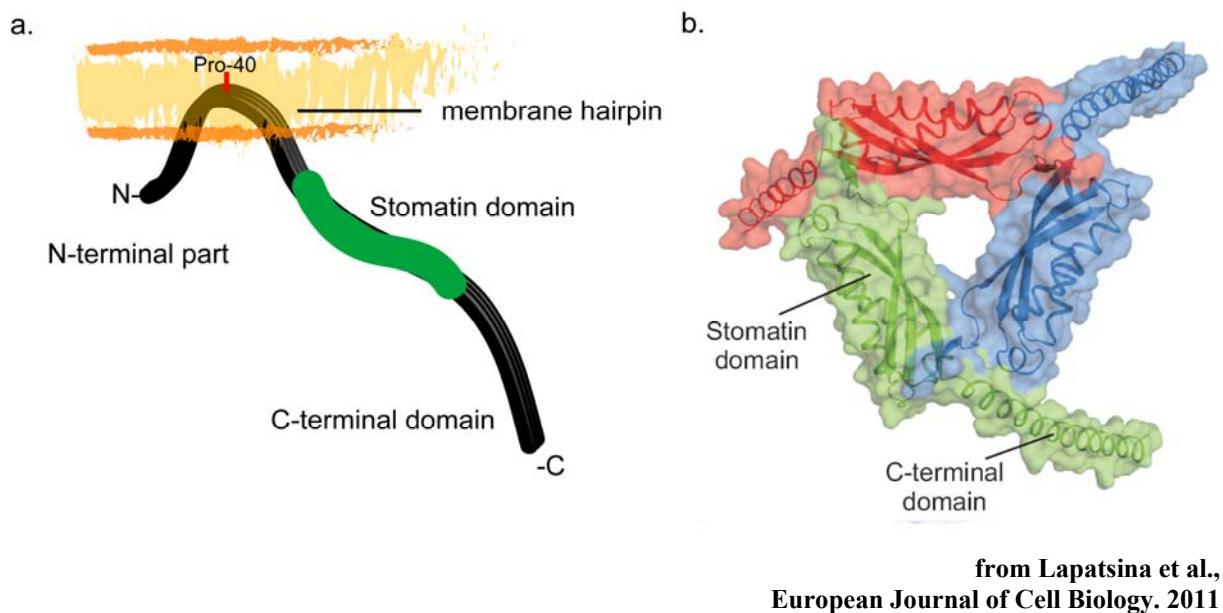
Figure 4. Domain organisation of STOML-3 protein.
(a) STOML-3 is an integral membrane protein with a single, relatively short, hydrophobic membrane insertion domain, followed by the core stomatin domain. A single conserved proline residue in the hydrophobic region is required for the formation of the hairpin structure. Both N- and C- termini of the protein are intracellular. **(b)** A homology model of trimeric STOML-3, based on the known structure of the phStomatin trimer was created using SWISS-MODEL (with help from Janco Brand).

1.3.5 Role of STOML-3 in mechanosensation

The STOML-3 protein was first identified as an olfactory neurone specific protein of unknown function (Kobayakawa et al, 2002). STOML-3 shares about 77% of similarity in its amino acid sequence with *C. elegans* MEC-2 (**Figure 3**). Unlike stomatin, which is expressed almost ubiquitously in the mouse, STOML-3 expression is restricted to just a few tissues

including mechanosensory neurones of the DRG (Wetzel et al, 2007). Null *stoml-3* animals demonstrate reduced tactile acuity in comparison with wild-type animals. Around 40% of skin mechanoreceptors in these mice are insensitive to mechanical stimulation, however, their electrical excitability is unaffected. It is known that almost all large-diameter sensory neurones isolated from wild-type mice possess a fast and sensitive mechanically gated current (Hu & Lewin, 2006; Lechner et al, 2009). By analyzing *stoml-3-/-* mice it was found, that the mechanically gated currents require the presence of STOML-3 protein, as they were absent in large diameter neurones isolated from the knock-out animals. Moreover these mechanosensitive currents could be rescued after reintroduction of a cDNA encoding wild-type STOML-3 (Wetzel et al, 2007). Interestingly, it was found that STOML-3 is necessary not just for the function of mammalian mechanotransduction complexes but it also plays a physiological role in regulating ASIC channel subunits in sensory neurones. Like Stomatin, STOML-3 is capable of inhibiting the amplitude of acid-gated currents mediated by ASICs; proton gated currents in sensory neurones from *stoml-3-/-* mice were larger than those in wild type animals (Wetzel et al, 2007). The molecular mechanisms that enable STOML-3 protein to modulate channels function are at present largely unknown.

1.4 Transport of plasma membrane proteins.

Neuronal cells have developed a complex plasma membrane organisation with structurally and functionally distinct domains within different parts of the cell. The protein content of these membrane domains is entirely dependent on sorting and delivery of fully processed membrane proteins and retention/recycling of the plasma membrane proteins (George J Siegel, 1999).

The biosynthetic pathway is responsible for newly synthesised protein delivery, which starts in the rough endoplasmic reticulum, which has a disordered appearance in DRG neurones (Kandel et al, 2000; Verkhratsky, 2005). After synthesis, proteins pass through the Golgi complex and are packed into vesicular carriers, which are subsequently transported into the designated parts of the cell and delivered to the plasma membrane by exocytic fusion (Craig & Banker, 1994) (**Figure 5**). Fusion of the vesicles occurs only with a correct target membrane. To maintain the protein composition of a specific membrane domain the recycling mechanism is under tight regulation, only certain proteins are internalised which are destined to be recycled. Thus, targeted transport vesicle fusion and regulated recycling processes are responsible for maintenance and proper balance of the plasma membrane composition.

Another important mechanism of protein delivery to the correct plasma membrane domain, which plays an important role in polarised cells, is transcytosis (Burack et al,; 2000 Sampo et al, 2003; Ahn et al, 1996). It is known that a number of proteins in polarized cells are delivered uniformly to the cell surface via transport vesicles and then are subsequently rapidly internalized and sorted to the correct plasma membrane compartment
 (Burack et al, 2000).
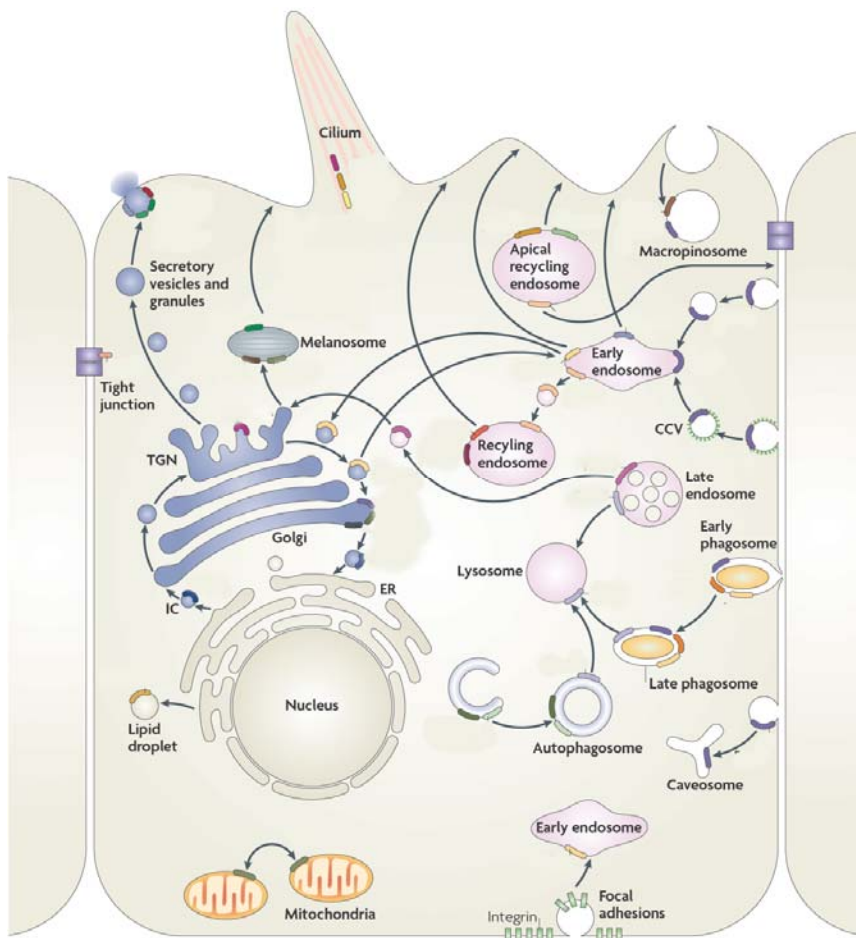
modified from Harald Stenmark Nature Reviews Molecular Cell Biology 2009

Figure 5. Protein trafficking in the polarised cell.
Proteins newly synthesised in the rough endoplasmic reticulum are translocated in vesicular carriers to the Golgi complex and subsequently to the *trans*-Golgi network (TGN). Once in the TGN, proteins get sorted to the plasma membrane. Resident proteins of each organelle along the secretory pathway achieve their localisation through retrieval mechanisms. Proteins localised on the plasma membrane undergo different types of endocytosis and either recycle back to the membrane or degrade in the lysosomal compartment.

In neuronal cells intracellular transport of newly sensitised or recycled cell components fall into three main categories.: fast anterograde axonal transport, slow axoplasmic flow and fast retrograde axonal transport. Essentially all newly synthesised proteins are exported by means of transport vesicles to the axon by fast anterograde axonal transport, a microtubule and kinesin dependent process. A net flow of endocytic vesicles, containing proteins targeted for

degradation, internalised growth factors, hormones and other molecules and vesicles involved in protein redistribution from axons to dendrites, is determined by fast retrograde transport (Vallee & Bloom, 1991). As in fast anterograde axonal transport, vesicles move along microtubules by means of dynein motor molecule (Dillman 3rd et al, 1996).

1.5 Purification of endogenous protein complexes.

The ensemble of expressed proteins in any cell is organized in multiprotein complexes. In the majority of cases the role and functional characteristics of a given protein can be understood only when interaction partners and their connections are defined. The biggest obstacle in determining the molecular nature of the mechanotransducer complex is the lack of a suitable *in vivo* system. Notably, there is no cell line known at the moment to display a mechanosensitive current similar to the one sensory neurones develop upon mechanical stimulation with the possible exception of the recently identified Piezo current in N2a cells (Coste et al, 2010). Thus, in an attempt to determine the moleculare conposition of mammalian mechanotransducer it was decided to employ an affinity purification methodology in combination with a genetic engineering approach. The role in cutaneous mechanosensaton in the mouse by now was clearly demonstrated only for STOML-3 (Wetzel et al, 2007) thus, we decided to use this protein as "molecular bait" for the affinity purification of the entire putative multiprotein complex involved in mechanosensation. Because of very pronounced homology between the members of the stomatin family of proteins there is no highly specific antibody available for an antibody-based protein purification method. To overcome this problem and, at the same time, use the real *in vivo* system we decided to create a knock-in mouse line, where STOML-3 protein was modified with N-terminal *OneSTrEP II* affinity tag*,* for purification. The construct was introduced under the endogenous *stoml-3* promoter, ensuring physiological level of the "bait" expression and thus, eliminating possible artefacts due to altered stoichiometry or composition of the complex.

1.5.1 One-STrEP-tag technology.

The *Strep*-tag[®] purification system is a relatively new technology based on highly selective interaction between the *Strep-tag II* peptide and an engineered form of streptavidin (*Strep*-Tactin). The *Strep*-tag *II* is the eight-amino acid peptide (sequence: Trp-Ser-His-Pro-Gln-Phe-Glu-Lys) that was developed as an affinity tool for purification of fusion proteins using streptavidin

columns. The peptide recognizes the same binding pocket of streptavidin where the natural ligand biotin normally binds (Schmidt et al, 1996). Due to lower *Strep*-tag *II* affinity to streptavidin, in comparison with biotin or its chemical analogues (K_D value of approximately 1.3×10^{-2} M for *Strep*-tag *II* and 4×10^{-15} M for biotin), these ligands can be used as a chemical competitor for elution of the tagged protein, ensuring very mild conditions during purification (Korndörfer & Skerra, 2002; Voss & Skerra, 1997). Over the years the Strep-tag/streptavidin system was systematically optimised, resulting in an improved binding capacity and flexibility (Korndörfer & Skerra, 2002; Voss & Skerra, 1997). The main advantage of the Strep-tag/streptavidin is an opportunity to carry on all the purification steps under mild physiological conditions, which allows isolation of sensitive proteins or native multimolecular complexes where intermolecular interactions can be rather weak. The *Strep*-tag *II* was successfully used for identification of interaction partners in a number of proteomic studies (Morita et al, 2007; Weber et al, 2008; Oellerich et al, 2009). Use of a tandem repeat of two *Strep*-tag *II* sequences has proved to deliver superior results in comparison with a single repeat (Junttila et al, 2005; Witte et al, 2004). This modified tag (*OneSTrEP-tag*) was chosen by us as a primary tool for purification of endogenous binding partners of the STOML-3 protein.

1.5.2 The principal workflow of protein purification using the Strep-tag/streptavidin system.

The relative simplicity and high specificity of the Strep-tag/streptavidin interaction allowed us to carry out the whole process of the affinity purification in just three steps (Figure 5): protein binding, washing, protein complexes elution with a competitor ligand binds to streptactin. The standard competitor used in this experiment is D- desthiobiotin, which binds streptactin with a high affinity (K_D value of approximately 1×10^{-13} M).
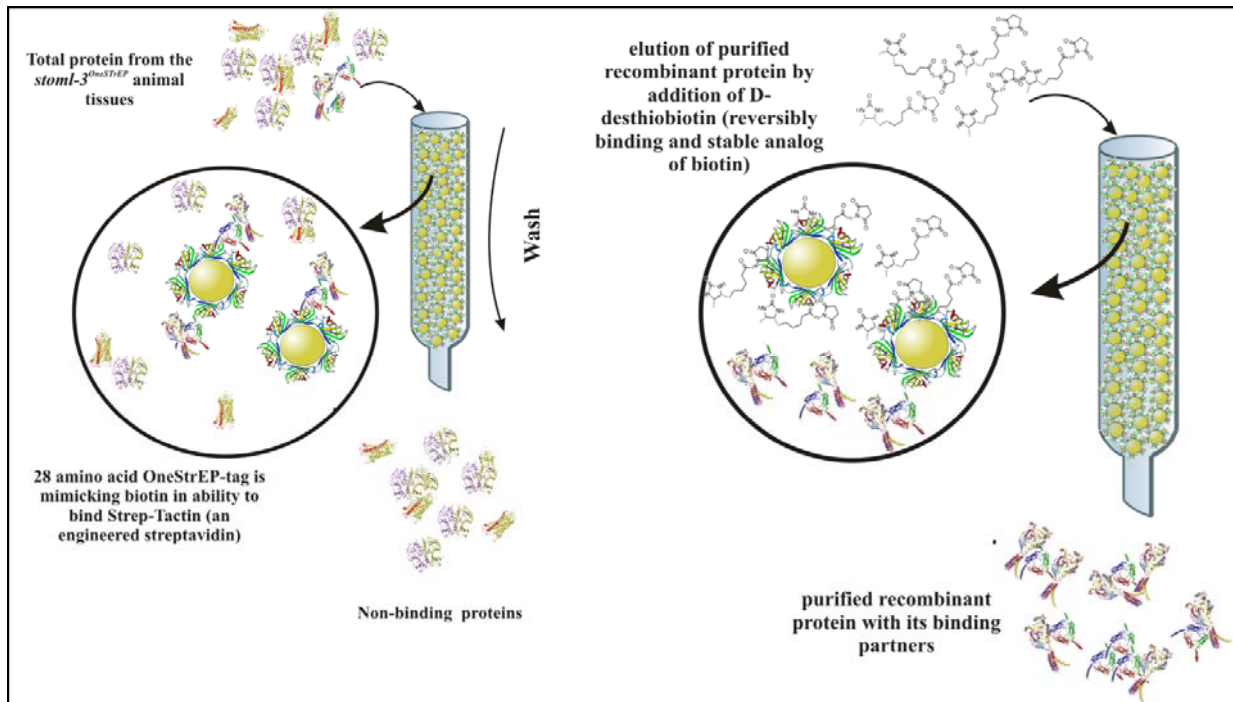
Figure 6. Protein purification using the Strep-tag/streptavidin system.
Left: total protein from the *Stoml-3^STrEP*animal tissues, where STOML-3 protein was modified with the OneSTrEP-tag sequence, was passed through the streptavidin column, after which the column was extensively washed in order to reduce nonspecific binding. **Right:** bound OneSTrEP- STOML-3 together with its binding partners can be eluted with D-desthiobiotin

1.6 Objectives of the work.

The unique effect of STOML-3 ablation on mechanosensation makes this protein an important subject for further studies and is also a potential pharmacological target. To date there is little information in the literature available about the molecular and cellular mechanisms by which STOML-3 functions (Wetzel et al, 2007). It is accepted that expression of STOML-3 is restricted to the nervous system; however, due to unavailability of specific antibody there are remained questions concerning the sites and level of STOML-3 protein expression. Thus, three main objectives of the present work can be formulated:

— To study the cell biology of STOML-3 and it dynamics.
— To chracterise the interaction partners of STOML-3, including putative components of the mammalian mechanotransducer.
— To characterise the endogenous STOML-3 expression pattern in the mouse.

The overall working hypothesis of this dissertation is that STOML-3 is an indispensable component of mammalian mechanotransducer. It is known that a multitude of proteins in any given organism are organised in functional multiprotein assemblies. Thus, interaction partners of STOML-3 protein must be expected to represent putative components of the mammalian

mechanosensing machinery. To verify this hypothesis I created a knock-in mouse line, where STOML-3 protein was modified with an affinity tag and expressed under the endogenous STOML-3 promoter; affinity purification of the protein together with interacting proteins is expected to shed light on the native mechanotransduction complex.

The first mammalian member of stomatin family of proteins, stomatin, was first reported as an essential component of erythrocyte membrane in the early nineties. Since this time other family members were discovered and a number of effects on cellular and organismic level related to the stomatins were reported (Wetzel et al, 2007; Huber et al, 2003; Boute et al, 2000b; Huber et al, 2006; Da Cruz et al, 2008; Tondera et al, 2009; Da Cruz et al, 2010). In spite of this, nothing is known about how these proteins function and which cellular processes underlie their effects. Thus, to widen our knowledge about stomatin family members and in particular about STOML-3 protein, in this work I used cell biology techniques combined with confocal and live-cell imaging to characterise the protein dynamics and distribution of STOML-3 in sensory neurones.

In addition, to verify STOML-3 expression pattern in the mouse I have created a β-galactosidase- expressing *stoml-3* reporter line, which in combination with the aforementioned knock-in *stoml-3* provides a useful tool to investigate the temporal and spatial profile of *stoml-3* mRNA expression.

2. Materials and Methods.

2.1 Preface.

2.1.1 Chemicals.

Name	Supplier
Agarose, ultra-pure	Invitrogen GmbH, Karlsruhe, Germany
Antibiotic-Antimycotic	Invitrogen GmbH (Gibco), Karlsruhe, Germany
Ammonium chloride	Carl Roth GmbH & Co. KG, Karlsruhe, Germany
Ampicillin sodium salt	Sigma-Aldrich Chemie GmbH, Schnelldorf, Germany
Arabinose	Carl Roth GmbH & Co. KG, Karlsruhe, Germany
Aqua-Polymount	Polysciences Europe GmbH
BES	Sigma-Aldrich Chemie GmbH, Schnelldorf, Germany
Bovine serum albumin (BSA)	Sigma-Aldrich Chemie GmbH, Schnelldorf, Germany
Bromphenolblue	Carl Roth GmbH & Co. KG, Karlsruhe, Germany
Calcium chloride dihydrate	Merck KgaA, Darmstadt, Germany
Collagenase Type IV	Sigma-Aldrich Chemie GmbH, Schnelldorf, Germany
Dimethyl sulfoxide (DMSO)	Merck KgaA, Darmstadt, Germany
DOC	Invitrogen GmbH, Karlsruhe, Germany
dNTP-Mix	Invitrogen GmbH, Karlsruhe, Germany
DTT	Invitrogen GmbH, Karlsruhe, Germany
EDTA disodium-dihydrate	Carl Roth GmbH & Co. KG, Karlsruhe, Germany
Ethanol	Carl Roth GmbH & Co. KG, Karlsruhe, Germany
Ethidium bromide	Carl Roth GmbH & Co. KG, Karlsruhe, Germany
FBS (fetal bovine serum)	Invitrogen GmbH (Gibco), Karlsruhe, Germany
FugeneHD	Roche Pharma AG, Grenzach-Wyhlen, Germany
D-(+)-glucose	Sigma-Aldrich Chemie GmbH, Schnelldorf, Germany
D-MEM	Invitrogen GmbH (Gibco), Karlsruhe, Germany
DNAse I	Sigma-Aldrich Chemie GmbH, Schnelldorf, Germany
Ganciclovir	Sigma-Aldrich Chemie GmbH, Schnelldorf, Germany
Geneticin	Invitrogen GmbH (Gibco), Karlsruhe, Germany
Glacial acetic acid	Carl Roth GmbH & Co. KG, Karlsruhe, Germany
Glutaraldehyde	Sigma-Aldrich Chemie GmbH, Schnelldorf, Germany
GlutaMAXTM	Invitrogen GmbH (Gibco), Karlsruhe, Germany
Glycine	Carl Roth GmbH & Co. KG, Karlsruhe, Germany
Glycerol	Carl Roth GmbH & Co. KG, Karlsruhe, Germany
HBSS (10x)	Invitrogen GmbH (Gibco), Karlsruhe, Germany
HEPES	Carl Roth GmbH & Co. KG, Karlsruhe, Germany
Horse serum	Invitrogen GmbH (Gibco), Karlsruhe, Germany
IPTG	Sigma-Aldrich Chemie GmbH, Schnelldorf, Germany
Isopropanol	Carl Roth GmbH & Co. KG, Karlsruhe, Germany

Ketamin 10 %	WDT eG, Garbsen, Germany
N-Lauroylsarcosine	Sigma-Aldrich Chemie GmbH, Schnelldorf, Germany
Lipofectamine™ 2000	Invitrogen GmbH, Karlsruhe, Germany
ß-mercaptoethanol	Sigma-Aldrich Chemie GmbH, Schnelldorf, Germany
Methanol	Carl Roth GmbH & Co. KG, Karlsruhe, Germany
MgCl2 (50 mM)	Invitrogen GmbH, Karlsruhe, Germany
Mitomycin C	Sigma-Aldrich Chemie GmbH, Schnelldorf, Germany
O.C.T.™ Tissue Tek	Sakura Finetek, Zoeterwoude, Netherlands
Oligonucleotides	Invitrogen GmbH, Karlsruhe, Germany
Opti-MEM®	Invitrogen GmbH (Gibco), Karlsruhe, Germany
Paraformaldehyde	Sigma-Aldrich Chemie GmbH, Schnelldorf, Germany
PBS (10x)	Invitrogen GmbH (Gibco), Karlsruhe, Germany
PCR Rxn buffer (10x)	Invitrogen GmbH, Karlsruhe, Germany
Penicillin/streptomycin	Invitrogen GmbH (Gibco), Karlsruhe, Germany
Peptone	Carl Roth GmbH & Co. KG, Karlsruhe, Germany
Poly-L-lysine 0.01 %	Sigma-Aldrich Chemie GmbH, Schnelldorf, Germany
Protease inhibitor tablets complete mini	Roche Pharma AG, Grenzach-Wyhlen, Germany
Proteinase K	Sigma-Aldrich Chemie GmbH, Schnelldorf, Germany
Rompun® (2% Xylazin)	Bayer Vital GmbH, Leverkusen, Germany
Sodium chloride	Carl Roth GmbH & Co. KG, Karlsruhe, Germany
Sodium hydrogen sulfate	Sigma-Aldrich Chemie GmbH, Schnelldorf, Germany
Sodium citrate	Sigma-Aldrich Chemie GmbH, Schnelldorf, Germany
Sodium hydroxide	Sigma-Aldrich Chemie GmbH, Schnelldorf, Germany
Sucrose	Sigma-Aldrich Chemie GmbH, Schnelldorf, Germany
TEA	Sigma-Aldrich Chemie GmbH, Schnelldorf, Germany
TRIS	Carl Roth GmbH & Co. KG, Karlsruhe, Germany
Triton X-100	Sigma-Aldrich Chemie GmbH, Schnelldorf, Germany
Trizol	Invitrogen GmbH (Gibco), Karlsruhe, Germany
Trypsin-EDTA (0.25 %)	Invitrogen GmbH (Gibco), Karlsruhe, Germany
Trypsin inhibitor Type I-S (soybean)	Sigma-Aldrich Chemie GmbH, Schnelldorf, Germany
Tween 20	Serva Electrophoresis GmbH, Heidelberg, Germany
Urea	Sigma-Aldrich Chemie GmbH, Schnelldorf, Germany
X-Gal (bromo-chloro-indolyl-galactopyranoside)	Carl Roth GmbH & Co. KG, Karlsruhe, Germany
Yeast extract	Carl Roth GmbH & Co. KG, Karlsruhe, Germany

2.1.2 Buffers and solutions.

Name	Composition
0.2M $Na_2H_2PO_4$	15.5% 1M Na_2HPO_4, 4.5% 1M NaH_2PO_4 in MQ, pH7.4
0.3% Glutaraldehyde	0.3% Glutaraldehyde, 2 mM MgCl2, 1.25mM EGTA in PBS. pH-7.4
4% PFA	4% paraformaldehyde, 2 mM MgCl2, 1.25mM EGTA in PBS. pH 7.2-7.4
10x PBS	80g/l NaCl, 2g/l KH_2PO4, 2g/l KCl, 21.6g/l $Na_2HPO4 \bullet 7H2O$
20x BBS	50mM BES, 280mM NaCl, 1.5mM Na_2HPO_4, pH6.9 (with NaOH)
50x TAE	242g/l Tris base, 5.71 % (v/v) Glacial acetic acid, 0.05M EDTA, pH8.0
Blocking buffer for immunostaining	1x PBS with 10% goat serum and 0.3% TritonX-100
Citrate buffer	10mM citric acid, 0.05% Tween 20, pH6
LB agar	LB-medium + 1.5% (w/v) agar
LB medium	10g tryptone, 5g yeast extract, 10g NaCl in 1 liter H_2O
Lysis buffer 1	50mM Tris-HCl, 150mM NaCl, 1mM EDTA, 0.5% DOC, 0.5% Triton-X100, 0.1% SDS, 1mM DTT, protease inhibitors. pH-7.4
Lysis buffer 2	50mM Tris-HCl, 150mM NaCl, 2mM MgCl, 1.5% *n*-Octylglucoside, 10% glycerol , protease inhibitors. pH-7.4
Lysis buffer 3	50mM Tris-HCl, 150mM NaCl, 1mM EDTA, 1% Triton-X100, 0.3% SDS, 9M Urea
SSC 20X	3M NaCl, 300 mM sodium citrate, pH 7.0
TBS 10x	0.5M Tris-HCl pH7.9, 1.5M NaCl
TBS-T	TBS + 0.05% Tween-20
TE buffer	10mM Tris pH8.0, 1mM EDTA
X-gal buffer	35 mM K4[Fe(CN)6]•3H2O, 35 mM K3[Fe(CN)6], 2mM MgCl2, 0.02% Nonidet P-40, 0.01% Na deoxycholate, 10mg/ml X-gal in dimethylformamide in PBS

2.1.3 Bacteria strains.

Name	Genotype
E.coli TOP10	F- mcrA Δ(mrr-hsdRMS-mcrBC) φ80lacZΔM15 ΔlacX74 nupG recA1 araD139 Δ(ara-leu)7697 galE15 galK16 rpsL(Str^R) endA1 λ$^-$
E.coli DH5a	F$^-$ endA1 glnV44 thi-1 recA1 relA1 gyrA96 deoR nupG Φ80d*lacZ*ΔM15 Δ(*lacZYA-argF*)U169, hsdR17(r$_K^-$ m$_K^+$), λ−
E.coli Hb101	F$^-$ mcrB mrr hsdS20(r$_B^-$ m$_B^-$) recA13 leuB6 ara-14 proA2 lacY1 galK2 xyl-5 mtl-1 rpsL20(Sm^R) glnV44 λ$^-$
SURE	endA1 glnV44 thi-1 gyrA96 relA1 lac recB recJ sbcC umuC::Tn5 uvrC e14- Δ(mcrCB-hsdSMR-mrr)171 F'[proAB$^+$ lacI^q lacZΔM15 Tn10]
DY380	F- *mcrA* Δ(*mrr-hsd*RMS-*mcr*BC) Φ80d*lacZ* M15 *ΔlacX74 deoR recA1 endA1 araD139 Δ(ara, leu) 7649 galU galK rspL nupG [λcI857 (cro-bioA) <> tet]
EL350	F- *mcrA* Δ(*mrr-hsd*RMS-*mcr*BC) Φ80d*lacZ* M15 *ΔlacX74 deoR recA1 endA1 araD139 Δ(ara, leu) 7649 galU galK rspL nupG [λcI857 [(cro-bioA) <> araC-PBADcre]

2.1.4 Primers.

Name	Sequence 5'-3'
Cloning primers	
clcA-F	ACGTATGAATTCATGGCCGAGTTGGATCCATTC
clcA-R	ATCGTAGGTACCGTGCACCAGGGGGGCCTGC
flot1-F	ATCGTAGCTAGCATGTTTTTCACTTGTGGCCCAAATG
flot1-R	ATACTGAAGCTTGCGCTGTCCTTAAAGGCTTGTTGTG
flot2-F	ATGTACGAATTCATGGGCAACTGCCACACGGTG
flot2-R	ATCGTAGGATCCCACCTGTGCACCAGTGGCGTTC
LAMP1N3-F	ACTGTAGCTAGCATGGCGGCCCCCGGCGCCCG
LAMP1N3-R	CTGTAAAGCGGATGGTCTGATAGCCGGCGTGACTCCTCTTCC
LifCherry-F	AGCTTCGAATTCATGGGCGTGGCGGATCTGATTAAAAAATTTGAAAG CATTAGCAAAGAAGAAGTGAGCAAGGGCGAGGAGGA
LifCherry-R	ATCGTAGCGGCCGCTTACTTGTACAGCTCGTCCATGCCGC
Rab13-F	ACTGATCCTGCAGAGGCCAAAGCCTACGACCACCTC
Rab13-R	AGCTACGGATCCTCAGCCTAACAAGCACTTGTTCTTCTTC
Rab35C1-F	AGCTTCGAATTCAATGGCCCGGGACTACGACCAC
Rab35C1-R	TAGCTAGGTACCTTAGCAGCAGCGTTTCTTTCGTTTACTG
stomStrep-F	ATCGTGGTCTCAGCGCAATGTCTGACAAACGGCAGTCCAG
stomStrep-R	ATCGTGGTCTCAGATATCAGTGATTAGAACCCATGATGCCC

	Mutagenic primers
Rab11aS25N-F	GATTCTGGTGTTGGAAAGAATAACCTCCTGTCTCGATTTAC
Rab11aS25N-R	GTAAATCGAGACAGGAGGTTATTCTTTCCAACACCAGAATC
Rab11Q70L-F	CAGATATGGGACACAGCAGGGCTGGAGCGGTACAGGGCTATAAC
Rab11Q70L-R	GTTATAGCCCTGTACCGCTCCAGCCCTGCTGTGTCCCATATCTG
Rab35-S22N-F	CGACAGCGGTGTGGGCAAGAACAGCTTGCTGTTACGATTCGC
Rab35-S22N-R	GCGAATCGTAACAGCAAGCTGTTCTTGCCCACACCGCTGTCG

2.1.5 Antibodies and markers.

Name	Concentration/dilution	Application	Supplier
Alexa Fluor 488 goat anti-rabbit IgG	1:1000	ICC/IF, IHC	Invitrogen GmbH (Molecular probes), Karlsruhe, Germany
Alexa Fluor 633 goat anti-rabbit IgG	1:1000	ICC/IF, IHC	Invitrogen GmbH (Molecular probes), Karlsruhe, Germany
Alexa Fluor 488 goat anti-mouse IgG	1:1000	ICC/IF, IHC	Invitrogen GmbH (Molecular probes), Karlsruhe, Germany
Alexa Fluor 488 goat anti-mouse IgG	1:1000	ICC/IF, IHC	Invitrogen GmbH (Molecular probes), Karlsruhe, Germany
Alexa Fluor 633 phalloidin	1:20 (10 Units/ml)	ICC/IF	Invitrogen GmbH (Molecular probes), Karlsruhe, Germany
Alexa Fluor 488–WGA	30μg/ml	ICC/IF	Invitrogen GmbH (Molecular probes), Karlsruhe, Germany
Alexa Fluor 633–WGA	30μg/ml	ICC/IF	Invitrogen GmbH (Molecular probes), Karlsruhe, Germany
Alexa Fluor 350 – WGA	30μg/ml	ICC/IF	Invitrogen GmbH (Molecular probes), Karlsruhe, Germany
Cy2 goat anti-rabbit IgG	1:1000	ICC/IF, IHC	Jackson ImmunoResearch Europe Ltd., Suffolk, UK
Cy3 donkey anti-chicken IgG	1:1000	ICC/IF, IHC	Jackson ImmunoResearch Europe Ltd., Suffolk, UK
anti – OneSTrEP mouse monoclonal	ICC/IF, IHC - 1:1000 WB 1:800	ICC/IF, IHC, WB	IBA GmbH, Germany
anti – OneSTrEP rabbit polyclonal	1:1000	ICC/IF, IHC, WB	Abnova Corporation, US
Anti-Flag M2, monoclonal, mouse	1:2000	WB, IP	Sigma-Aldrich Chemie GmbH, Schnelldorf, Germany
Anti-Flag M2, HRP conjugate	1:3000	WB	Sigma-Aldrich Chemie GmbH, Schnelldorf, Germany
Ani-OMP	1:500	IHC	Abcam, Cambridge, UK
Anti-NeuroD	1:1000	IHC	Abcam, Cambridge, UK
Anti- Histone H3 (phospho S10) monoclonal mouse	1:1000	IHC	Abcam, Cambridge, UK

Anti Ia1	1:500	IHC	
Anti-GFAP	1:500	IHC	Thermo Scientific Pierce
Anti-alpha-Tubulin , monoclonal mouse	1:1000	ICC/IF	Sigma-Aldrich Chemie GmbH, Schnelldorf, Germany
4´6-diamidino-2-phenylindole, dilactate (DAPI)	300 nM	ICC/IF, IHC	Invitrogen GmbH (Molecular probes), Karlsruhe, Germany
Goat anti-mouse-HRP	1:1000	WB	Sigma-Aldrich Chemie GmbH, Schnelldorf, Germany
Goat anti-rabbit-HRP	1:1000	WB	Sigma-Aldrich Chemie GmbH, Schnelldorf, Germany
MitoTracker Red CM-H_2Xros	1mM	ICC/IF	Invitrogen GmbH (Molecular probes), Karlsruhe, Germany

2.1.6 Enzymes for molecular biology.

Name	Source
Restriction enzymes	New England Biolabs GmbH, Frankfurt, Germany
Dnase (TypeI)	Sigma-Aldrich Chemie GmbH, Schnelldorf, Germany
T4 DNA Ligase	New England Biolabs GmbH, Frankfurt, Germany
Polymerase, PhusionHF	New England Biolabs GmbH, Frankfurt, Germany
Polymerase, KOD	Merck KGaA, Darmstadt, Germany
Polymerase, Taq	Invitrogen GmbH, Karlsruhe, Germany
Polymerase I, Large (*Klenow*) Fragment	Stratagen GmbH, Waldbronn, Germany
RecA	New England Biolabs GmbH, Frankfurt, Germany
Shrimp alkaline phosphatase	USB Europe GmBH, Staufen, Germany

2.1.7 Kits.

Name	Supplier
Amersham™ ECL plus WB detection kit	GE Healthcare, Munich, Germany
CloneJET™ PCR Cloning Kit	FERMENTAS GmbH
EndoFree® plasmid maxi kit	Qiagen GmbH, Hilden, Germany
mMessage mMachine® SP6 kit	Applied Biosystems (Ambion), Austin, TX, USA
Mini-PROTEAN® 4-12% Bis-Tris gels	Bio-Rad Laboratories, GmbH, München, Germany
Plasma membrane protein extraction kit	BioVision Research, Mountain View, CA, USA
Prime-It II Random Primer Labelling Kit	Stratagen GmbH, Waldbronn, Germany
Strep-tag Starter Kit	IBA GmbH, Göttingen, Germany
QIAfilter™ plasmid maxi kit	Qiagen GmbH, Hilden, Germany
QIAquick® gel extraction kit	Qiagen GmbH, Hilden, Germany
QIAprep® spin miniprep kit	Qiagen GmbH, Hilden, Germany
TOPO TA cloning® kit	Invitrogen GmbH (Gibco), Karlsruhe, Germany

2.1.8 Cell culture media.

Name	Compositiom
HEK293 growth medium	DMEM (or Minimum Essential Medium, a Modification [a-MEM]), 100 units/ml penicillin, 100 µg/ml streptomycin, 4 mM L-glutamine,10% fetal bovine serum
CHO growth medium	F-12 medium, 100 units/ml penicillin, 100 µg/ml streptomycin, 10% fetal bovine serum
DRG neurone growth medium	DMEM medium, 100 units/ml penicillin, 100 µg/ml streptomycin, 4 mM L-glutamine, glucose, 10% fetal bovine serum
MEF growth medium	DMEM medium with glutamax, 12% fetal bovine serum, 100µM non essential aminoacids (10mM, 100X), 100 units/ml penicillin, 100 µg/ml streptomycin, 0.1mM mercapto-ethanol
ES cell growth medium	DMEM medium with glutamax, 15% fetal bovine serum, 100µM non essential aminoacids (10mM, 100X), 100 units/ml penicillin, 100 µg/ml streptomycin, 0.1mM mercapto-ethanol, 180µl LIF per 600ml of a total volume (conditioned medium of LIF expressing COS cells).

2.2 Molecular biology.

2.2.1 Extraction of mRNA from animal tissues and cDNA preparation.

Tissues (dorsal root ganglia (DRGs), brain or spinal cord) were dissected and immediately transferred into eppendorf tubes containing an appropriate volume of Trizol reagent (normally 1ml per 100mg of tissue). The samples were homogenised using a glass homogenizer and incubated for 5 minutes at room temperature. Afterwards 0.2ml of chloroform per 1ml of Trizol used initially was added; samples were vigorously mixed and incubated for 3 more minutes on a bench. To separate RNA, the tissue homogenate was centrifuged for 10 minutes at 12000g, 4C° and afterwards the resulted colorless upper aqueous phase was transferred into a fresh tube. To precipitate RNA 0.5ml of isopropanol per 1ml of Trizol volume used was added and samples were incubated for 10 minutes at room temperature. Next RNA was separated by centrifugation at 12000g for 10 minutes, washed with 75% ethanol, air-dried and dissolved in 30µl of RNAse-free water. One to three µg of total RNA was used for cDNA synthesis using SuperScript™ III Reverse Transcriptase according to the manufacture's protocol.

2.2.2 Amplification of DNA fragments by PCR reaction.

All DNA fragments aimed for molecular cloning or site-directed mutagenesis were amplified from cDNA, BACs or plasmids using Phusion® High-Fidelity DNA polymerase (New England Biolabs). Genotyping of animals, colony and analytical PCR assays were performed with Taq-DNA polymerase (Invitrogen). All primers used in this work were synthesised by Invitrogen.

Standard PCR mix. for Taq polymerase	Cycling protocol for Taq polymerase:
20-100ng of template	Initial denaturation: 94°C 2min
1 x PCR buffer	Denaturation: 94°C 30–60sec
2mM MgCl$_2$	Annealing: primer-dependent 30–60sec
0.2mM dNTPs	Extension: 72°C 30–60sec
0.5mM primer 3´	Cycles: 25–35
0.5mM primer 5´	Final extension 72°C 10min
5U Taq DNA polymerase	Storage: 4°C
H$_2$O to 30µl reaction volume.	

Standard PCR mix. for Phusion®	Cycling protocol for Phusion®
20-100ng of template	Initial denaturation: 98°C 30sec.
1x HF or GC buffer	Denaturation: 98°C 15sec
0.2mM dNTPs	Annealing: primer-dependent 20-30sec
0.5μM primer 3´	Extension: 72°C 30sec/kb
0.5μM primer 5´	Cycles: 25–35
1U of Phusion®	Final extension 72°C 10min
H$_2$O to 50μl reaction volume.	Storage: 4°C

2.2.3 Agarose gel electrophoresis.

DNA samples were separated on 0.5-2 % agarose gels in the EasyCast™ gel system (Owl Thermo Scientific). Gel was prepared by microwaving of the appropriate amount of agarose powder in 1X SB buffer. 0.01 % of SYBR Green (Invitrogen) was added to the pre-cooled agarose solution and the gel was poured into the gel slides and allowed to polymerize. DNA samples were mixed with 6x DNA loading dye and ~200-500 ng of DNA (analytic gels) or 1-4 μg of DNA (preparative gels) were added per gel pocket. The Smart DNA ladder (Eurogen) was used as a DNA size marker. Electrophoresis was carried out at 70-120 volts for 40-60 minutes and gels were subsequently analysed using the Safe Imager™ blue light (Invitrogen).

2.2.4 Gel purification of DNA fragments.

For extraction of all PCR amplified and enzyme digested fragments after agarose gel electrophoresis the QIAquick® gel extraction kit (Qiagen, Germany) was used. The DNA bands of interest were cut out from 1% agarose gel under the Safe Imager™ illumination and melted in QC buffer at 55 °C. The extraction was performed according to the producer's manual.

2.2.5 Restriction digestion and subcloning.

DNA was enzymatically digested using specific endonucleases (New England Biolabs, USA) with 10 U of the restriction enzyme and 1x final dilution of the required restriction buffer added to 0.5-1 μg for plasmid DNA. The final volume was adjusted to 20-30μl with MQ water and the samples were incubated for 1–2 h at the temperature required for the respective

restriction enzyme. Ligation reaction was carried out as the sticky end ligation with 3-5 fold molar ratios of inserts to vectors. Typical volume for a ligation mixture was 20µl containing 2000 units (in 1µl) of Quick T4 DNA ligase (New England Biolabs, USA) and 1x ligation buffer. Ligation reaction was carried out at room temperature for 30 minutes and after what mixture was quickly cooled down on ice. Five to 7 µl from the reaction mixture was used for transformation into bacteria.

2.2.6 Construction of expression vectors for cell biological experiments.

All expression vectors used in this work were made using standard molecular-biological techniques. Genes of interest were amplified from mouse cDNA using gene-specific primers, containing suitable sites for each subsequent subcloning into the expression vector backbones.

2.2.7 Plasmid DNA extraction.

Plasmid DNA was extracted using the QIAprep® spin miniprep kit or the QIAfilter™ plasmid maxi kit (Qiagen, Germany). All steps were performed according to the manufacture's protocol. Concentrations of obtained DNA were measured using the GeneQuant 1300 photometer (GE Healthcare). All DNA preparations were stored at -20 °C.

2.2.8 Sequencing.

Sequencing of DNA samples was done by LGC Genomics, Berlin. All sequencing results were analyzed with Vector NTI 10.3 (Invitrogen) and FinchTV (Geospiza Inc.).

2.2.9 Southern blot (alkaline method).

For the analyses of neomycin resistant ES-cell clones and genotyping of the resulting mouse lines the following Southern Blotting method was used. DNA fragments of digested genomic DNA from ES clones or animal tails were separated on a 0.9% agarose gel using TAE buffer, stained with ethidium bromide and photographed with a ruler in order to be able to identify the size of DNA fragments. The gel was incubated in 0.25N HCl for 10 minutes with agitation in order to depurinate DNA fragments and break large fragments into smaller pieces, what allows more efficient DNA transfer from a gel to a membrane. To denature double-stranded DNA and thus improve binding of negatively charged DNA to the positively charged

membrane, the depurinated gel was transferred into 0.4N NaOH and incubated with agitation two times, 15 minutes each. For DNA transfer a capillary transfer system using 0.4N NaOH as a carrier buffer was set up. After overnight transfer the membrane was backed at + 80C° for 2 hours in order to fix DNA fragments. The membrane was washed twice in 20X SCC followed by 5 minute incubation in 2X SCC buffer.

2.2.10 Hybridisation with radioactively labeled DNA probes.

DNA fragments, for radiolabeled probe synthesis, were amplified from a BAC containing the gene of interest and gel purified. Radioactive probes were synthesised using Prime-It II random primer labelling kit (Stratagene) according to the manufacturer's protocol. In all experiments $[\alpha- ^{32}P]dCTP$ isotope (PerkinElmer) was used. Prior actual hybridisation with the probe, membranes were pre-hybridised in a heated hybridisation buffer (GE Healthcare) for at least 2 hours at 65C° in order to block nonspecific binding. The radioactive probe was boiled for at least 5 minutes, immediately transferred on ice for 5 minutes and added to the hybridisation buffer. Membranes were incubated with the probe overnight at 65C° with constant rotation. After hybridisation the hybridisation buffer was discarded and membranes were washed 2 times for 5 minutes in 2X SSC – 0.1% SDS buffer and 1 time for 30 minutes in the oven with rotation. After this, membranes were transferred into bigger containers with a 0.1 SCC-0.5% SDS buffer and washed 2-3 times on 65C° preheated water-baths. Washed membranes were slightly air-dried, wrapped into plastic and exposed to X-Ray film in exposure cassettes at -80 C°. Exposure time varied from 24 hours to one week.

2.3 Construction of gene targeting vectors.

Initially conditional knockout (cko) or targeting vectors were made using the so called recombineering approach to introduce functional elements such as *loxP*, *frt* sites as well as positive and negative selection markers into BAC DNA by homologous recombination in bacteria. The region of interest already containing *loxP* sites and positive and negative selection markers was excised from the BAC and used to transform ES cells for further recombination. The production of such constructs appears to be complicated due to presence of *loxP* sites in the most BAC vector backbones and significant BAC size (Semprini et al, 2007). Thus the method described by Liu et al., where subcloning of 10–15-kb into a high-copy plasmid vector from a BAC by gap repair, was employed in this work (Liu et al, 2003).

This method based on homologous recombination mediated by the λ phage Red proteins, which are expressed from a defective temperature-sensitive λ prophage. The efficiency of this recombination is nevertheless relatively low and increases with the length of the homologous DNA arms used. Thus, to make a construction process more efficient and straightforward a novel approach in construction of my targeting vectors was used. I combined a megaprimer-based approach, which is used for site-directed mutagenesis and design of chimeric proteins, with two-step long-range PCR in order to introduce long (300-500bp) "mini-arms" to selection markers, *loxP* and *frt* sites necessary for subsequent recombination in bacteria.

2.3.1 Subcloning DNA via GAP-repair

To make subcloning by GAP-repair possible, a BAC bearing the gene of interest must be co-transformed with linearised high-copy plasmid, containing flanking homology sequences to the BAC and selection markers into an *E. coli* strain that expresses λ phage Red proteins (e.g EL350, DY380) (Lee et al, 2001). To prepare a subcloning vector for the gene targeting the next strategy was used. In the first step two pairs of specific primers, containing at the same time homologous sequences to the subcloning vector and a BAC containing *Stoml-3* genomic sequence (for primer sequences and vector maps see **Appendix**) were used to amplify two sequences (400 bp.) from the BAC (**Figure 6a**). The PCR products were gel-purified and used as the first set of primers in PCR reaction, in which whole subcloning vector (pDTA) was amplified. After 12 initial PCR cycles two flanking primers, which bind to the 5' end of the first amplified fragment and 3' end of the second fragment, were added directly into PCR tubes and the amplification program was run till the end. The product of this reaction was digested with DpnI endonuclease in order to remove template vector used for PCR and afterwards gel-purified. The products corresponded to the linearised pDTA to which homological sequences for recombination were "sewed" (**Figure 6b**). This construct was used to retrieve a region of *stoml-3* gene for cko targeting vector construction. EL350 cells co-transformed with BAC and prepared on the previous step pDTA plasmid were grown on Amp agar plates for selection for at least 15 hours at 30C°. Due to the large size of BACs and absence of selection pressure, initial BAC (chloramphenicol resistance) used for transformation was eliminated. The resulting colonies were tested for correct recombination and positive clones used for further vector construction.
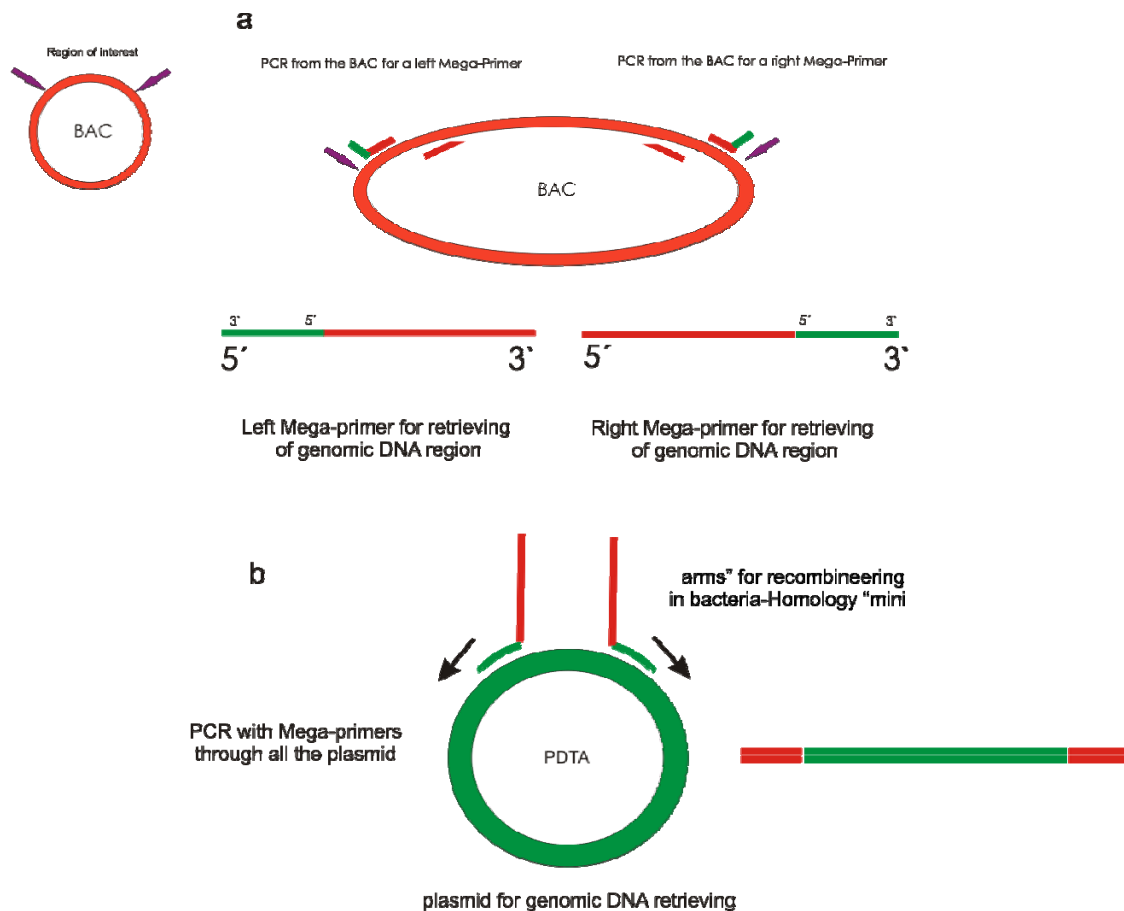
Figure 7. A principal scheme of megaprimer approach for targeting vector construction.
(a) on the first step two sets of primers, containing homology sequences to a subcloning pDTA vector (marked in green) were used to amplify "mini-arms" necessary for targeting construct recombination in bacteria (marked in red). **(b)** two "mini-arms" from the first step were used as primes to amplify the whole subcloning vector and thus, to adjust sequences necessary for recombination to the vector backbone, containing DTA (negative selection marker).

2.3.2 Targeting of a single *lox*P site into the subcloned plasmid DNA

In the next step a single *loxP* site was introduced into the subcloned DNA fragment upstream of the first *stoml-3* exon sequence. This was accomplished by introducing a floxed neomycin resistance (*Neo*) cassette via homologous recombination into the subcloned DNA region, and subsequent removal of this cassette by *cre* recombinase, that was expressed by EL350 cells upon arabinose induction. Removal of the floxed *Neo* gene leaves a single *loxP* site in the same orientation at the targeted locus. To introduce the floxed *Neo* cassette it was flanked with 300bp-long homologous „arms" using the same mega-primer approach described above (**Figure 6a,b**). EL350 cells were co-transformed with the vector prepared in the previous step and with a floxed *Neo* cassette containing homologous sequences for recombination. Correctly recombined constructs were selected on kanamycin (Kan.) plates and verified by analytical restriction and sequencing. One of the positive clones was used to remove *Neo* via *cre*-mediated excision. Expression of *cre*-recombinase was induced by EL350 cell incubation

in arabinose containing medium over 1 hour. After incubation cells were collected by centrifugation and plated on ampicillin (Amp.) and kanamycin. agar plates. Colonies from the Amp. plates were analysed, the Kan. plate did not support bacterial growth, indicating efficiency of *Neo*-cassette excision.

2.3.3 Targeting of the second *loxP* site and neomycin resistance selection marker.

The final step in construction of a targeting vector is an introduction of a second *loxP* site into the subcloned DNA fragment together with a positive selection marker. To achieve this, a construct, containing *Neo* flanked by *frt* and *loxP* sites only from one side, was used to introduce homological sequences for recombination using the methods described above. Recombination of this construct with the vector from the second step resulted in the construction of the final targeting vector (**Figure 30**).

Vectors for *Stoml-3^{OneSTrEP}* knock-in and *Stoml-3^{LacZ}* reporter allele (**Figure 31 and 32**) were constructed using the same methodology.

2.4 Cell biology.

2.4.1 Preparation of MEF cell culture.

Mouse embryonic fibroblasts (MEFs) were prepared as feeder cells to maintain mouse embryonic stem cells (ES cells) in undifferentiated state during clone selection.

Prior to MEF preparation, mating of the mice containing neomycin resistance cassette in their genome (e.g. any knock-out mouse line, where a neomycin resistance cassette was used to disrupt a gene sequence), was set up. Mouse embryos from one or two pregnant animals (for one preparation 7 to 9 embryos was used) were dissected aseptically at 14,5-15,5 dpc, cleaned from all membranes and placed in a Petri dish with sterile PBS. Limbs, viscera and brain were removed; the trunks were washed in PBS and DMEM without serum after which they were minced with sterile razor-blades into small pieces and passed several times through a 10ml glass pipette. The minced embryos were transferred into a 50ml Falcon tube containing 15ml of trypsin/EDTA buffer and incubated at 37C° for 15 minutes while stirring. To reduce viscosity, several drops of DNAse were added to the tissue mixture. After 15 minutes of incubation the tube content was passed several times through a glass pipette and incubated for next 15 minutes while stirring. At the end of incubation time an equal volume of serum-

containing medium was added to the trypsinized tissues. The content of the tube was spun at 1000rpm for 10 minutes. The obtained cell pellet was resuspended in a cell culture medium and plated at a rate one dissected embryo per one 15Ø tissue culture dish. On the next day the medium was changed. Fibroblasts were grown to confluence, after which they were split from 1:6 to 1:10 and grown again to confluence. For ES cell cultures, MEFs from the third or later passages were used.

2.4.2 ES cell cultivation, electroporation and selection of positive clones.

Prior to the ES cell work a sufficient amount of neomycin resistant MEF cells was prepared as described above. All the cell culture plastic used during ES cultivation was covered with 0.1% gelatine solution in the following way: sufficient amount to cover a dish surface of 0,1% sterile gelatin was added and incubated for 5 minutes at the room temperature. After incubation the left over liquid was carefully removed with a pipette and covered dishes were left to dry under the hood for at least for 5 minutes.

2.4.2.1 Linearization of the targeting vector.

For linearization 80 to 100 μg of the verified and thoroughly sequenced targeting vector was used. The vector was digested with 40U of NotI-HF endonuclease (New England Biolabs, USA) overnight in 300μl reaction volume containing appropriate buffer and BSA. A small aliquot from the restriction mixture was separated in an agarose gel to verify if the digestion was complete. Afterwards the whole volume of the digested DNA was mixed with 300μl of phenol/chloroform (1:1) and spun in a pre-cooled micro-centrifuge for 10 minutes. The top aqueous layer was carefully transferred to a new tube and mixed with an equal volume of chloroform in order to remove phenol traces. The mixture was centrifuged for 10 more minutes, aqueous layer transferred to the new tube and sodium acetate/ethanol mix (with a 0,3 M final concentration of sodium acetate) was added in order to precipitate DNA. The tube was incubated overnight at -20C° and afterwards spun at 14000rpm for 15 minutes at 4C°. The obtained DNA pellet was washed once with ice-cold 70% ethanol, dried and resuspended in 50μl of sterile TE buffer (pH 8).

2.4.2.2 Feeder cells preparation for ES cell culture.

Freshly prepared or frozen MEF cells from no more than 4 passages were seeded onto 15cm culture dishes and grown to confluence. The growth medium was changed every second day.

Confluent dishes were trypsinized in the following way: the growth medium was aspirated and cells washed once with PBS, 3ml of trypsin/EDTA per 15Ø dish was added and incubated at 37C° until cells detached, 5ml of the medium (containing serum) was added, cells were gently pipetted up and down, transferred into a falcon tube and centrifuged at 1100 rpm for 3 minutes. The collected cells were resuspended in a feeder growth medium, plated onto three 15cm dishes and grown to confluence. Upon confluence normal feeder medium was substituted with a medium containing mitomycin C (final concentration 0,01mg/ml) and plates were incubated for 2-3 h at 37C°, after what the medium was removed and cells trypsinized as ascribed above. The mitomycin treated cells were seeded onto new dishes (see **Appendix** for dilutions) and used for ES-cells cultivation for up to 2 weeks.

2.4.2.3 Thawing of frozen ES cells and preparation for electroporation with a targeting construct.

A vial of frozen ES cells was thawed at 37C° in a water bath; cell suspension was transferred to a tube with 10ml of ES cell medium. The tube was swirled several times and centrifuged at 900 rpm for 3 minutes. The cell pellet was thoroughly resuspended in 5 ml of a new ES cell medium to break up all cell clumps. The obtained single-cell suspension was seeded onto a 6cm dish with feeder MEF cells and grown for 2 days. Next cells were re-plated on one 10cm feeder dish and grown for 2 more days to achieve a dense culture state (but not confluent), when single colonies are round in shape with sharp visible edges (**Figure 7**). The ES cell colonies were trypsinased with 2.5ml of trypsin/EDTA mixture for 5 minutes at 37C° followed by careful pipetting and centrifugation to achieve full separation of the cells. A number of single cells was estimated and cell suspension was concentrated to approximately to 1.2×10^7 cells in 800μl PBS volume. Twenty to 40μg of linearized targeting vector was mixed with the cells and this mixture was transferred into a cuvette for electroporation. The electroporator parameters used were as follows: impulse length – 2ms, capacity – 1200μF. After electroporation the cuvette was kept on ice for a few minutes for cell recovery. The electroporated cells were transferred to a tube containing 30ml of ES cell medium with LIF and seeded to three 10cm dishes with mitomycin inactivated feeder cells.
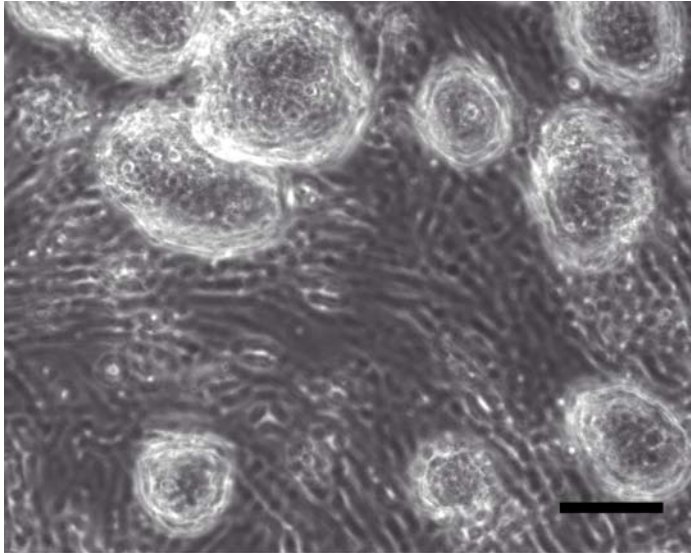
Figure 8. Non-differentiated ES-cell colonies that can be used for electroporation of a targeting construct. Bar – 100μm.

2.4.2.4 Selection and picking of neomycin resistant ES-cell colonies.

After electroporation the ES-cells grew undisturbed for 48 hours until the medium was changed with to one containing G418 (400 μg/ml of active G418). Selection medium was changed once daily over 7 days. On the 8th day single undifferentiated ES cell colonies were picked and cultured for additional 1-2 days in 96-well plates on feeder cells. Grown ES-cell colonies were trypsinised and split into two new 96-well plates; one plate without feeder cells for screening (replica plate –see below) and second one with feeder cells for freezing. To freeze ES cells down, 1 volume of ice-cold 2x freezing medium (ES medium with 13.3% DMSO) was added to semi-confluent, trypsinised 96-well plates that contained 1 volume of trypsin in them. The plates were sealed with adhesive PCR film (Thermo Scientific), wrapped in parafilm and gradually frozen at –80°C in Styrofoam boxes. To screen cell clones for homologous recombination, a replica plates coated with 0.1% gelatine (Sigma) were made of each 96-well plate. These plates were grown to full confluence and used for DNA preparation and subsequent Southern blot analyses.

2.4.2.5 Manipulation of blastocyst and transfer into pseudopregnant mice.

Isolation of blastocysts (C57BL/6 background), injection of ES cells (129/Ola background) into their inner cavity and their transfer into uteri of foster mothers in order to create chimeric mice were done in Transgenic Core Facility (TCF) MDC Berlin-Buch.

2.4.3 Cultivation and transfection of primary and stable cell lines.

2.4.3.1 Establishment of stable cell lines.

A sub-confluent 10cm dish of HEK293 cells was transfected with *stoml-3-OneSTrEP* construct using FuGENE HD (Roche) transfection reagent according to the manufacturer's instructions. On the next day standard HEK293 growth medium was replaced with a medium containing 400-600µg/ml of G418 for selection of cells with stably incorporated *stoml-3-OneSTrEP-tag* construct. The selection medium was changed every day during two weeks. G418 resistant grown colonies were picked with a pipette on an inverted light microscope and transferred to wells in a 24-well plate. Upon confluence clones were picked and trypsinised and split into two wells of a 6-well plate. Cells from one of these wells were used to control expression of the protein with Western Blot. Clones with a good expression level of STOML3-STrEP protein were split into three 10cm dishes. Two of these dished were frozen and the third one was used for further cultivation. The maximal G418 concentration used for maintenance of the stable line was 200µg/ml.

2.4.3.2 Primary DRG cell culture and transfection.

For dissociated DRG cell cultures, ganglia from 4-10 week old animals were dissected into ice-cold PBS after which they were incubated with 1µg/ml collagenase type IV dissolved in 1ml PBS at 37°C for 30 min. In the next step collagenase was substituted for 100µl 0.5% trypsin in 1ml PBS and ganglia were incubated for a further 30 minutes at 37°C. After incubation trypsin was carefully removed and 5ml of pre-warmed DRG-culture medium added to inhibit the remaining enzyme activity. The suspension was centrifuged at 170 x g for 3 minutes after which enzyme-treated DRGs were passed through 23G injection needle to dissociate them into single cells. Dissociated cells were collected by centrifugation at 170 x g for 3 minutes, cell debris were discarded with the medium, cell pellet resuspended in 1ml of DRG medium and cells plated on poly-L-lysin and laminin coated coverslips (about 60-120µl of the cell suspension per coverslip). Plated cells were incubated in the Steri-Cult200 incubator for 4 hours for attachment to the coverslip after what additional DRG medium was added to cover the coverslips completely. Sensory neurones were grown for 24 – 30 hours at 37°C in a Steri-Cult200 incubator.

For electroporation dissociated neuronal cells were centrifuged as described above, pellet resuspended in the electroporation medium (Lonza), appropriate amount of an expression vector was added and mixture was transferred into an electroporation cuvette followed by

actual electroporation using Amaxa machine (pre-installed program A-030). After this 0.5 ml of DRG medium was added and transfected cells were plated on poly-L-lysin and laminin coated coverslips. After 4 hours additional medium was added to float the coverslips.

2.4.4 Immunocytochemistry.

Cultivated DRG neurones were fixed with 4% paraformaldehyde in PBS (pH 7.4) for 10 - 15 min at room temperature, washed with PBS and subsequently permeabilized with 0.05% Triton-X for 10 minutes at room temperature. Non-specific binding of antibody was blocked by incubating the culture in 3% goat serum at 37^oC for 30min. Incubation with primary Abs was done overnight at 4^oC or alternatively for 45min. at 37^oC in 3% goat serum. After this coverslips were washed two times with PBS and incubated with fluorescently-labelled secondary Ab for 45min. at 37^oC. After several wash steps coverslips were mounted and examined using a LeicaSP5 confocal microscope.

2.4.5 WGA labelling of the neuronal cell culture.

For WGA labeling, DRG neurones transiently transfected 24 hours prior the experiment with a wild type *stoml-3-mCherry* construct, were incubated at 37°C with 30μg/ml Alexa Fluor 488-WGA (Invitrogen) in HBSS with 0.1mM Ca^{2+}, 1mM Mg^{2+} and 1% bovine serum albumin (BSA) during 1, 1.5 and 2 hours. Further the cells were washed to remove the unbound labelled WGA and fixed with 4% paraformaldehyde for subsequent microscopic analysis.

2.4.6. Confocal imaging and data processing.

2.4.6.1 Manual particle tracking.

To estimate movement speed of STOML-3 positive vesicles, 24-36 hours before the experiment DRG neurones were transfected either with *stoml-3egfp* or *stoml-3-mCherry* constructs and plated on μ-dishes (Ibidi) for subsequent live cell imaging. Image series of live DRG neurones expressing tagged STOML-3 protein were recorded with 40.0x oil objective (NA 1.25) on the Leica SP5 confocal microscope. Detection of particles and their trajectories tracing was done manually using ImageJ version 1.42q (National Institutes of Health, USA) Manual Tracking plugin (Sbalzarini and Koumoutsakos, 2005). For movement analyses 13

cells from 5 different transfections were used (n of particles 235). The speed of single particle was calculated as an average speed in μm/sec.

2.4.6.2 Manipulation of the cytoskeletal dynamics of neurones.

To destabilise the microtubular cytoskeleton STOML-3 transfected primary neuronal cultures were treated with 5 or 8mM nocodazole for at least 20 minutes prior to imaging. As a control condition application of the same amount of microtubules stabilising agent taxol was used. DMSO stocks of the substances were dissolved in 0.5ml of neuronal growth medium and after that added to STOML-3 or EGFP-transfected neurones.

2.5 Histology.

2.5.1 Animal perfusion.

Prior to the perfusion mice were anaesthetised with Rompun+ ketavet mixture. 0.5 ml 2% Rompun (20mg/ml Xylazine) and 0.5ml Ketavet (100mg/ml Ketavet) were made in 9.0 ml of PBS, the dose of 0.02 ml/g body weight (~0.45ml) was injected intraperitonealy. Surgical-plane anaesthesia was assured by the absence of toe pinch evoked reflexes. The thoracic cavity was opened by cutting the diaphragm from one lateral aspect to the other lateral aspect. Both lateral aspects of the rib cage were cut in a caudal to rostral direction up to 2nd rib and folded-back to expose thoracic organs. The right atrial-chamber was lacerated with scissors while the 25G perfusion needle attached to the saline syringe was carefully inserted into the left ventricular chamber of the mouse. Mice were perfused with ice-cold PBS until liver blanching, followed by 4% PFA or 0,4% glutaraldehyde perfusion during next 20-30 minutes. At the completion of the perfusion required tissues were dissected, post-fixed during 4h in 4% PFA and dehydrated in 30% sucrose overnight at 4C°. Tissue samples, aimed for X-gal detection of β–galactosidase activity, prior dehydration were post-fixed in 0,4% glutaraldehyde for 30 minutes at 4C°.

2.5.2 Preparation of histochemical slices.

Dehydrated tissue samples were embedded in O.C.T. Tissue-Teks (Sakura Finetek, Netherlands), frozen on dry ice and stored at -80C° prior use. For further histochemical experiments frozen embedded tissues were sectioned on Cryostat (Leica CM3050S) on to

slides and dried at room temperature. The thickness of sections was dependent on tissue type and the type of staining used. For dorsal root ganglia sections thickness was normally about 15μm.

2.5.3 Immunohistochemistry.

Freshly prepared or stored at -20C° slides were fixed to the gelatine covered glass slides with ice-cold acetone for 10 minutes followed by triple washing in 1X TBS and incubation for 2 hours at room temperature in a pre-incubation buffer, containing 1% BSA and 0.05% Triton-X-100. After 2 hours the buffer was changed to an incubation buffer, containing first antibody, 5% goat serum and 0.05% Triton-X-100, and incubated overnight at 4C°. Concentrations of the antibodies used were determined empirically for each particular case. Next day sections were washed three times with 1X TBS buffer for 10 minutes and incubation buffer, containing secondary antibody was applied for 2 hours at room temperature. Finally, slices were washed 3 times with 1X TBS 10 minutes each, air-dried and coverslipped.

2.5.4 Epitope recovery (citrate method).

To recover antigens masked in some samples by fixation in cross linking fixatives such as PFA, I used the so called citrate method. Prior to recovery tissue sections were dehydrated and citrate buffer (10mM citric acid, 0.05% Tween 20, pH6) was preheated till 95C°. Slides were in the staining dish containing the buffer and incubated for 20-30 minutes in the oven at 80-90C°. After this the staining dish with slides was removed to room temperature and cooled down for 20 minutes. Slides were washed several times with a 1X TBS-Tween20 buffer and used for immunostaining.

2.5.5 Detection of $\tilde{\beta}$-galactosidase activity.

.
Glutaraldehyde fixed tissues were frozen and sectioned on to slides. Prior to staining, all the slides used were rinsed several times in 1X PBS. Fresh X-gal buffer, containing 35mM potassium ferrocyanide, 35mM potassium ferricyanide, 2mM $MgCl_2$ and 1mg/ml X-gal, was prepared for every experiment. Slides were placed into a histochemical chamber and flooded with the X-gal buffer. Staining was carried out protected from light at 37C° for 24h. Following overnight staining, samples were intensively washed with 1X PBS and coverslipped for further imaging.

2.5.6 Whole mount staining and cleaning of LacZ expressing embryos.

Mouse embryos were dissected into ice cold PBS, all membranes (including the amnion) were removed. Prepared embryos were fixed for 2-2.5h in 0.5% glutaraldehyde and rinsed thoroughly in ice-cold PBS. Fresh X-gal buffer (see description above) was prepared and embryos were incubated in X-gal buffer overnight at 37C° protected from light. Stained embryos were washed in PBS to remove the rest of staining solution and fixed in 4% PFA overnight at 4C°. In some experiments embryos older than 15dpc were skinned prior staining to facilitate staining of internal organs or viscera was removed to facilitate carcass staining. Embryos older than 13dpc were cleared for subsequent visualisation. For this embryos were incubated in series of solutions containing 20%, 50%, 80% and 100% glycerol (v/v) brought to the final volume with 1% KOH (w/v) at 30C°: Each incubation step last from 4 to 7 days, after which the solution was changed. Cleaned embryos were stored and visualised in 100% glycerol.

2.6 Protein analyses.

2.6.1 Preparation of total protein extracts from cell culture and animal tissues.

Prior to protein extract preparation cultivated cells were washed free of culture medium and incubated for 5-10 minutes in PBS in the cell culture incubator, to reduce contamination with protein from the serum. After incubation PBS was substituted with RIPA lyses buffer supplemented with a protease inhibitor cocktail (Roche), cells were collected using cell scrapper and homogenised on ice in glass-teflon homogeniser with 6-10 strokes. Homogenised samples were incubated for 20-30 minutes with rotation followed by centrifugation for 20 minutes at 16000g.

For preparation of total protein from the mouse tissues fresh-dissected or alternatively flash-frozen samples were used. Tissues were minced with a razorblade and homogenised in the lyses buffer (50mM Tris-HCl, 150mM NaCl, 1mM EDTA, 0.5% DOC, 1% Triton-X100, 0.3% SDS, 1mM DTT, protease inhibitors. pH-7.4 or 50mM Tris-HCl, 150mM NaCl, 1mM EDTA, 1% Triton-X100, 0.3% SDS, 9M Urea) using *Ultrathorax*. Homogenised samples were incubated for 20-30 minutes with rotation followed by centrifugation for 10 minutes at 16000g. A pellet, containing cells and cell debris was discarded and a supernatant was transferred into a new tube and centrifuged for 30 more minutes. All the steps were performed

at 4C° or on ice to reduce protein degradation. Protein concentrations were estimated using the Bradford essay (Bradford, 1976).

2.6.2 Co-immunoprecipitation.

For co-immunoprecipitation experiments a CHO cell line was co-transfected with plasmids encoding proteins of interest for at least 24 hours prior to use. Total protein extract from transfected cells was prepared as described above. Co-immunoprecipitation was carried out according the manufacturer's protocol (Dynabeads® Protein G, Invitrogen). In brief, 1.5mg of dynabeads were used for protein-specific antibody binding, total protein extract was added to the beads and incubated for 10 minutes with rotation at room temperature. The beads with precipitated proteins were intensively washed, separated on a magnet and used to elute bound proteins under denaturing conditions with a protein sample buffer. For control, protein samples were collected at every step of the protocol. Obtained protein eluate and samples of the total protein extract were separated on the SDS-gel, blotted on nitrocellulose membrane and subjected standard antibody detection.

2.6.3 SDS-PAGE and Western blotting.

Before separation on a SDS gels, protein samples were diluted 1:3 with 4x SDS sample loading buffer and denatured for 5 minutes at 95C°. Cooled samples were then loaded on 12% SDS gel and proteins separated in 1x Tris-glycin buffer at 120-150V on Mini-PROTEAN III system (BioRad). After separation of proteins the SDS-PAGE gel was rinsed with distillate to reduce SDS amount and proteins were blotted on nitrocellulose membrane using wet-blotting Mini Trans-Blot system (BioRad) according to the manufacture's instructions. The membrane was rinsed with 1x TBS buffer and incubated in blocking buffer for non-specific binding of antibody with shaking for 1 hour at room temperature. Blocked membrane was washed 2 times 5 minutes each in 1x TBS-0.5% Tween buffer followed by incubation in the primary antibody diluted in 1x TBS – 0.5% Tween buffer for 1 hour with shaking. In the next step non-bound antibody were washed from the membrane in 1x TBS – 0.5% Tween buffer (3 times 5 minutes each) and membrane was incubated in the secondary peroxidase-conjugated antibody pre-diluted in 1x TBS – 0.5% Tween buffer. The membrane was washed again in the same manner and developed with ECL reagent (Pierce). Chemiluminescence signal was detected after exposure of the membranes to ECL films (GE Healthcare).

3. Results.

3.1 Cell biology of stomatin-like protein-3.

STOML-3 is a membrane-associated protein in the stomatin family of proteins and it displays a restricted neuronal pattern of expression. We have recently shown that STOML-3 is required for normal touch sensation in the mouse (Wetzel et al, 2007), but the cellular functions of STOML-3 and the molecular mechanisms by which it functions are unknown. Due to high similarity with other stomatin family members (e.g. stomatin and STOML-1), direct *in vitro* and *in vivo* studies using protein-specific antibodies are significantly hindered. Thus, in this work I utilised cell biological approaches, supported by *in vivo* genetic models, in an attempt to elucidate the cellular functions of STOML-3 and its relevant interaction partners.

3.1.1 Characterisation of STOML-3 sub-cellular localisation in sensory neurones.

Almost all members of the stomatin family of proteins are predicted to be membrane associated proteins with both termini localised intracellularly. Short hydrophobic domains as well as palmitoylation, are important for membrane targeting of stomatin proteins (Snyers et al, 1999a; Stewart et al, 1993). The membrane localisation of STOML-3, as well as other stomatin family members, was confirmed by us and others using transfection of different cell lines and endogenous protein purification from the erythrocyte membrane (Zhu et al, 1999; Zhang et al, 2004; Wang et al, 1991; Snyers et al, 1999b). In order to carry out more detailed characterisation of the sub-cellular topology and dynamics of STOM-3 in DRG neurones I transfected primary neuronal cultures with fluorescently-labelled *Stoml-3* constructs, in combination with staining of the endogenous protein in sensory neurones from the *Stoml-3*[STrEP] mouse, which will be described later in this thesis.

3.1.1.1 Membrane localisation of STOML-3.

To analyse the sub-cellular localisation of STOML-3 in the cell type in which the protein is normally expressed, acutely prepared DRG neurones from C57BL/6j animals were transfected with *Stoml-3-EGFP* or *Stoml-3-mCherry* C-terminal tagged constructs using the Amaxa Nucleofector® kit and subsequently cultivated on µ-IBD dishes for 24h for further microscopy analyses. For analyses of endogenous protein distribution, DRG neuronal cultures from *stoml-*

3^{STrEP} mice were cultured on glass coverslips for 24h after which they were fixed and immunostained with an antibody directed against the OneSTrEP tag.

Immunofluorescence microscopy analyses revealed distinct plasma membrane staining of STOML-3 in both types of DRG neuronal culture (from wild type and from Stoml-3^{STrEP} mice), which corresponds to the expected localisation of the protein (**Figure 9b, d).** Additional, unexpected protein localisation was observed in an intracellular vesicular compartment upon transfection with fluorescently labelled STOML-3 (**Figure 9a**). A similar pattern was obtained from staining of endogenous STOML-3, which supports the idea that overexpression recapitulates endogenous expression patterns of the protein. (**Figure 9c).**
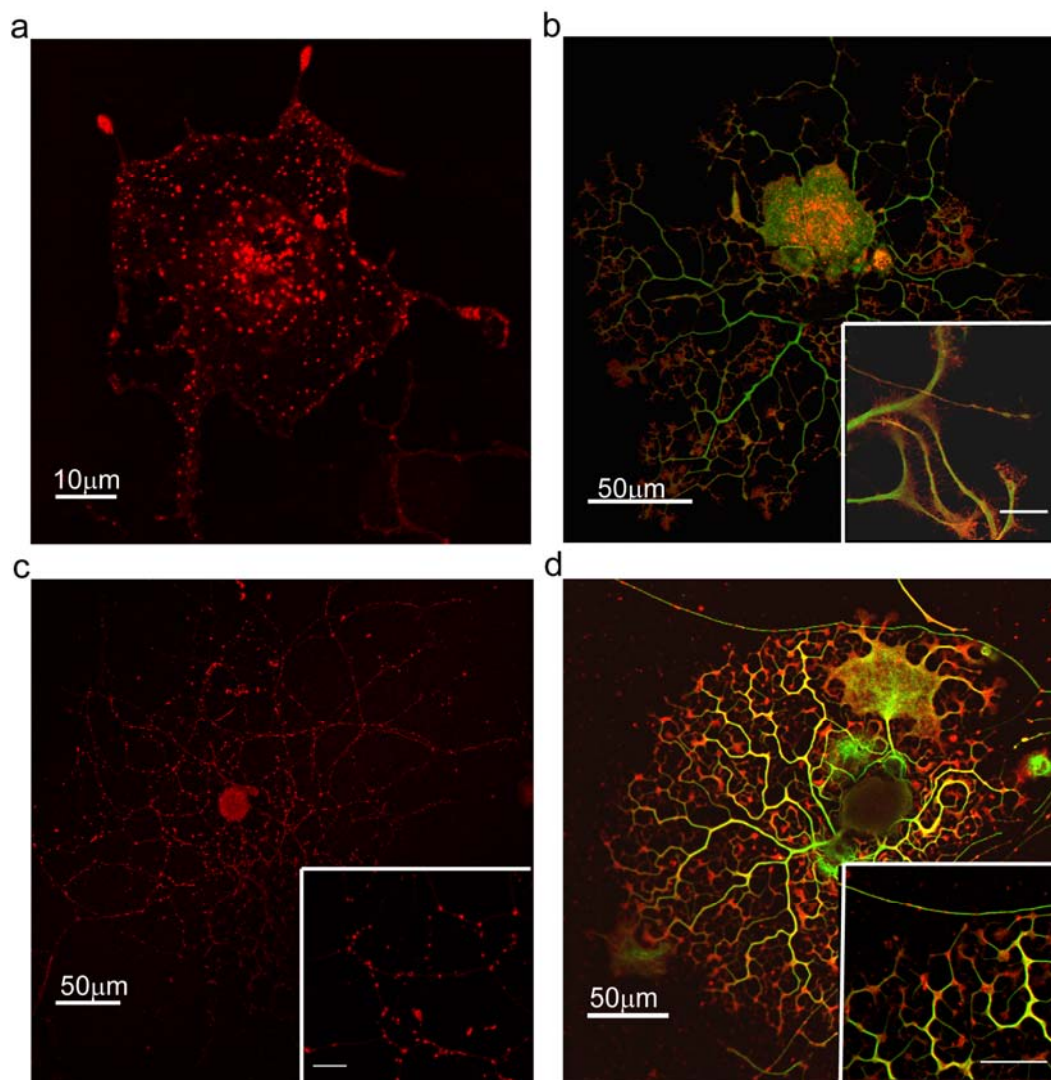
Figure 9. Sub-cellular localisation of STOML-3 protein in mouse DRG neurones.

(**a,b**) acutely prepared DRG neurones were transfected with mCherry-tagged STOML-3 protein, after 24 h cells were fixed and analysed using a confocal microscope.(**c,d**) DRG neurones from a Stoml-3^{STrEP} mouse were cultivated for 24 h, fixed and immunostained with an antibody directed against OneSTrEP-tag (AlexaFluor633, red channel). (**a,c**) both types of cell culture demonstrated characteristic localisation of the STOML-3 protein to vesicular compartments. (**b,d**) STOML3-mCherry and STOML3-OneSTrEP cultures were counterstained using an anti-tubulin antibody (AlexaFluor488, green channel). In addition to the described vesicular localisation, STOML-3 was localised to the plasma membrane. (**b,d**) insert bars – 20μm, (**c**) insert bar – 10μm.

To further study the membrane localisation of STOML-3 protein, TIRF imaging of transfected DRG neuronal cultures was performed. The TIRF system is based on selective illumination and excitation of a fluorophore in a restricted region of the specimen using an evanescent wave, this allows illumination of a very thin near-membrane layer and elimination of any background signal from intracellular components (**Figure 10a).**

A DRG neuronal culture transfected with the *Stoml-3-mCherry* construct was visualised using an Olympus Cell^R TIRF illumination microscope. STOML-3 was readily detected in the plasma membrane of the neurone, as well as in vesicles localised in very close proximity to the plasma membrane (**Figure 10b)**.
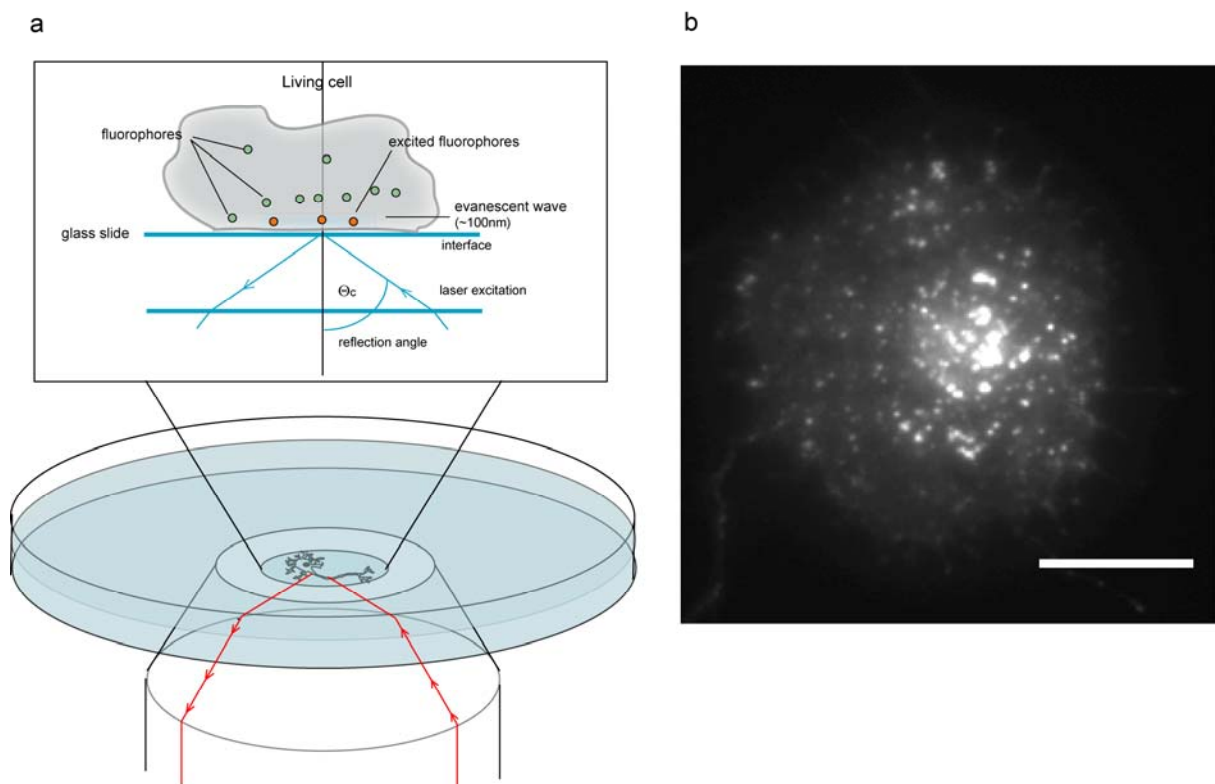
Figure 10. STOML-3 shows membrane, as well as vesicular, localisation in the evanescent field.
a. a scheme of the TIRF imaging technique. **b.** TIRF image of a STOML3-mCherry transfected DRG sensory neurone. In addition to the plasma membrane localisation, a number of relatively static STOML-3 positive vesicles could easily be distinguished. Scale-bar -15μm

3.1.1.2 STOML-3 is localised to a heterogeneous, mobile vesicular compartment.

To further investigate this vesicular compartment further imaging of living DRG neuronal cultures, transfected with fluorescently labelled STOML-3, was performed. The observed intracellular pool of STOML-3 represents a heterogeneous, highly mobile vesicular

population (**Figure 11**). The average speed of movement for a particle in a given field is 0.62 ± 0.02 μm/s (range between 0.3 and 1.2 μm/s), which corresponds to the speed of kinesin-based transport (Gagliano et al, 2010). The bi-directional movement, speed and alternation between mobile and immobile states are consistent with transport events in sensory axons (Cai et al, 2007; Cui et al, 2007; Gagliano et al, 2010; Shtridelman et al, 2009).
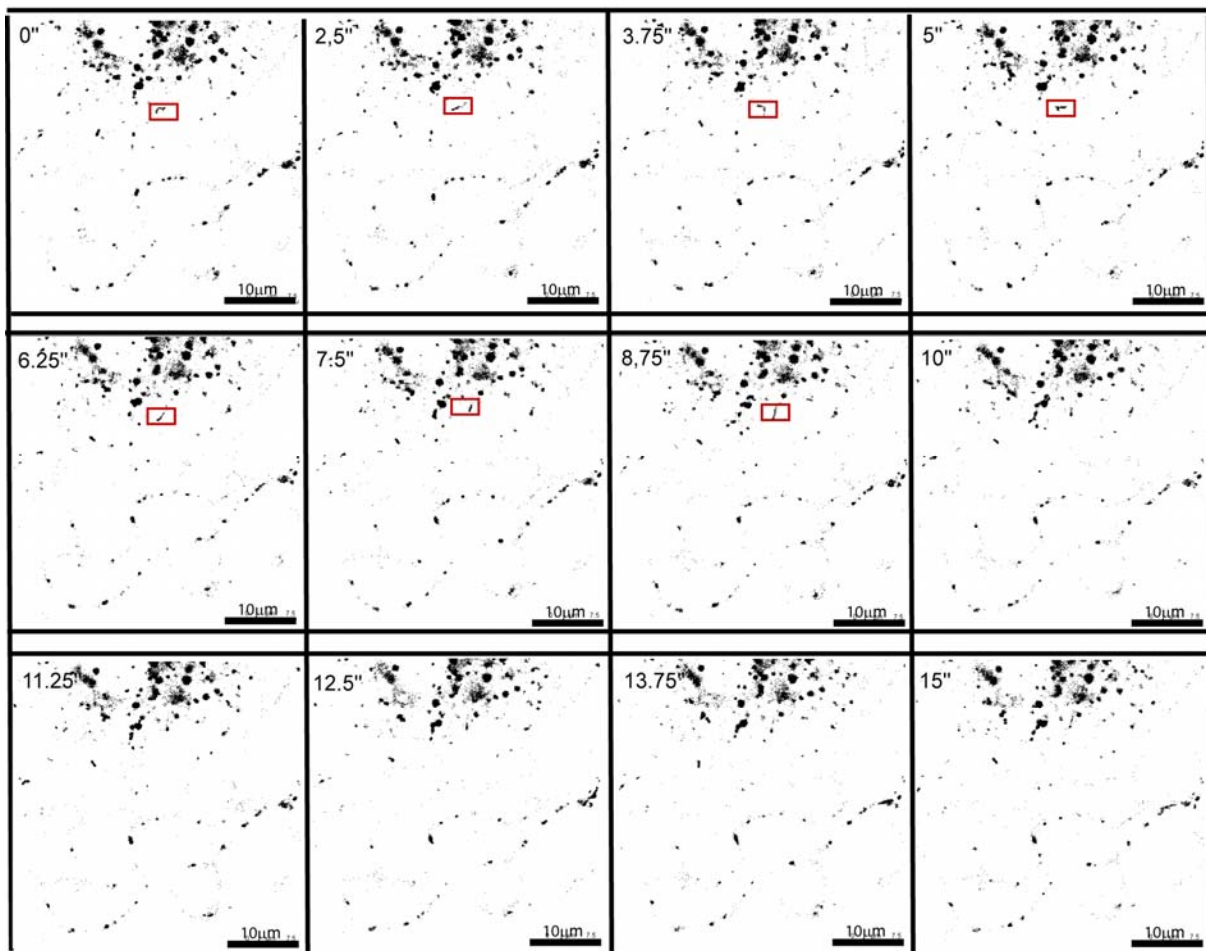
Figure 11. Time course of STOML-3 positive vesicles movements.
Acutely prepared DRG neurones were transfected with the EGFP-tagged STOML-3 construct and cultivated for at least 24 hours prior to live cell imaging. Series of images were acquired at 0.8 frames/second using a Leica SP5 microscope and analysed using ImageJ software. On the presented image series a large number of mobile STOML-3 positive vesicles could be observed. The predominant subpopulation was round in shape; but in addition, a rare subpopulation of vesicles with elongated morphology was also observed (red square).

Among the vesicular pool two main vesicular morphologies could be readily identified. The prevalent population was round in shape and was ~0.5μm in diameter (**Figure 12a**, blue circles). The second vesicular population was comparatively rare and consists of vesicles with an elongated morphology > 1μm in length (**Figure 12a**, white box). The larger vesicles were found to move at higher speeds (mean speed of 1.59 ± 0.15 μm/s) **(Figure 12b)**
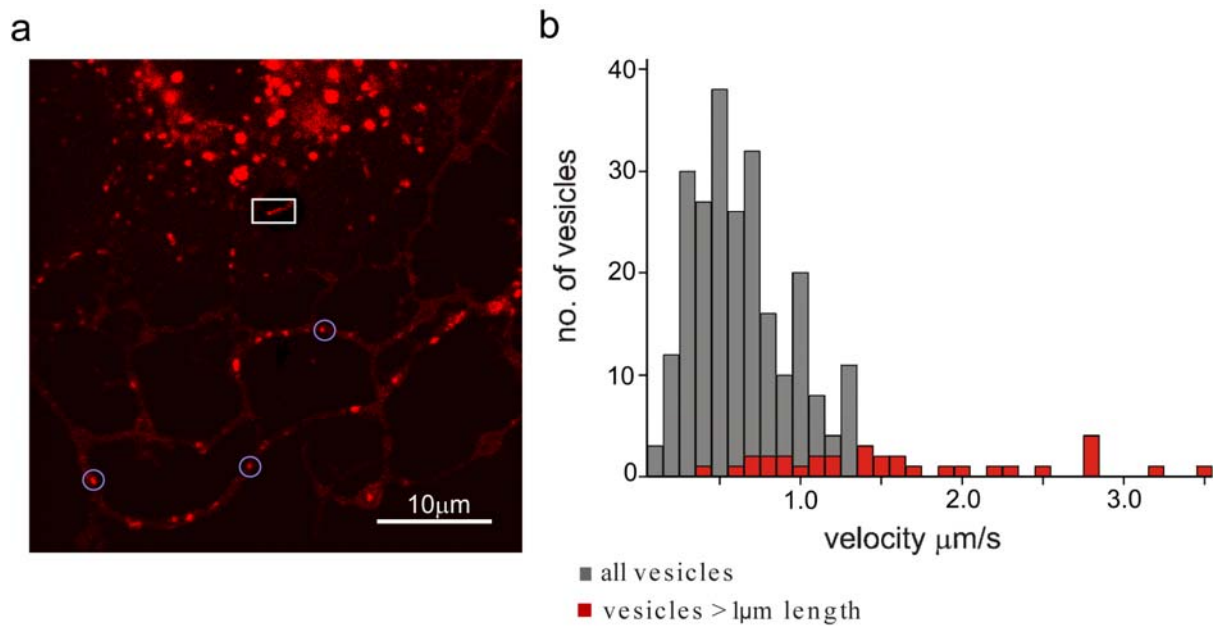
Figure 12. STOML-3 positive vesicular pool can be subdivided into two main subpopulations.
Time series of STOML3-mCherry transfected neurones were acquired using a Leica SP5 microscope. The analysis of vesicular velocities and morphology was conducted using ImageJ software. The majority of vesicles had a round-shape morphology with an average diameter of 0.5μm; the velocity of these particles was 0.4-0.7 μm/s on average. A significantly smaller subpopulation of elongated STOML-3 positive vesicles with an average length of 1μm was shown to have higher velocity, up to 3.5μm/s.

The population of elongated STOML-3 positive vesicles was exclusively observed in DRG neurones. Expression of EGFP-tagged STOML-3 in CHO and HEK293 cell lines resulted in the plasma membrane and vesicular localisation of the protein. Notably, the vesicular compartment contained only round vesicles with a diameter of ~0.5μm and a large proportion of the protein was localised in the perinuclear region, characteristic of the trans-Golgi network (**Figure 13**).
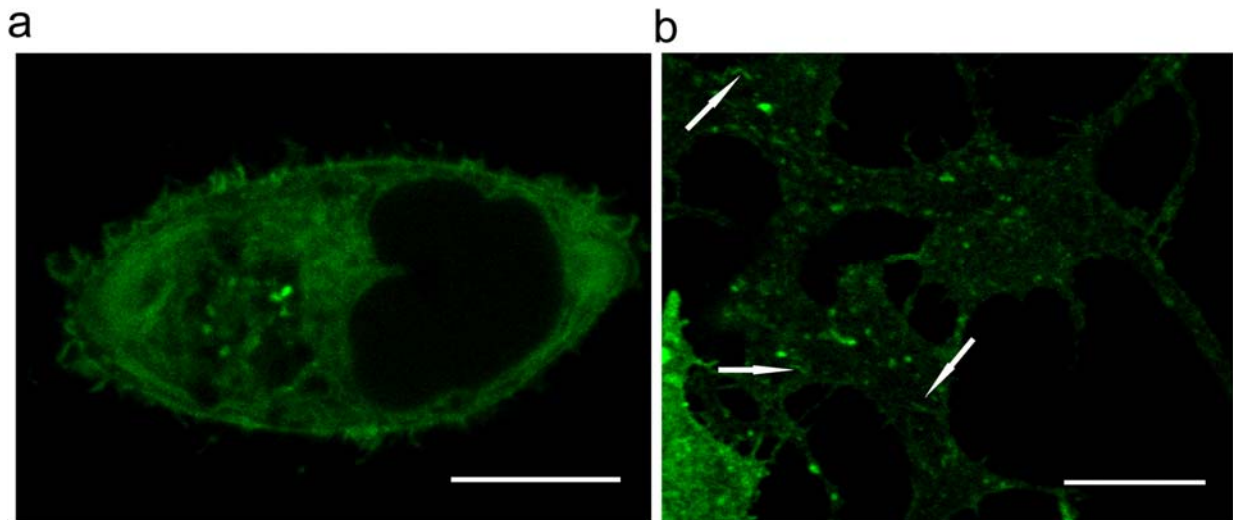
Figure 13. Elongated STOML-3 positive vesicles are characteristic of DRG sensory neurones.
Expression of EGFP-tagged STOML-3 in different cell lines demonstrated a different cellular distribution profile of the protein compared to one observed in DRG neurones. **(a)** In CHO cells the STOML-3 pattern switched from the characteristic vesicular in DRG neurones to a more reticular one with no elongated vesicles observed. **(b, arrow labels)** expression of STOML-3 in neurones resulted in redistribution of the protein to the heterogeneous vesicular compartment. Presence of the long vesicles was readily observed in all experiments, bars – 10μm.

3.1.1.3 Motility of the STOML-3 positive vesicular compartment is cytoskeleton dependent.

Neurones are highly polarized cells with a characteristic morphology and pronounced partitioning of the cell into molecularly and functionally distinct compartments: axonal and dendritic. The length of these two compartments is in many cases very large and can reach in humans more than one meter, corresponding to several centimeters in the mouse. To provide neuronal terminals with "building blocks" and functional components, cell need to transport a large number of organelles, proteins and protein complexes, as well as, mRNAs to distant cell parts. The long distance transport is microtubule-dependent and carried out by members of superfamilies of specialized motor proteins. Anterograde transport is performed by kinesins, while retrograde transportation is dynamin-dependent (Danino & Hinshaw, 2001; Hirokawa et al, 2009). Thus, motility of STOML-3 positive vesicles is expected to be cytoskeleton dependent. To confirm this, acutely prepared DRG neuronal cultures were transfected with fluorescently labelled STOML-3 together with EB3, a microtubule tip-binding protein. One day after transfection, cells were visualised using a confocal microscope in the live imaging mode. Tubulin dynamics and motility of STOML-3 positive vesicles were recorded as two channel movies (**Figure 14 a,c).** The trajectory of vesicle movement corresponds to the orientation of the microtubules as determined by the EB3-EGFP protein signal. In addition,

co-labeling of the transfected culture with tubulin demonstrates close localisation of STOML-3 vesicles to the cytoskeletal "tracks" (**Figure 14b**), supporting the live imaging data.
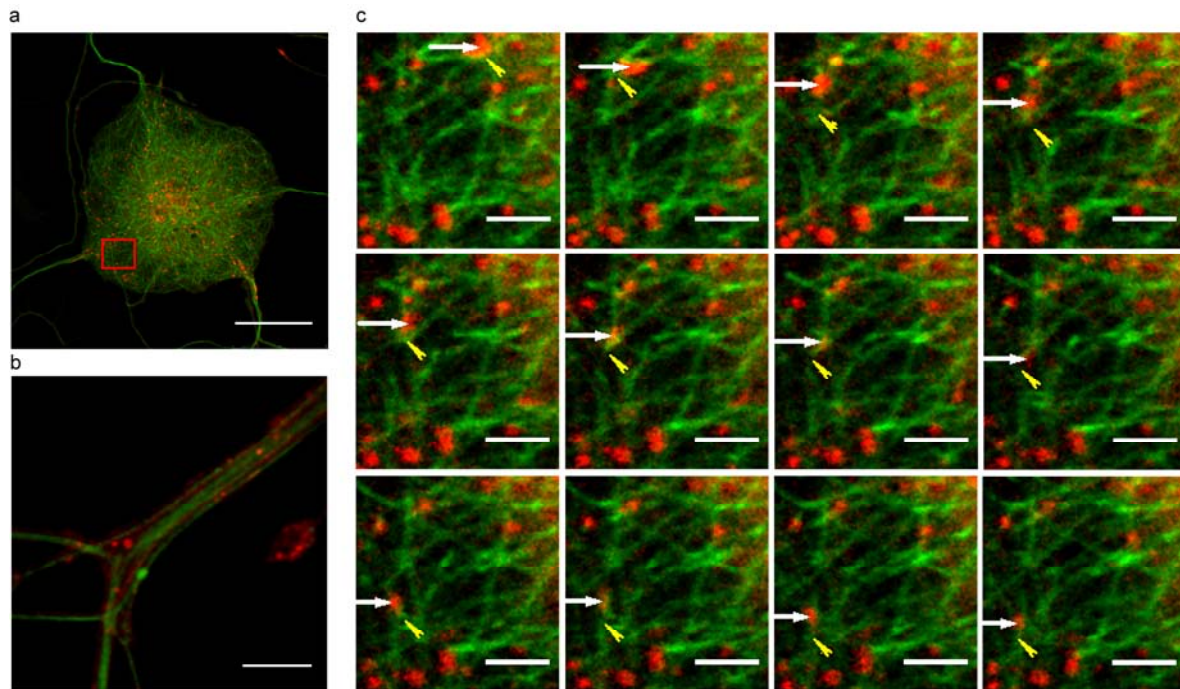
Figure 14. STOML-3 positive vesicles are transported in a microtubule-dependent manner.
(a,c).STOML-3-mCherry transfected DRG neurones were co-transfected with an EB3-EGFP construct in order to visualise the dynamics of microtubule assembly; the vector of vesicle movement corresponds to the direction of filament growth (**a**), Scale bar – 20μm. **(c).** Time course of STOML-3 vesicle movement along growing microtubules. White arrows track a displacement of a vesicle, yellow arrows denote assembling of microtubule filaments; time difference between two consequent images from the panel is 2,5 seconds, Scale bar – 2,5 μm. **(b).** Antibody staining of α−tubulin (AlexaFluor 633) reveals localization of the vesicles in close proximity to the tubulin labeled "tracks". Scale bar – 5μm.

3.1.1.4 Disruption of microtubules promotes fusion of STOML-3 vesicles with the plasma membrane.

To further confirm involvement of the cytoskeleton in the motility of STOML-3 positive vesicles, the acutely prepared cultures of DRG sensory neurones, transfected with *Stoml-3-EGFP* fusion construct, were treated with 5μM nocodazole, an agent which interferes with the polymerization of microtubules and leads to their collapse. Partial disruption of microtubule dynamics resulted in decoupling of the STOML-3 positive vesicles from the cytoskeleton and subsequent fusion with the plasma membrane (**Figure 15a**). Increases in the membrane-associated STOML-3 pool led to a progressive bending of the membrane (**Figure 15a insert**). Notably, EGFP transfected neurones treated with the same concentration of nocodazole showed no changes in cell membrane curvature over time (**Figure 15b**), which supports the hypothesis that STOML-3 has a direct effect upon plasma membrane properties. At the same

time, application of 5µm taxol, a microtubule stabilising agent, produced no apparent effect on distribution and dynamics of STOML-3 positive compartment (**Figure 15c).**
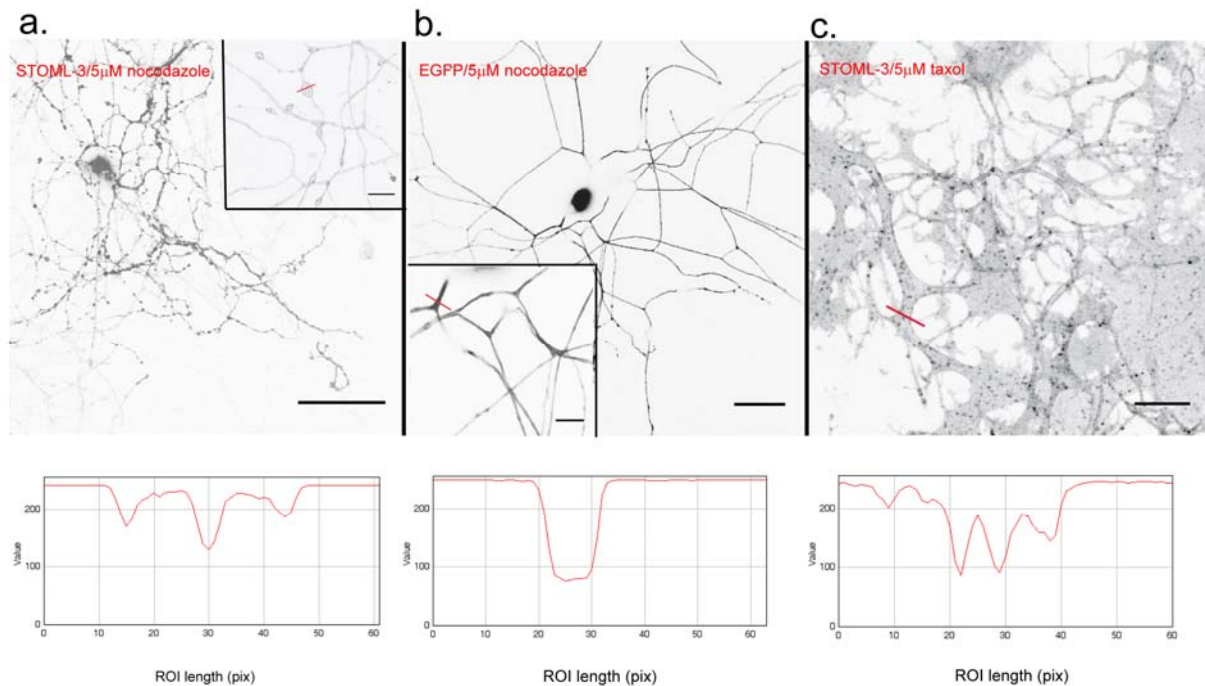
Figure 15. Disruption of the cytoskeleton leads to redistribution of STOML-3 from the vesicular compartment to the plasma membrane.

Application of 5 µM nocodazole, a microtubule destabilising agent, to a DRG neuronal culture transfected with EGFP-labelled STOML-3 led to a detachment of the STOML-3 positive vesicles and subsequent fusion of the vesicle content with the plasma membrane **(a, and a corresponding surface plot at the bottom);** scale bar – 50µm. Increase in STOML-3 content on the plasma membrane resulted in its progressive bending **(a inset)**. Application of the same conditions to EGFP transfected neurones revealed no effect on the membrane curvature **(b)**; scale bar - 50µm. The microtubules stabilising chemical taxol also did not have any effect on the protein redistribution or membrane morphology **(c)**; scale bar – 10µm. Inset scale bars - 10µm. Bottom row of surface plots illustrates a difference in the EGFP fluorophore distribution in three different conditions. ROIs (region of interest) are marked with red lines **(a-c)**. Pronounced reverse peaks on **the first plot** demonstrate predominantly membrane localization of the protein upon nocodazole application; additional peak in the middle corresponds to a vesicle. In comparison, EGFP transfected cells shows even distribution of the signal alone the neurite **(plot two)**; STOML3-EGFP transfected neurones after taxol application have no changes in the protein redistribution with multiple vesicles alone neurites **(plot three).** Red lines denote areas used to build the surface plots.

3.1.2 Molecular characterisation of STOML-3.

3.1.2.1 The STOML-3 positive vesicular pool is distinct from the neuronal mitochondria compartment.

The presence of relatively long vesicles (~1µm) that display a complex pattern of motility, combined with evidence in the literature about mitochondrial localisation of one of the stomatin family members, STOML-2 (Tondera et al, 2009; Hájek et al, 2007), prompted me to test the hypothesis that the STOML-3 vesicular compartment represents a mobile

mitochondria pool in DRG neurones. It is known that mitochondria are actively transported down the processes in neuronal cell bodies in order to support the normal physiological state of the cell in response to active growth and changes in metabolic state (Morris & Hollenbeck, 1993; Kang et al, 2008). Approximately one third of axonal mitochondria is mobile and undergoes saltatory, bidirectional, stop-and-start movements with frequent change in the direction of movement (Stowers et al, 2002; Górska-Andrzejak et al, 2003). The speed of mitochondrial movement is 0.2-2μm/s, dependent on the cell state (Zhang et al, 2010).

To test the hypothesis that the long STOML-3-positive vesicles represent mitochondria in DRG neurones, the following experiment was performed. Acutely prepared, live DRG cell cultures were transfected with *Stoml3-EGFP* construct and after at least 24 hours, which is necessary for expression, mitochondria were labelled alive with *MitoTracker* Red CM-H2Xros (Invitrogen). The culture was used for live-cell imaging using a confocal microscope where two fluorescent channels were simultaneously recorded. Analyses of acquired movies revealed no overlap between the STOML-3-positive vesicular pool and mitochondrial compartment in DRG neurones (**Figure 16)**.
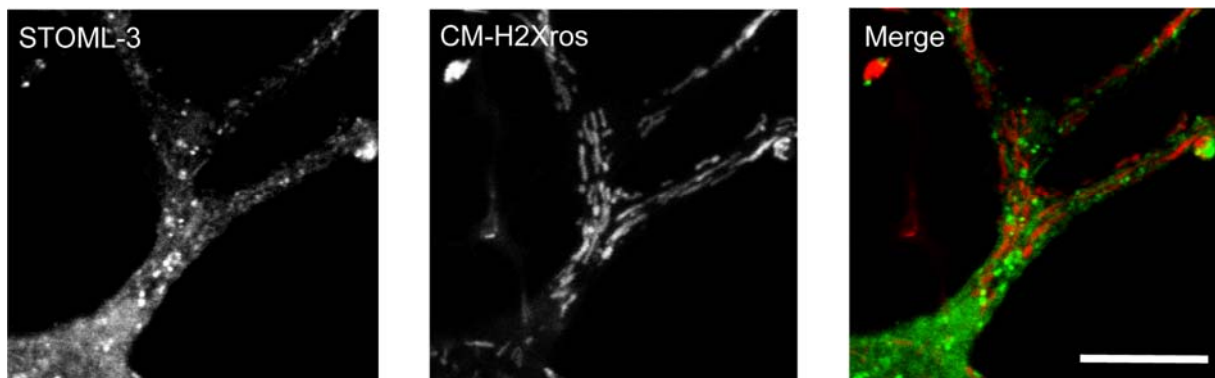
Figure 16. STOML-3 does not localise to mitochondria in sensory neurones.
Acutely prepared DRG neurones were transfected with the *STOML-3-EGFP* construct and subsequently labelled with a live mitochondrial marker - Red CM-H2Xros. Live-cell imaging of double labelled DRG neurones showed no apparent localisation of STOML-3 in the mitochondrial compartment of the cell. Scale bar – 10μm.

3.1.2.2 STOML-3 positive vesicles define a clathrin-independent trafficking pathway.

The level of membrane expression of a particular protein is tightly regulated by different intracellular events process. Direct tuning of protein trafficking is a more rapid event in comparison with the regulation of protein content in the cell at either the transcriptional or translational level particularly in neuronal cells. Thus, precise regulation of trafficking is crucial for immediate adaptation in a dynamic environment. All membrane proteins share a common pathway in the cell, which starts with synthesis in the endoplasmic reticulum (ER),

followed by processing and sorting in the Golgi network, before final export to the plasma membrane. Some membrane proteins may remain on the cell surface for a prolonged time or are internalised via the endocytic compartment. Internalised proteins can undergo further direct, or indirect, recycling back to the cell membrane or be transferred into the lysosomal compartment for subsequent degradation. For neuronal cells, regulation of the cell surface level of protein complexes via protein internalisation and recycling is crucial. We postulate that STOML-3 is involved in mechanosensation and participates in formation of multimolecular mechanosensing complexes. Thus, STOML-3 containing vesicles could represent a distinct endocytic pathway involved in transportation of the protein and thus, regulation of its surface expression. Approximately seven endocytic pathways have been described to date (Doherty & McMahon, 2009). Among these pathways, the clathrin-dependent mechanism is the best characterised and thought to be the most common in certain conditions. Clathrin-mediated endocytosis (CME) is a continuous process characteristic to all mammalian cells and is responsible for the uptake of essential nutrients, as well as intracellular communication during development and regulation of membrane protein content (Conner & Schmid, 2003; Di Fiore & De Camilli, 2001; Brodsky et al, 2001; Schmid, 1997). Rapid clearance and downregulation of activated receptors, ion channels and transporters and recycling of synaptic vesicle membrane proteins are the most studied roles of CME in mammalian cells (De Camilli & Takei, 1996; Beattie et al, 2000).

To test whether the STOML-3 positive vesicular pool represents clathrin-dependent pathway of protein trafficking, immunostaining of DRG neurones was performed. Anti-clathrin (heavy chain) staining of DRG neurones, transfected with fluorescently labelled STOML-3, clearly demonstrated distinct localisation to different vesicular compartments and domains on the plasma membrane (**Figure 17**). Thus, we can conclude that STOML-3 vesicle trafficking is clathrin-independent in DRG neurones (data from 6 cells, 2 experiments).
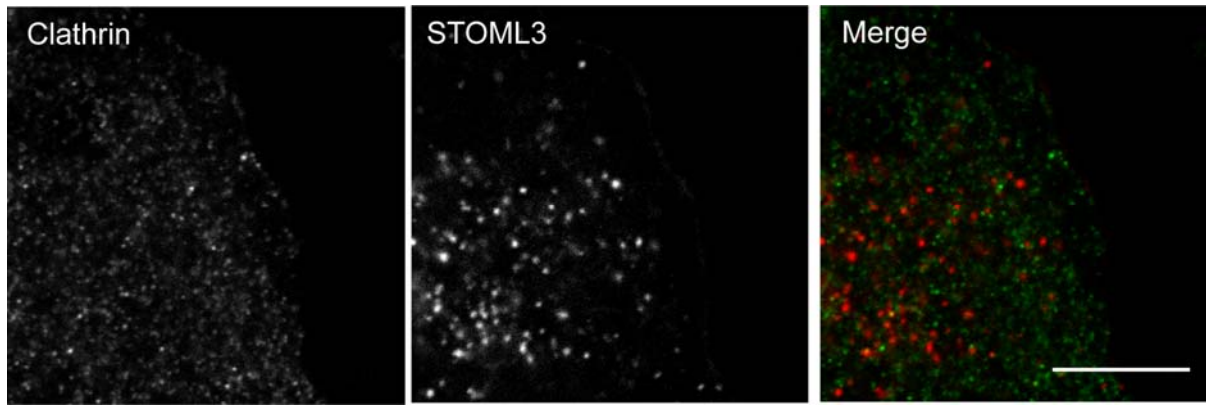
Figure 17. Trafficking of STOML-3 positive vesicles is clathrin independent.
DRG neurones transfected with the STOML-3-mCherry construct were fixed and immunostained with an anti-clathrin antibody (AlexaFluor 488). Confocal images of the vesicular compartment and cell membrane were acquired. No co-localisation between STOML-3 positive vesicles and clathrin coated pits was observed. Scale bar – 10μm.

3.1.2.3 Only a small proportion of STOML-3 positive vesicles is present in the lysosomal compartment.

In certain conditions membrane proteins undergo internalisation and subsequent degradation in the lysosomal compartment. Massive overexpression, which occurs when transfecting the protein of interest into the cells *in vitro*, can lead to degradation of the excessive protein in lysosomes. Thus, to verify the relevance of the primary DRG cell culture system used and exclude the possible artefact produced by protein overexpression, localisation of fluorescently labelled STOML-3 in the lysosomal compartment was examined. Analyses of two-channel confocal images revealed that only a small number (normally less than 10%) of the STOML-3 protein co-localised with the lysosomal marker Lamp-1 in DRG neurones which appear to be healthy in a bright field (phase bright cell bodies) (**Figure 18**). Data from 2 independent transfections, 8 cells.
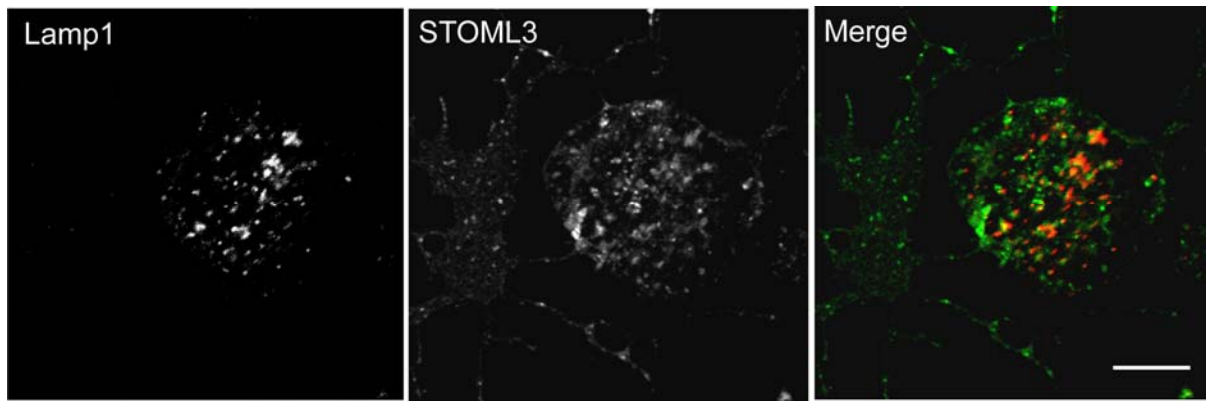
Figure 18. STOML-3 containing vesicles do not co-localise with a lysosomal marker Lamp1.
DRG neurones co-transfected with STOML-3-EGFP and lysosomal marker Lamp1-mCherry constructs were fixed and visualized using a confocal microscope. Two channel images of transfected cells were analysed for co-localisation. Only a small number of STOML-3 containing vesicles was defined as lysosomal compartment, based upon Lamp1 co-staining. Scale bar -10μm.

3.1.2.4 The vesicular compartment is defined as a Rab11 positive recycling pool.

Rab proteins are small GTPases known to be involved in intracellular membrane dynamics (Pfeffer & Aivazian, 2004). In mammals, there are more than 60 known members of the Rab family of proteins, which localise to different cellular compartments (Zerial & McBride, 2001a; Pereira-Leal & Seabra, 2001; Schwartz et al, 2007). The different Rab GTPases are specifically localised to the cytosolic face of intracellular membranes and function as regulators of distinct steps in membrane trafficking (Smythe, 2002; Somsel Rodman & Wandinger-Ness, 2000; Zerial & McBride, 2001b). Thus, identification of Rab proteins localised to the STOML-3 positive vesicles could help to answer the question about the nature of this vesicular pool. To do so, a number of mouse Rab proteins were cloned into an EGFP containing expression vector and these constructs were subsequently transfected together with mCherry tagged STOML-3 into DRG neurones. Two channel fluorescent images were acquired using a confocal microscope and analysed for co-localisation of two fluorescent signals. From 6 Rab proteins analysed, obvious co-localisation was observed only for Rab11 protein (**Figure 22a**), known to be implicated in vesicle recycling and regulation of membrane proteins transport (Eva et al, 2010; Kamiguchi & Lemmon, 2000; Park et al, 2004). Two of the 6 analysed Rab proteins demonstrated cytoplasmic localisation in DRG sensory neurones and are not described in any further detail here.

Rab5 is a small nucleotide-binding protein, which is localised to early endosomes, caveolosomes and the plasma membrane, where it mediates endocytosis and endosome fusion of clathrin-coated vesicles (Barbieri et al, 1996a; Gorvel et al, 1991). A significant number of studies have identified a role for early endosomes in the transport of growth factors, their

receptors and activated signalling proteins in neurons (Saxena et al, 2005; Campenot & MacInnis, 2004; Averill et al, 2001; Reynolds et al, 2001; Delcroix et al, 1999; Delcroix et al, 2004, 2003; Howe et al, 2001). To function, Rab proteins constantly switch between two conformational states, where the GTP-bound state is "active" and the GDP-bound form is "inactive". Rab5 protein with a glutamine for leucine substitution in the GTPase domain (Q79L) is constitutively active and is known to cause the formation of enlarged early endosomes by stimulation of endosome fusion (Barbieri et al, 1996b; Stenmark et al, 1994).

To verify if STOML-3 positive vesicles could represent the early endocytic compartment, EGFP-tagged STOML-3 protein was transfected together with Rab5Q79L mutant into DRG neurones. Confocal images of double-transfected cells were acquired and analysed for localisation of STOML-3 to the enlarged Rab5Q79L early endosomes. No co-localisation of the proteins was detected (**Figure 19**) (data from 3 independent transfections).
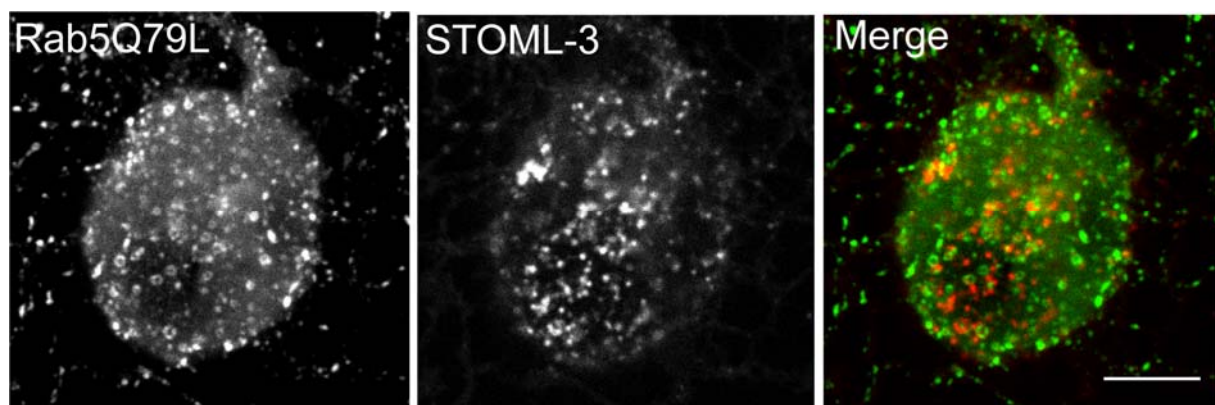
Figure 19. STOML-3 does not localise to the early endosomal compartment.
DRG neuronal cultures were co-transfected with mCherry-labeled STOML-3 and EGFP-labeled Rab5Q79L, two channel confocal images were acquired and analysed for co-localisation. The constitutively active Rab5Q79L mutant produces significantly enlarged endosomes compared to the wild type Rab5. Thus, localisation of STOML-3 to Rab5 early endosomal compartment would result in enlargement of STOML-3 positive vesicles. No changes in STOML-3 vesicle size or double labelling with the proteins were observed. Scale bar – 10μm.

It has been shown that Rab13 is involved in regulation of protein trafficking between the trans-Golgi network (TGN) and recycling endosomes (RE) in polarised epithelial cells. Overexpression of Rab13 mutant forms inhibits the delivery of proteins sorted through RE to the cell surface (Nokes et al, 2008). In MDCK cells Rab13 plays an important role in formation and integrity of tight junctions by recruiting protein components to junctional complexes (Marzesco et al, 2002; Marzesco & Zahraoui, 2005; Yamamoto et al, 2003). It has also been demonstrated that Rab13 is upregulated during regeneration of neuronal processes and involved in neurite outgrowth in PC12 cells (Sakane et al, 2010), most probably by

delivering adhesion molecules to the growing tips of the neurites. In order to verify if STOML-3 localised in Rab13 positive endosomes, double transfections with fluorescent protein-tagged STOML-3 and Rab13 were carried out. Two channel images of PFA fixed DRG neurones were acquired and analysed for co-localisation. The distribution of Rab13 in DRG neurones was predominantly membrane-associated, with a small number of vesicles although these were different from the vesicles containing STOML-3 (**Figure 20**). Thus, STOML-3 positive vesicular pool is different from Rab13 endosomes (data from 8 cells)
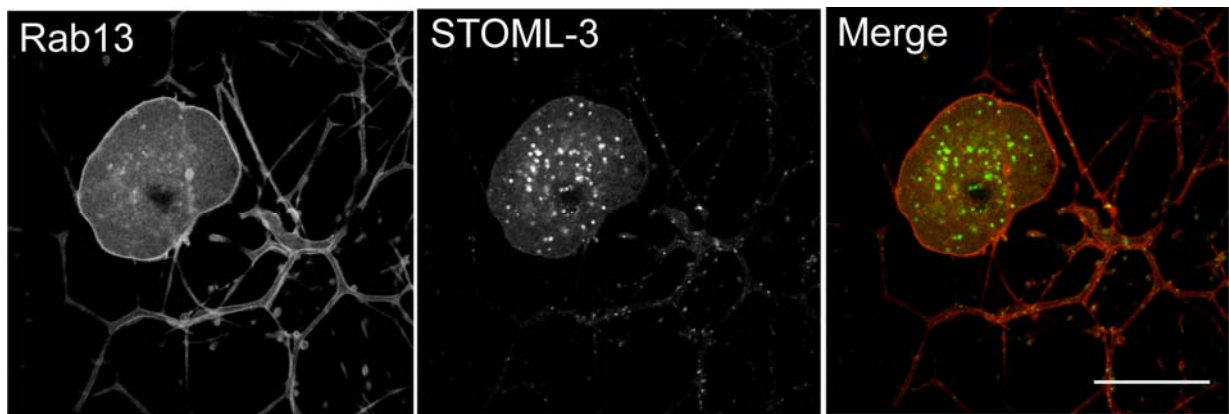
Figure 20. The STOML-3 vesicular compartment is different from Rab13 positive endosomes.
Double transfection of DRG neurones with STOML3-EGFP and Rab13-mCherry constructs revealed a distinct localisation pattern of the protein, where STOML-3 was localised to the characteristic vesicular pool and Rab13 demonstrated a predominantly plasma membrane-bound state. Scale bar – 20μm.

Rab14 is known to be localised to biosynthetic (notably ER, Golgi and Trans-Golgi network), as well as endosomal, compartments and regulates the transport of carrier membranes between these two compartments (Junutula et al, 2004; Proikas-Cezanne et al, 2006). It has also been shown that the protein is involved in regulation of apical protein targeting in polarised MDCK cells (Kitt et al, 2008). Co-transfection of DRG neurones with STOML-3 and Rab14 constructs demonstrated no apparent co-localisation in the vesicular compartment (data from 20 cells, 2 independent transfections) (**Figure 21**).
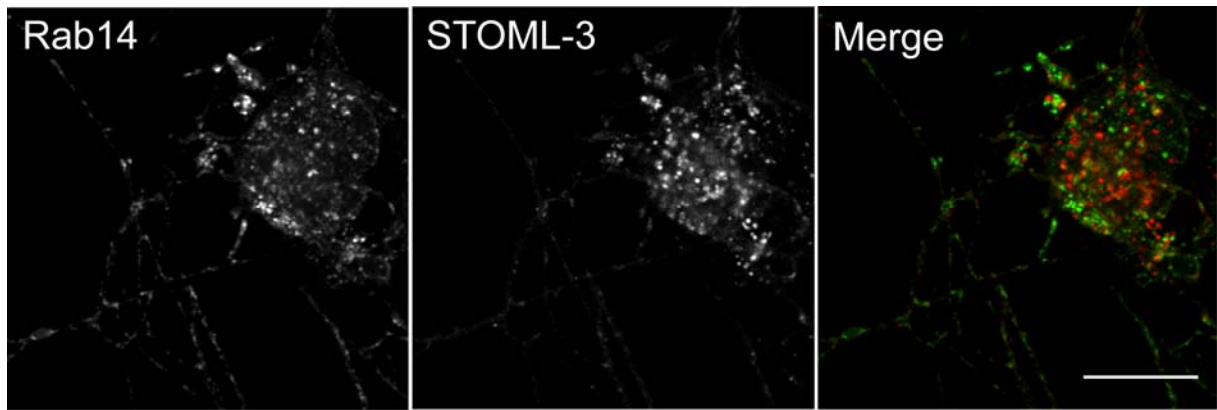
Figure 21. The STOML-3 protein is localised to a different compartment than the Rab14 positive endosomal compartment.
Analyses of confocal images of DRG neurones transfected with STOML3-mCherry together with Rab14-EGFP demonstrated the localisation of the proteins into distinct non-overlapping compartments. Scale bar – 15μm.

The Rab11 family of small monomeric GTPases are known to be involved not only in endocytic membrane trafficking, but also in the regulation of other membrane transport pathways. The Rab11 protein family consists of three members: Rab11a, Rab11b, Rab25 (Goldenring et al, 2001, 1993). Rab11a regulates protein recycling from endosomes back to plasma membrane and is enriched in the tubular-vesicular compartment, known as recycling endosomes and plays an important role in sorting and targeting of proteins during cell polarisation, outgrowth and motility (Apodaca et al, 1994; Ren et al, 1998a; Ullrich et al, 1996a). In addition, Rab11a is known to be associated with post-Golgi membranes, including the trans-Golgi network (Schwartz et al, 2007; Ullrich et al, 1996a). Thus, overexpression of a dominant negative Rab11 mutant (Rab11S25S) leads to inhibition of transporting, recycling and sorting of different membrane proteins and their accumulation in the perinuclear region (Cayouette et al, 2010; Ren et al, 1998b; Schlierf et al, 2000; Ullrich et al, 1996b). A number of studies have shown a role of Rab11 GTPase in the transport and targeting of different membrane proteins in neurones, such as AMPA receptors in dendrites (Brown et al, 2007; Correia et al, 2008; Lisé et al, 2006; Park et al, 2004; Wang et al, 2008), axonal trafficking of Trk receptors (Ascaño et al, 2009) , integrins and other adhesion molecules during axonal growth (Eva et al, 2010; Kamiguchi & Lemmon, 2000).

DRG neurones were co-transfected with STOML-3 and Rab11 constructs. Pronounced co-localisation of these two proteins was observed in the same vesicles along a neurite "tree" (nsfections) (**Figure 22a**). To investigate this further, I over-expressed a dominant-negative mutant of Rab11 (S25N) and a constitutively active Rab11 (Q70L) form together with STOML-3 construct. The dominant-negative S25N mutant led to an accumulation of STOML-3 in the cell body and a visible reduction in trafficking of STOML3 positive vesicles

(data from 17 cells, 3 transfections) (**Figure 22b**). In comparison with S25N mutant, the constitutively active form Q70L demonstrated pronounced co-localization with STOML-3 in characteristic enlarged vesicles in DRG neurone axons (data from 15 cells, 2 independent transfections) (**Figure 22c**).
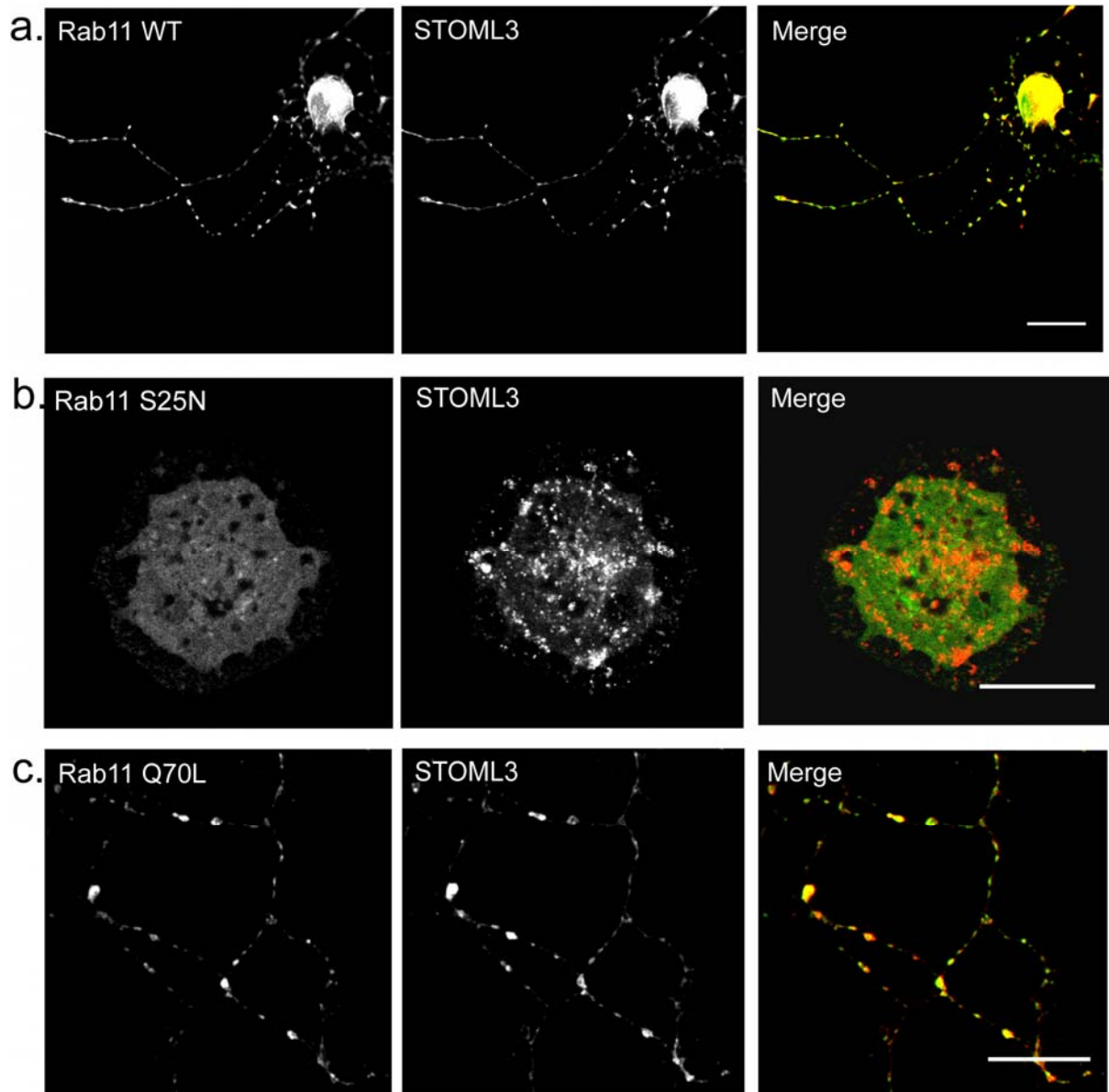
Figure 22. STOML-3 is localised to the Rab11 positive endosomal compartment.
Acutely prepared DRG cultures were transfected with the STOML-3-mCherry construct and one of the Rab11-EGFP constructs (WT, Q70L, S25N); confocal images of fixed cells were analysed for co-localisation. **(a)** More than a half of STOML-3 vesicle pool was Rab11a positive (upper row; scale bar – 40μm). **(b)** Co-expression of STOML-3 and Rab11aS25N (non-membrane-associated dominant-negative mutant) led to accumulation of STOML-3 positive vesicles in neurone cell bodies and a significant decrease of vesicle number in neurites (middle row; 20μm). **(c)** Overexpression of the constitutively active mutant Rab11Q70L resulted in enlargement of STOML3/Rab11Q70L double positive endosomes (bottom row; 15μm); redistribution of STOML-3 vesicles was similar with one in case of the wild type Rab11 protein co-expression.

3.1.2.5 Membrane dynamics of STOML-3.

To address the question of STOML-3 dynamics more directly, the internalisation pattern of the protein was surveyed using fluorescently labelled Wheat Germ Agglutinin (WGA) as a tool for endocytosis visualisation. Wheat germ agglutinin is a carbohydrate-binding protein that selectively recognises the sugar residues N-acetylglucosamine and N-acetylneuraminic acid (sialic acid), which are predominantly found on externally exposed plasma membrane proteins. Thus, application of fluorescent WGA allows cell surface labelling in a non-specific manner. To follow the dynamics of membrane-localised STOML-3, DRG neuronal cell cultures, transfected with the fluorescently tagged STOML-3 protein, were pulse-labelled with WGA and then visualised 60, 90 and 120 minutes after the start of the incubation. No major overlap between STOML-3 positive vesicles and WGA containing endocytic vesicles was observed (**Figure 23**). Nevertheless, a partial co-localisation between STOML-3 and WGA vesicular pools was detected. This co-localisation was significantly reduced with longer incubation times, which can be explained by the tendency of WGA to accumulate in the trans-Golgi network (TGN) (Raub et al, 1990), as well as by the recycling of vesicular content. For the control experiment triple labelling of the identically treated DRG neuronal culture was performed. A marker of the early endosomal compartment - EE1 was largely colocalised with the WGA-AlexaFlour containing vesicles at all points of incubation (**Figure 23**).
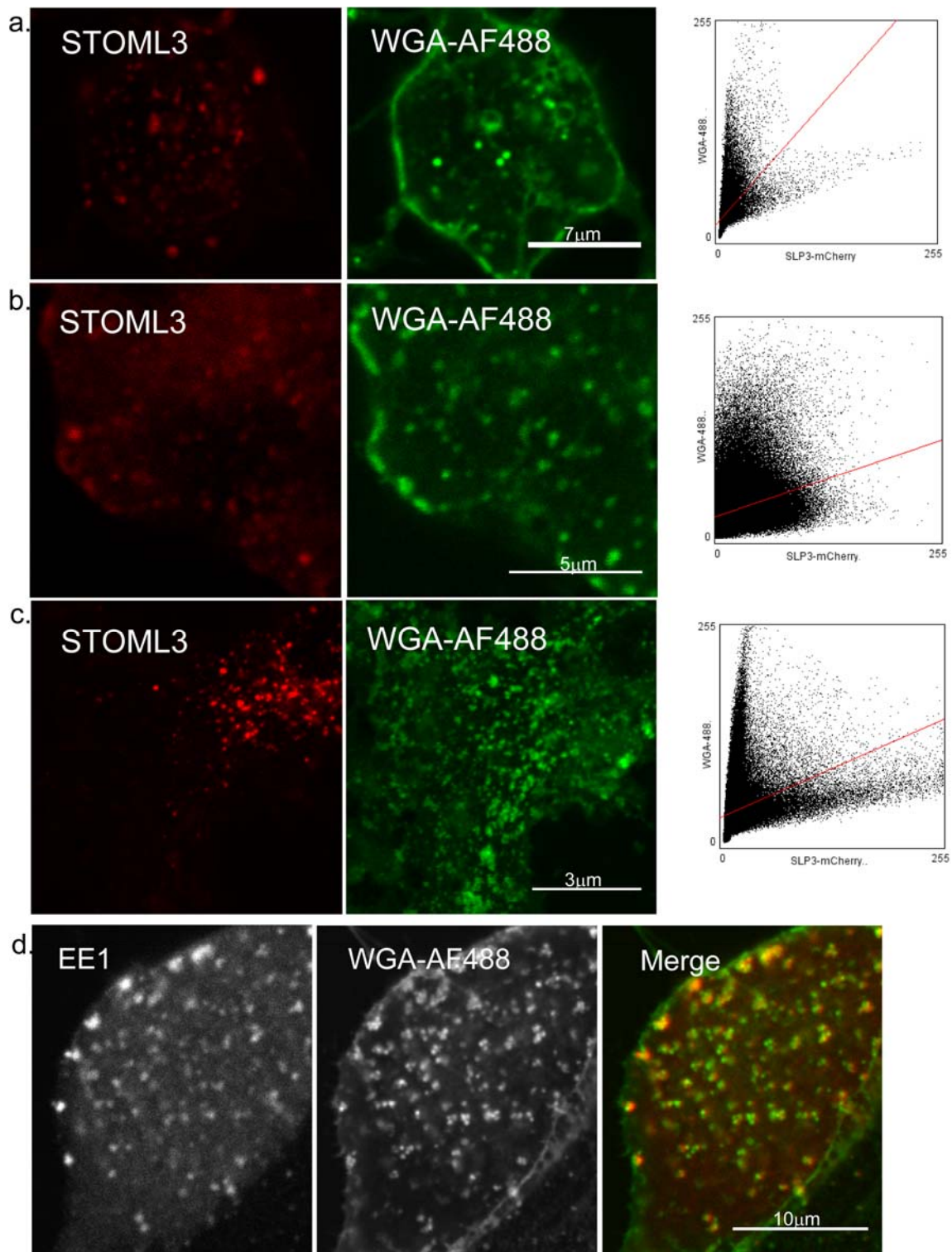
Figure 23. A small proportion of STOML-3 undergoes internalisation through early endosomes over time.

STOML3-mCherry transfected DRG neurones were labelled with WGA-488 for 60, 90 and 120 min., fixed and imaged using confocal scanning microscope. The results of co-localization analyses for all three time points are displayed as pixel distribution diagrams (right column).

In a control experiment (lower row), EE1-mCherry transfected DRG neurones were incubated for 90 min with WGA-488 and imaged using a confocal microscope after fixation. Early endosomal marker -1 was localised to the majority of WGA labeled vesicles (data from 4 labeling experiments).

3.1.3 STOML-3 interaction partners.

3.1.3.1 Different members of the stomatin family co-localised to the STOML-3 vesicular pool and interact with each other.

The stomatin family of proteins in mammals is represented by five proteins, which share 40 to 84% sequence similarity in the stomatin-domain and have a similar membrane topology and primary domain organisation (Lapatsina et al, 2011). It is known that different members of the family can form higher-order oligomers (Snyers et al, 1999b, 1998), but it is not clear if different family members can oligomerise with each other, forming hetero-oligomeric complexes. Using Western blot analysis I could demonstrate, that different stomatin family members immunoprecipitate with each other, and can, thus, potentially interact with each other and form hetero-oligomeric complexes (**Figure 24**).
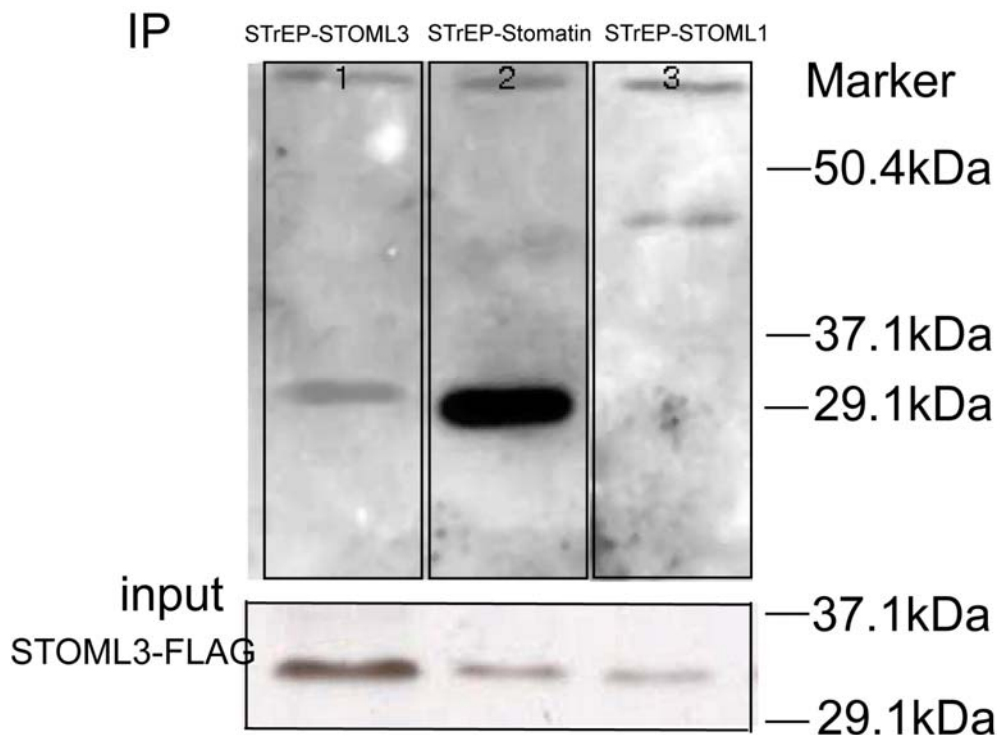
Figure 24. Stomatin and STOML-1 interact and can be precipitated together with STOML-3.
FLAG-STOML3 was transfected together with STrEP-STOML-3, STrEP-Stomatin or STrEP-STOML1 constructs into HEK293 cells. After 24 hours cells were collected and total protein extract was prepared for immunoprecipitation of the proteins using an antibody directed against the FLAG tag. Input – total protein, immuno-blot against FLAG-tagged STOML-3. Lane1 – STrEP-STOML-3 (~35kDa), lane2 – STrEP-Stomatin (~34,4kDa), lane3 – STrEP-STOML-1 (~46kDa); immuno-blot against STrEP-tag.

To examine live distribution of several close STOML-3 relatives, DRG neurones were co-transfected with plasmids encoding fluorescently labelled family members and the level of co-localisation was analysed. The highest degree of co-localisation was observed for the protein most similar to STOML-3, stomatin (>80%), overlap coefficient: r=0.94, Pearson's

coefficient: r=0.919 (**Figure 25a**). A lower level of co-localisation was observed in the case of STOML-1, which is less similar to STOML-3 (about 60%) than stomatin, overlap coefficient: r=0.598, Pearson's coefficient: r=0.439 (**Figure 25b**).
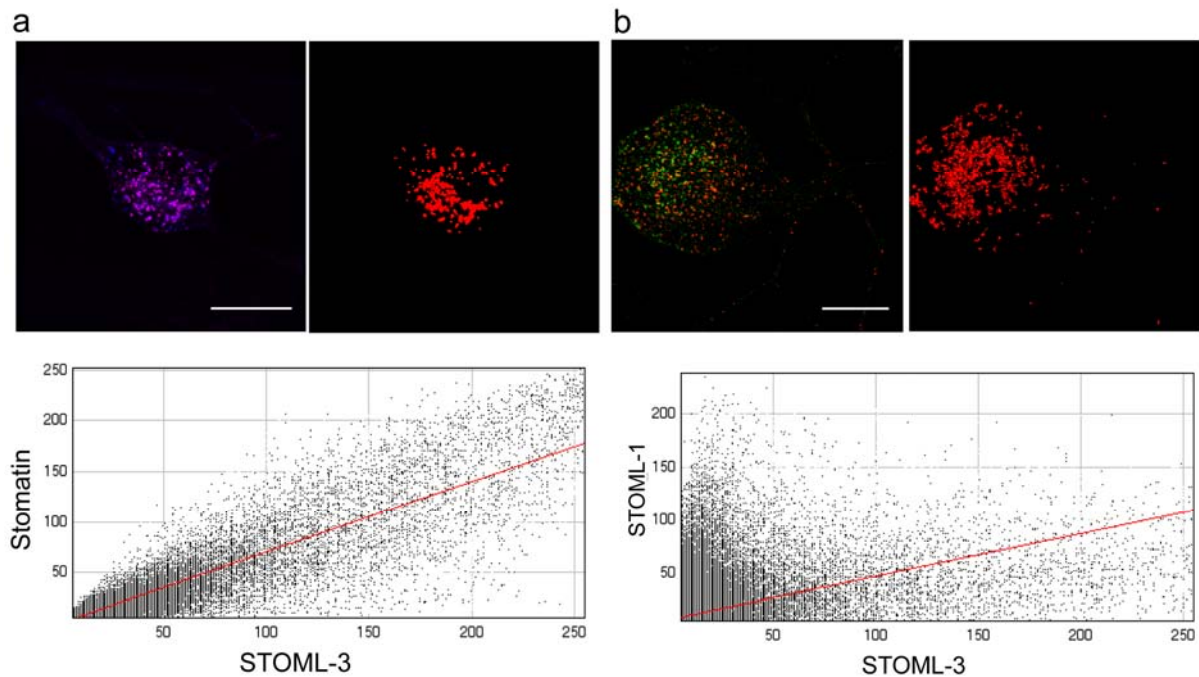
Figure 25. STOML-3 interacts with other members of the stomatin family of proteins; the extent of co-localisation correlates with the degree of similarity of the proteins analysed.

STOML3-mCherry and Stomatin-pAmCyan or EGFP-STOML1, were co-transfected into DRG neurones and the co-localisation rate was analysed using a package of ImageJ plug-ins (JACoP). Co-localisation analysis between Stomatin/STOML-3 (data from 3 co-transfection experiments for each stomatin protein) **(a)** and between STOML-1/ STOML-3 **(b)**. Left **a,b** images – an overlay of two separate confocal acquisition images, bars are 20μm; right **a,b** images – co-localisation mask based on distance between centres of mass calculated for two channels; bottom **a,b** graphs - pixel distribution diagram illustrating the result of co-localisation analyses (graph axes – grey value)

No apparent co-localisation was observed while co-expressing STOML-3 with Flotillin-1 and Flotillin-2, proteins, which like stomatins belong to the SPFH family (**Figure 26**).
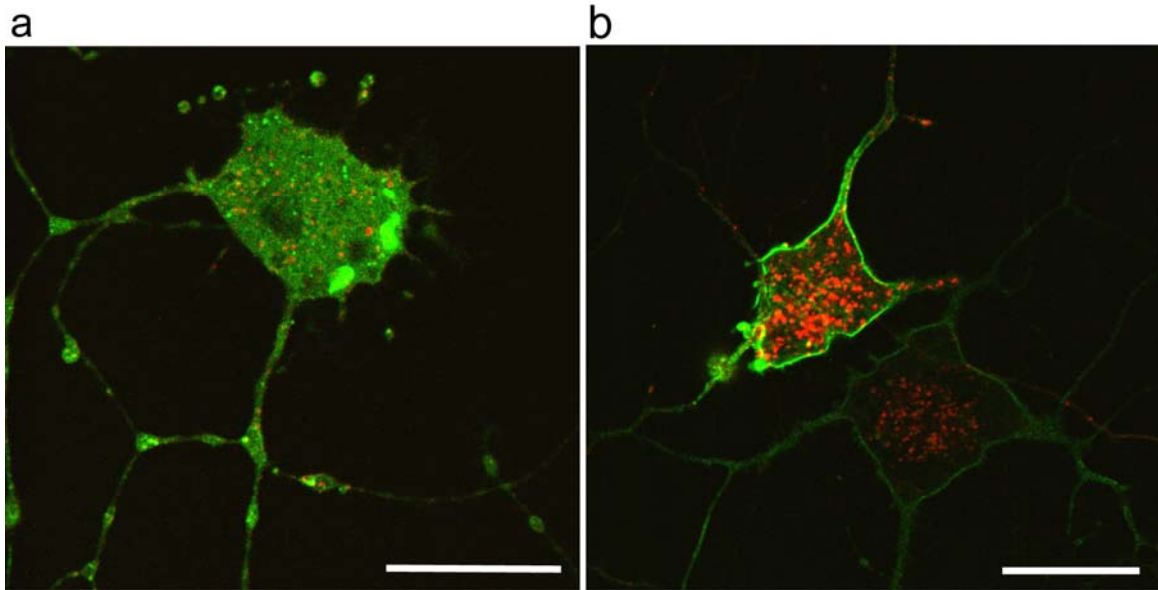
Figure 26. STOML-3 does not co-localise with Flotilin-1 and Flotilin-2 proteins.
Co-transfected DRG neurones were analysed for co-localisation between STOML3-EGFP and Flotillin1-mCherry **(a)** and between STOML3-mCherry and Flotillin2-EGFP **(b)**. No apparent co-localisation was observed in both cases. Scale bars – 25μm.

3.1.3.2 ASIC2a and ASIC3 are localised to the STOML-3-positive vesicular compartment.

Stomatin family members are known to interact with and modulate functions of different ASIC subunits (Price et al, 2004). In *C.elegans*, MEC4/10 (homologous to mammalian ASIC channels) and MEC-2 (close homolog of STOML-3 from *C.elegans*) form the core component of the mechanotransducing machinery. Thus, I asked if ASIC subunits localise to the STOML-3-positive vesicular compartment.

Cultures of primary DRG neurones were transfected with the *STOML-3-mCherry* construct together with *ASIC2a-EGFP* or *ASIC3-EGFP* and analysed using a confocal microscope. Analyses of two-channel images demonstrated obvious co-localisation of STOML-3 and ASIC fluorescent signals in the vesicular compartment (**Figure 27a and b**).
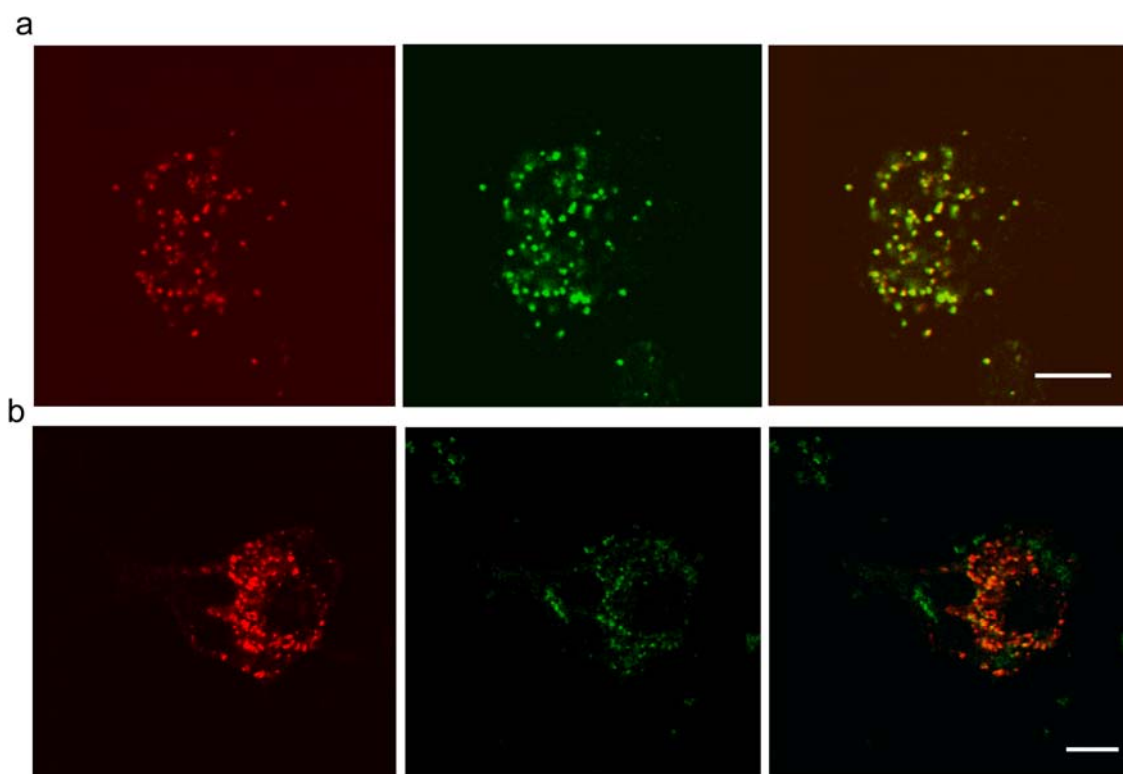
Figure 27. ASIC subunits localise to STOML-3-positive vesicles.

Primary cultures of DRG neurones were transfected with STOML-3-mCherry together with EGFP constructs of either ASIC2a or ASIC3, dual-colour images of the transfected cells were acquired and analysed for co-localisation. Both channels demonstrated obvious co-localisation with STOML-3 in the vesicular compartment. **(a)** STOML-3-mCherry/ASIC2a-EGFP; **(b)** STOML-3-mCherry/ASIC3-EGFP. Data from two independent transfections for each ASIC subunit, bars – 10μm.

### 3.1.3.3 OneSTrEP tag – streptavidin based purification of STOML-3 binding partners from a stably expressing HEK293 cell line.

To test the feasibility of membrane protein complex purification using the OneSTrEP tag / streptavidin system, a HEK293 cell line stably expressing STOML-3-OneSTrEP construct was established. Three to five 15cm confluent dishes were used for each preparation of total cell protein and subsequent purification using streptactin-containing affinity columns was conducted as described in the Materials and Methods. The purified proteins were separated on SDS gels and protein bands were visualised using the Imperial™ Protein Stain (Pierce) according to the manufacturer's protocol. For LC/MS/MS analysis (liquid chromatography–mass spectrometry), the whole SDS-gel was sliced into 22 parts, proteins from every individual slice were extracted and digested with trypsin. The mass-spec analysis identified a number of proteins which co-purified with STOML-3 (see the full list in the **Appendix**). Known interaction partners endogenously expressed in the HEK293 cell line (e.g. stomatin and prohibitin) were found (**Figure 28**). Thus, this result supported the idea, that the STrEP-tag can be successfully used for purification of protein complexes from animal tissues. A

number of proteins identified, e.g. Rab proteins, were cloned and used for co-localisation studies described above.
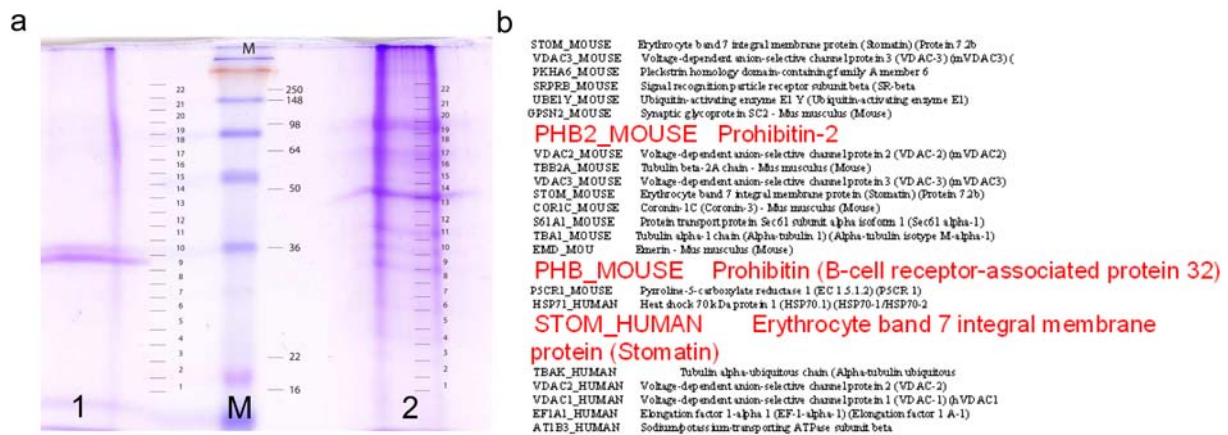

Figure 28. A number of proteins were co-purified from a HEK293 cell line together with OneSTrEP-STOML3.

A total protein extract from a HEK293 cell line stably expressing OneSTrEP-STOML3 construct was used for purification of STOML-3 interacting proteins using streptavidin columns. The purified proteins were separated on a SDS gel and LC/MS/MS analysed. **(a)**. SDS gel; line 1 – non-transfected HEK293 cell line (negative control), M – protein marker, 2 – protein co-purified with STOML-3. **(b)**. List of detected proteins; proteins known to be interaction partners of STOML-3 are marked in red.

3.1.3.4 Detection of OneSTrEP-STOML-3 protein expression in mouse tissues.

Our working hypothesis was that the STrEP-tag modified STOML-3 protein can be expressed in the mouse and subsequently detected in a total protein using Western Blot and thus, could be used for endogenous protein purification from animal tissues. To test this concept, three adult *Stoml-3^STrEP* mice were sacrificed and DRG, as well as sciatic nerves, were taken for total protein preparation as described in the Materials and Methods. Material obtained was separated on a 10% SDS gel and blotted on a nitrocellulose membrane. For STrEP-STOML-3 protein detection, HRP-labelled streptactin, as well as an HRP-conjugated anti-OneSTrEP antibody, were used. A band corresponding to the size of STOML-3 can be detected in the protein sample from the *Stoml-3^STrEP* animal; at the same time only weak background signal is detected in the control wild type sample (**Figure 29a**). Protein preparation using more harsh lysis and solubilisation conditions (e.g. 9M Urea containing buffer) resulted in a substantial increase in the Western Blot signal, which could be explained by epitope masking due to protein oligomerisation (**Figure 29b**). Thus, further optimisation of protein solubilisation methodology is necessary prior to actual purification of protein complexes using the *in vivo* OneSTrEP tag.
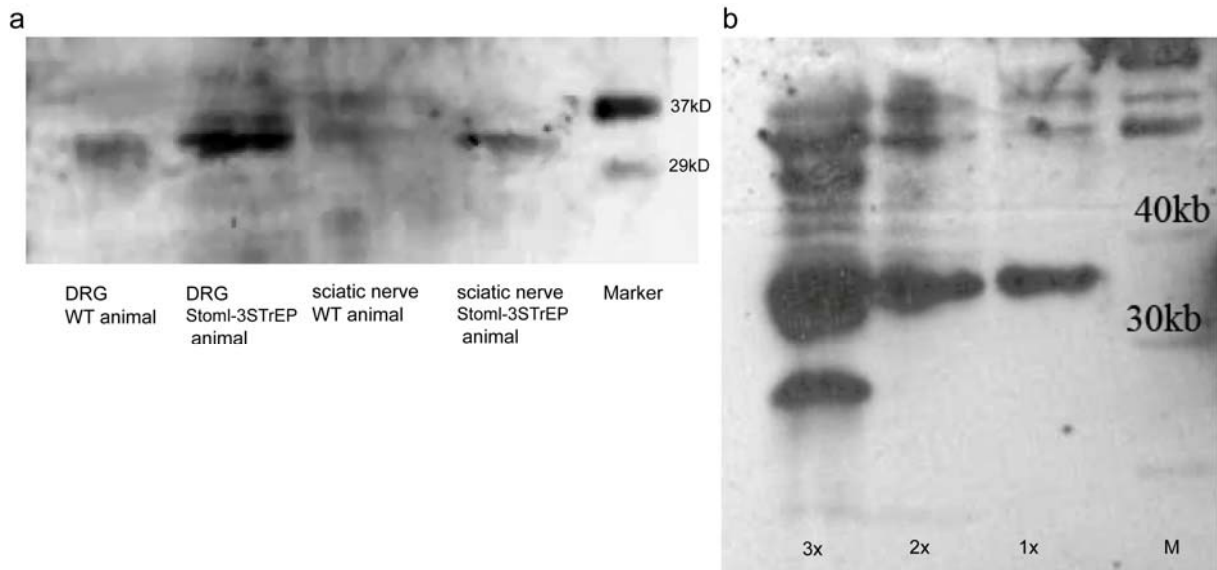
Figure 29. STOML-3 protein can be detected in the tissue protein extracts from Stoml-3^STrEP animals using an antibody directed against the STrEP-tag.

a. Dorsal root ganglia and sciatic nerve protein extracts were prepared from *Stoml-3^STrEP* and C57BL/6j mice and analysed with Western blot. The antibody directed against the STrEP tag detected a ~31kb protein band in separated protein extracts from the *Stoml-3^STrEP* mice, no signal was detected in case of C57BL/6j animals. **b.** Total protein extract was prepared from sciatic nerves of two *Stoml-3^STrEP* mice using 9M urea-containing buffer. Three different volumes of the sample (7, 14 and 21μl) were separated on the SDS-gel, antibody directed against OneSTrEP-tag recognised protein bands of expected size (~31kD).

3.2. Generation of STOML-3 knock-in mice.

3.2.1 Generation of *Stoml-3*^{LacZ} , *Stoml-3*^{Tm} and *Stoml-3*^{OneSTrEP} mice.

3.2.1.1 Conditional knock-out of the mouse *Stoml-3* gene.

To generate a targeted allele of *Stoml-3* the first exon of the gene was floxed with two *LoxP* sites using the recombineering-based method, which is described in detail in the Materials and Methods. Recombination between introduced *LoxP* sites, that could be achieved by crossing *Stoml-3*^{Tm} mice with *Cre* expressing mouse line, produces a frameshift mutation in the *Stoml-3* open reading frame and ablates the gene completely (**Figure 30**).
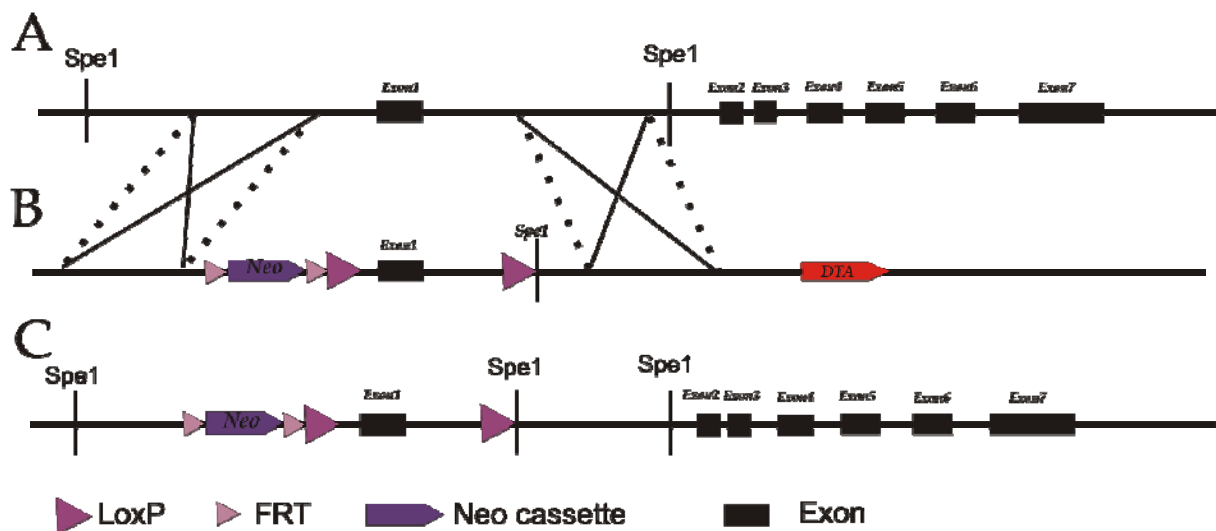
Figure 30. Graphical scheme of the stoml-3 conditional targeting strategy.
(a) wild-type *stoml-3* locus; **(b)** linearised conditional targeting vector, containing floxed first exon of *stoml-3* gene, positive (neomycin phosphotransferase II) and negative (*Diphtheria toxin* A fragment DT-A) selection markers; **(c)** recombinant allele.

The great advantage of making a conditional gene knock-out is the opportunity to "switch off" the gene of interest either in a temporal or spatial manner. Thus, by analysing animals where *Stoml-3* was ablated only in the peripheral nervous system, we would be able to separate central and peripheral impacts of *Stoml-3* deletion on mechanosensation and achieve more precise characterisation of the mutant phenotype reported before (Wetzel et al, 2007). For neuronal-specific deletion for breeding with *Stoml-3*^{Tm}, the *Isl*^{Cre} mouse line was used (Srinivas et al, 2001).

3.2.1.2 Generation of β-galactosidase expressing reporter line.

Bacterial β-galactosidase gene (*LacZ*) is a powerful tool for detection of *cis*-acting regulatory sequence activity. Once introduced under the promoter of the gene of interest, the endogenous pattern of expression and the time point in development when this gene is initially expressed could be deduced using an enzymatic reaction.

To create a reporter allele of the *Stoml-3* gene, the first exon of the gene was replaced with a β-galactosidase coding sequence. The gene promoter and regulatory elements were preserved (**Figure 31**). Due to this insertion inducing a frameshift mutation, no truncated STOML-3 protein is expected to be synthesised.
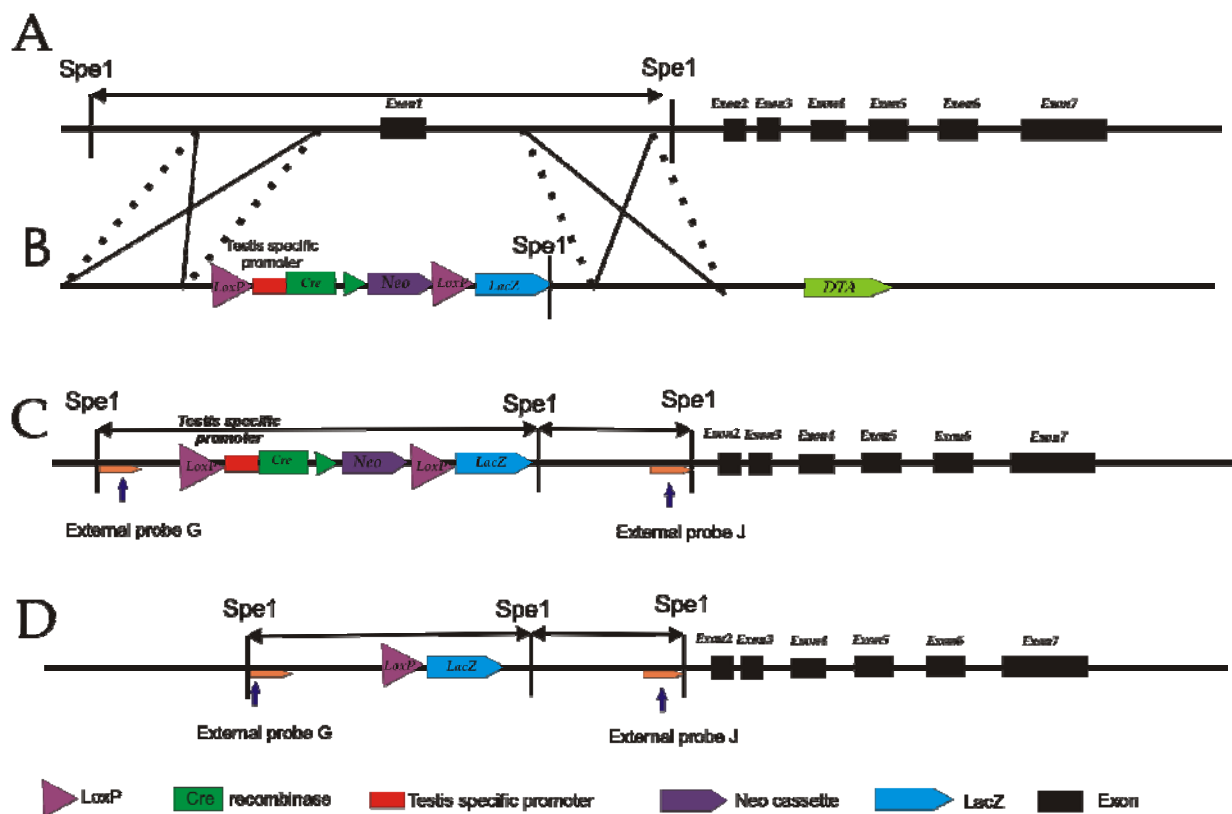
Figure 31. Graphical scheme of stoml-3-reporter line construction.

(a) wild-type *stoml-3* locus; **(b)** linearised targeting vector**,** containing the β-galactosidase coding sequence, positive (neomycin phosphotransferase II) selection marker floxed together with Cre-recombinase gene under the testes-specific promoter, and negative selection marker (*Diphtheria toxin* A fragment DT-A); **(c)** recombinant allele in ES-cells; **(d)** recombinant allele in mice (Neo-cassette and Cre-recombinase gene were excised upon activation of Cre expression in the mouse testes).

3.2.1.3 Generation of the *Stoml-3^STrEP* knock-in mouse line.

The coding sequence of the *Stoml-3* gene was analysed and the OneSTrEP tag sequence was inserted into the open reading frame at the 5'-end of the gene immediately after the start codon (**Figure 32**) using a recombineering-based method in E. coli (*Escherichia coli*) (Copeland et al, 2001; Liu et al, 2003). The endogenous *Stoml-3* promoter, as well as the *5'-UTR* sequence were preserved, thus ensuring normal mRNA processing and endogenous expression level of the modified protein.
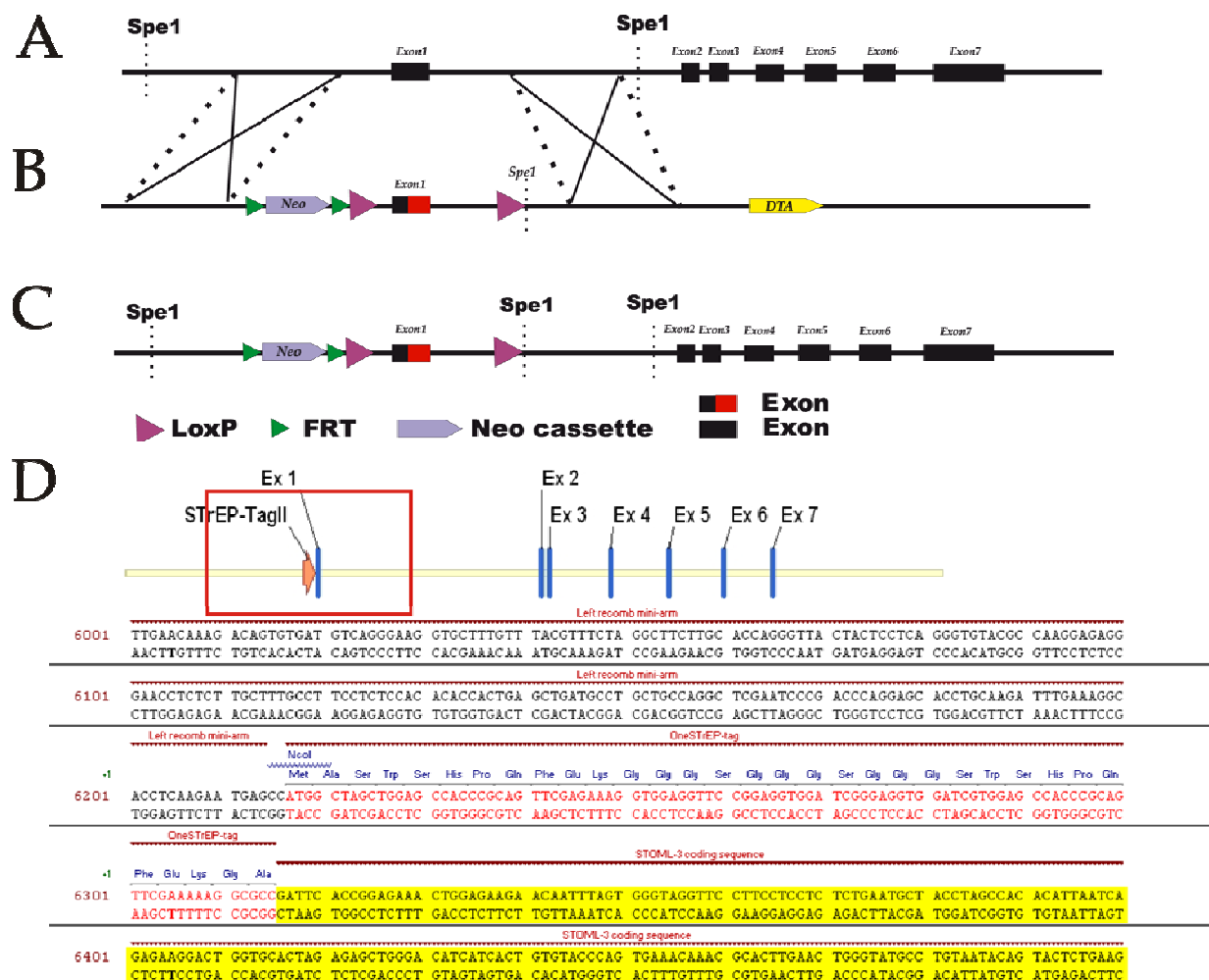
Figure 32. Scheme of Stoml-3^STrEP knock-in mouse line construction.
(a) wild-type *stoml-3* locus; **(b)** linearised targeting vector, containing OneSTrEP-modified first exon of the gene, positive (neomycin phosphotransferase II) and negative (*Diphtheria toxin* A fragment DT-A) selection markers; **(c)** recombinant allele; **(d)** tag-modified sequence of the first *stoml-3* exon.

To verify accurate recombination and the presence of the relatively small for the Southern blot detection tag, mice were first genotyped by Southern Blot analysis of SpeI digested genomic DNA (**Figure 33a**). After this, several positive animals were used to prepare cDNA

from DRGs with subsequent sequencing of 5' end of the *Stoml-3* gene in order to demonstrate the presence of an mRNA product containing the *OneSTrEP* tag sequence (**Figure 33b**).
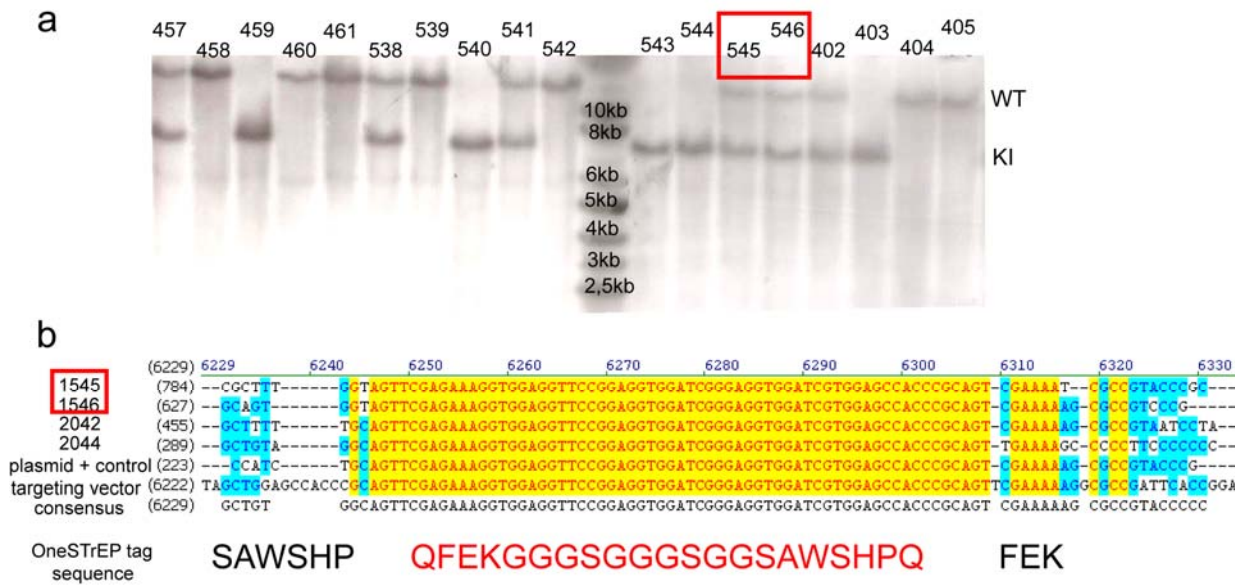
Figure 33. Verification of correct targeting.
(a) an example of *Stoml-3^STrEP* generated animal genotyping using Southern-blot analysis; **(b)** verification of OneSTrEP-tag presence in the generated mouse line. cDNA from two hetero- (1545, 1546) and two homozygote (2042, 2044) mice was sequenced using a primer that binds in the 5' end of the STrEP-tag sequence. As a positive control, the initial targeting vector and the original commercially available plasmid containing the STrEP-tag were used.

3.2.1.4 Verification of normal mechanosensitivity in *Stoml-3^STrEP* knock-in mice.

Even slight manipulation within coding or regulatory sequences of a gene can hinder processing, trafficking and entire protein function. Thus in order to verify whether the *Stoml-3^STrEP* knock-in mice display a normal sensitivity of sensory afferents in the skin, the electrical search protocol (Wetzel et al, 2007) was applied to 34 single fibres derived from 4 adult (>6 weeks) animals (*Stoml-3STrEP* hybrid strain, *C57Bl6* and *sv129* cross). 33 single fibres obtained from 4 wild-type animals (hybrid strain) were examined in the same way. No difference in the proportion of mechanosensitive fibres was observed among the *Stoml-3^STrEP* animals (**Figure 34a**). Experiments carried out in collaboration with Jan Walcher in the lab.
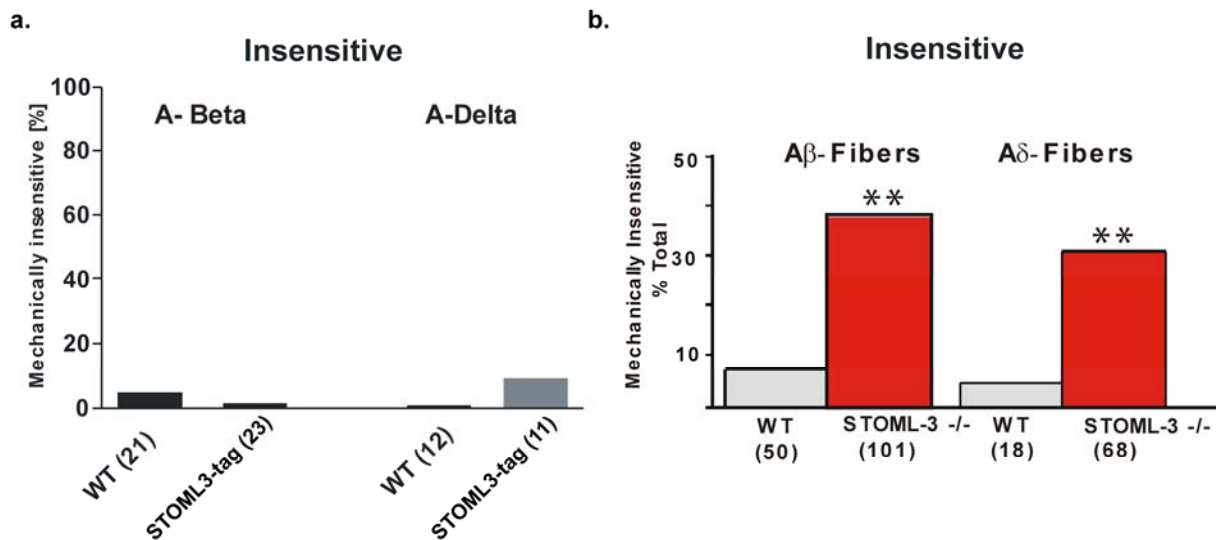
Figure 34. Stoml-3^{STrEP} knock-in mice have normal proportion of mechanosensitive A-beta and A-delta fibres.

(a) analyzed *Stoml-3^{STrEP}* animals have no difference in the proportion of mechanosensitive fibres, **(b) modified from Wetzel et al**. about 35% of mechanosensitive fibres do not respond to mechanical stimuli in STOML-3 null animals

3.2.2 Characterisation of the STOML-3 *in vivo* expression pattern using transgenic mice.

Stomatin like protein-3 (STOML-3) was first identified as an olfactory epithelium specific protein with unknown function (Kobayakawa et al., 2002). STOML-3 shares about 77% of protein sequence similarity with *C. elegans* MEC-2, which is known to play an important role in the formation of mechanosensitive complexes in mechanosensory neurones in *C. elegans* (Huang and Chalfie, 1994; Zhang et al., 2004). This high similarity prompted us to investigate further possible functions of STOML-3. Using RT-PCR and *in-situ* hybridizations we found that the protein is more widely expressed than was initially reported, with a significant level in DRG neurones. In our laboratory we were able to demonstrate that about 35% of skin mechanoreceptors do not respond to mechanical stimuli in STOML-3 knock-out mice; tactile-driven behaviour was also significantly impaired in these animals (Wetzel et al., 2007).

To characterise the *in vivo* expression pattern of STOML-3, a histochemical analysis of *Stoml-3^{STrEP}* and *Stoml-3^{LacZ}* mouse tissues was performed.

3.2.2.1 Expression pattern of STOML-3 in Stoml-3^{LacZ} mouse embryos.

Monitoring of gene expression using serial sections from different tissues is both time consuming and labour intensive. At the same time, examination of a whole embryo can give directions in further histochemical analysis of sections. Moreover, analyses of embryonic expression of the protein provides valuable information about the timing of the onset of

expression and changes in level and/or pattern of expression. Thus, initially detection of the β-galactosidase (β-gal) activity in whole *Stoml-3^LacZ* embryos was performed. Mouse embryos (13-15dpc.) were collected from pregnant *Stoml-3^LacZ* mice and used for detection of the β-gal. expression pattern using the X-gal reaction. After staining, whole embryos were cleaned and visualised using bright field illumination. A blue to violet colour indicates the presence of the β-galactosidase and thereby endogenous activity of the *Stoml-3* promoter. In the case of *Stoml-3^LacZ* animals, X-gal staining never gave a robust signal apart from in the olfactory epithelium, where visible colouration normally developed within a few hours. This can be explained by a low level of STOML-3 expression in DRGs. The overall pattern of the X-gal staining in the reporter line embryos encompassed different neuronal tissues: the olfactory epithelium, DRGs and nerves innervating different parts of the body (**Figure 35 and 36**). Additionally, staining of embryos older than 15dpc revealed significant colouration of the developing bone skeleton (five pups from the same litter).
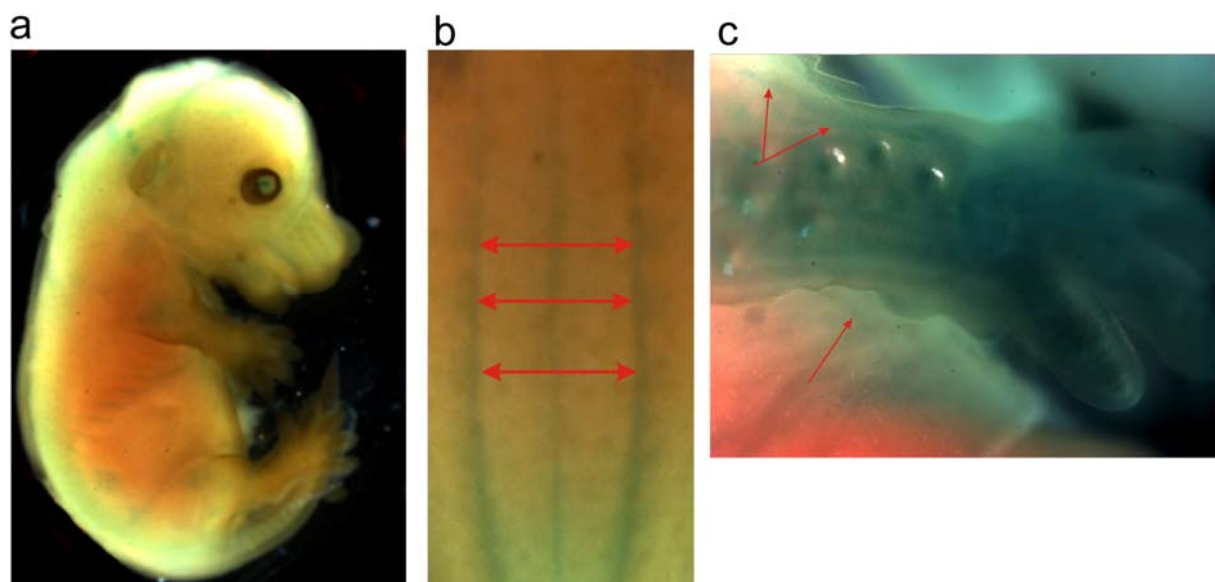
Figure 35. Expression pattern of STOML-3 in the mouse embryo.
15-16 day old embryos were collected from pregnant *Stoml-3^LacZ* mice, fixed and stained using X-gal. To make staining of internal organs more visible, embryos were cleaned in KOH/glycerol mixture prior to imaging. **(a)**. whole embryo stained with X-gal; **(b)** staining of DRG and spinal cord (dorsal view); **(c)** staining of the nerves innervating a forelimb. Staining of DRG and nerves marked with the red arrows.
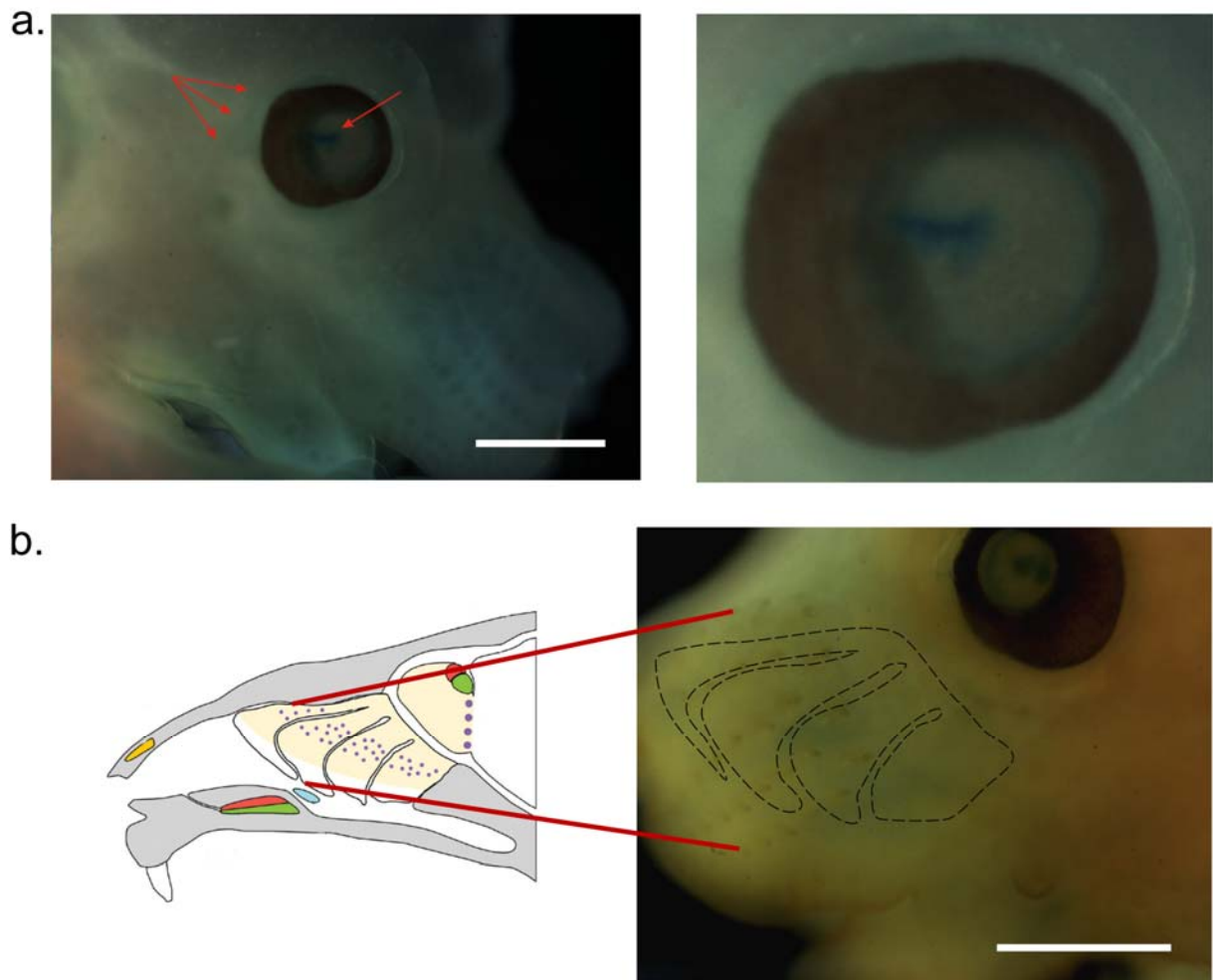
Figure 36. Expression of stoml-3 in different types of neuronal tissues.
(a) X-gal staining of the optic nerve from the *Stoml-3^{LacZ}* embryo. **(b)** expression of *stoml-3* in the olfactory epithelium of the *Stoml-3^{LacZ}* embryo, bar

3.2.2.2 Skeletal expression of the *stoml-3* gene.

Mammalian bone forms through two processes: endochondral and intramembranous ossification. Formation of the bone starts when terminal chondrocytes die at the end of so-called growth plates and their empty lacunae are invaded by cells involved in bone formation: osteoclasts, osteoblasts, endothelial cells, hematopoietic and stromal cells. During endochondral ossification, bone tissue is forming in the diaphysis of fetal long bones and these parts of the prospective bone skeleton are called primary ossification centres. In the mouse, terminal chondrocytes reach their maturation and are replaced by endochondral bone by E15.5. Secondary centres develop postnatally in the bone epiphysis. A characteristic feature of the intramembranous ossification is the condensation of skeletogenic cells into compact nodules. This process occurs at the sites of future skull bones and in the

perichondrium of growth plates at the level of prehypertrophic chondrocytes. The majority of the cells become osteoblastic and produce an organic matrix which is calcified through radial production of bony spicules from an ossification center.

Whole mount staining of embryos older than 15dpc. from *Stoml-3^LacZ* mice revealed development of prominent coloration of certain areas within the developing skeleton (**Figure 37a-d**). Characteristic patchy staining of the skull bones and central localisation of β-galactosidase positive cells in long bones, such as the humerus, tibia and scapula, indicate that the positive cells most probably belong to the bone-forming cell population, most likely to osteoblasts. Nevertheless, to confirm this hypothesis further histochemical analysis should be carried out.
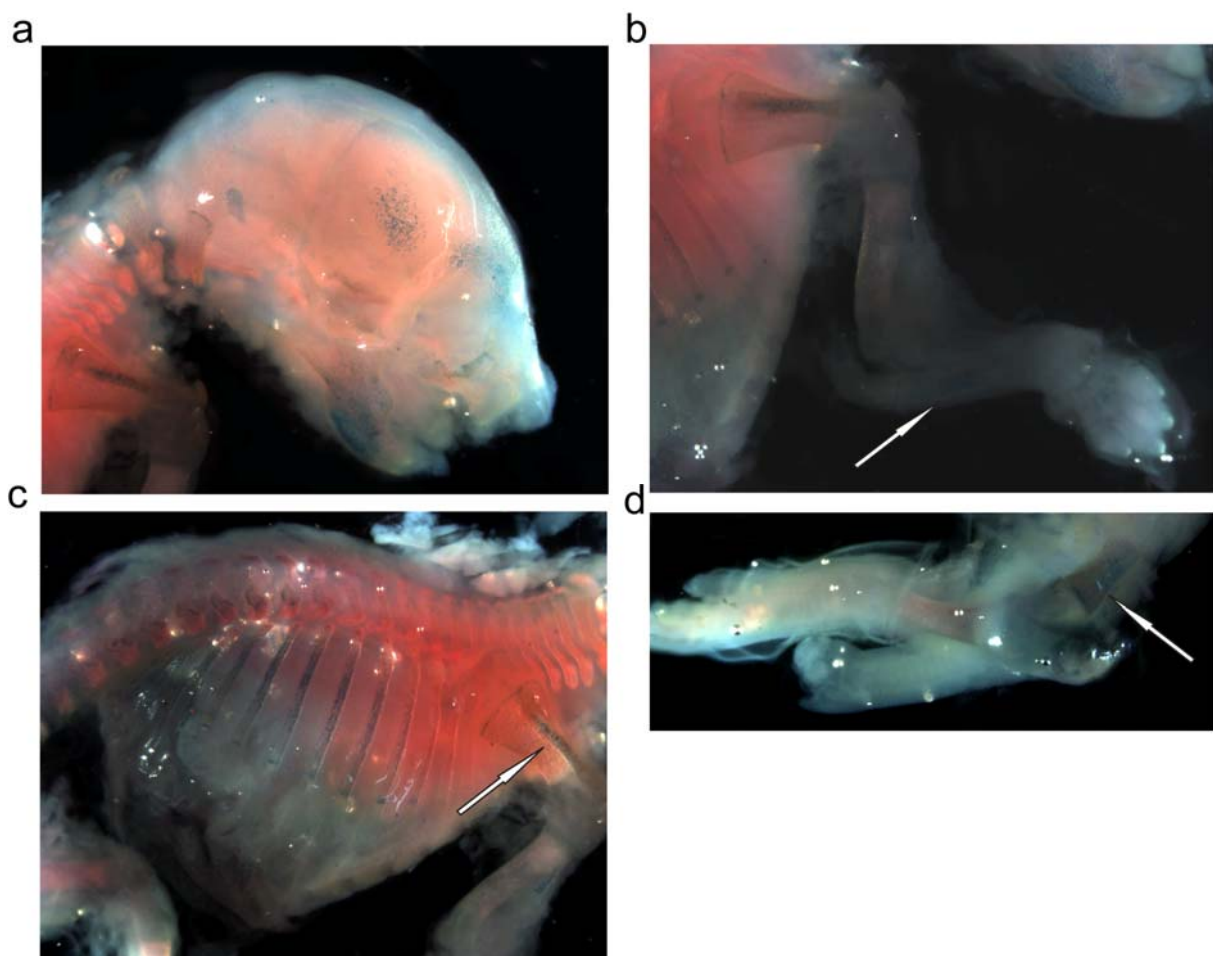
Figure 37. X-gal staining of developing bones in Stoml-3^LacZ embryos.

Embryos older than 15dpc. from *Stoml-3^LacZ* mice demonstrate prominent coloration of certain areas within the developing skeleton. **(a)** deskinned head of the mouse embryo with a prominent coloration of frontal, parietal bones and mandible; **(b)** a fore limb with stained scapula, humerus, radius and bones of forming metacarpus; **(c)** thoracal part of the embryo with a visible staining of ribs and forming vertebrae; **(d)** a hind limb with stained femur and tibia. Examples of X-gal positive ossification centres are marked with the white arrows

3.2.2.3 Histochemical and immunohistochemical analyses of the mouse olfactory system.

Adult olfactory epithelium is a pseudostratified epithelium composed of three main cell types arranged in a developmentally hierarchical manner atop a defined basal lamina, which separates the olfactory epithelium proper from its underlying lamina propria. The olfactory epithelium contains: basal cell progenitors, immature and mature olfactory neurones (ORNs) and sustentacular cells, olfactory neurones being the major cell type. The lamina propria contains axonal bundles, olfactory enscheating cells, connective tissue, blood vessels and Bowman's glands (**Figure 40a**). Each of these cell types can be distinguished topologically, morphologically, and by their distinct antigen expression profiles (Murdoch & Roskams, 2007). One of the most striking characteristics of the olfactory system is the constant substitution of old olfactory neurones with new, which have to find a pathway to a predefined glomerulus in the olfactory bulb and there form synapses with second-order projection neurones and interneurones with astonishing precision.

To conduct a more detailed characterisation of STOML-3 expression in the mouse olfactory system, tissue samples from *Stoml-3^{LacZ}* and *Stoml-3^{OneSTrEP}* mice were analysed using standard histochemical techniques. Adult mice were anesthetised and fixed by transcardiac perfusion of 4% PFA. Snouts were dissected and postfixed for 2 hours in 4% PFA. For X-gal staining snouts were dissected and nasal turbinates fixed for 30 minutes in 0,3% glutaraldehyde without preceding perfusion. Transverse sections of whole snouts or separate turbinate and olfactory bulbs were used for X-gal or antibody based staining of OneSTrEP-tagged STOML-3. Both approaches revealed robust expression of STOML-3 in the olfactory epithelium and a moderate level of expression within the glomerular level in the olfactory bulb (**Figure 38 and 39**). Four adunt *Stoml-3^{LacZ}* animals were used for olfactory epithelium analise.
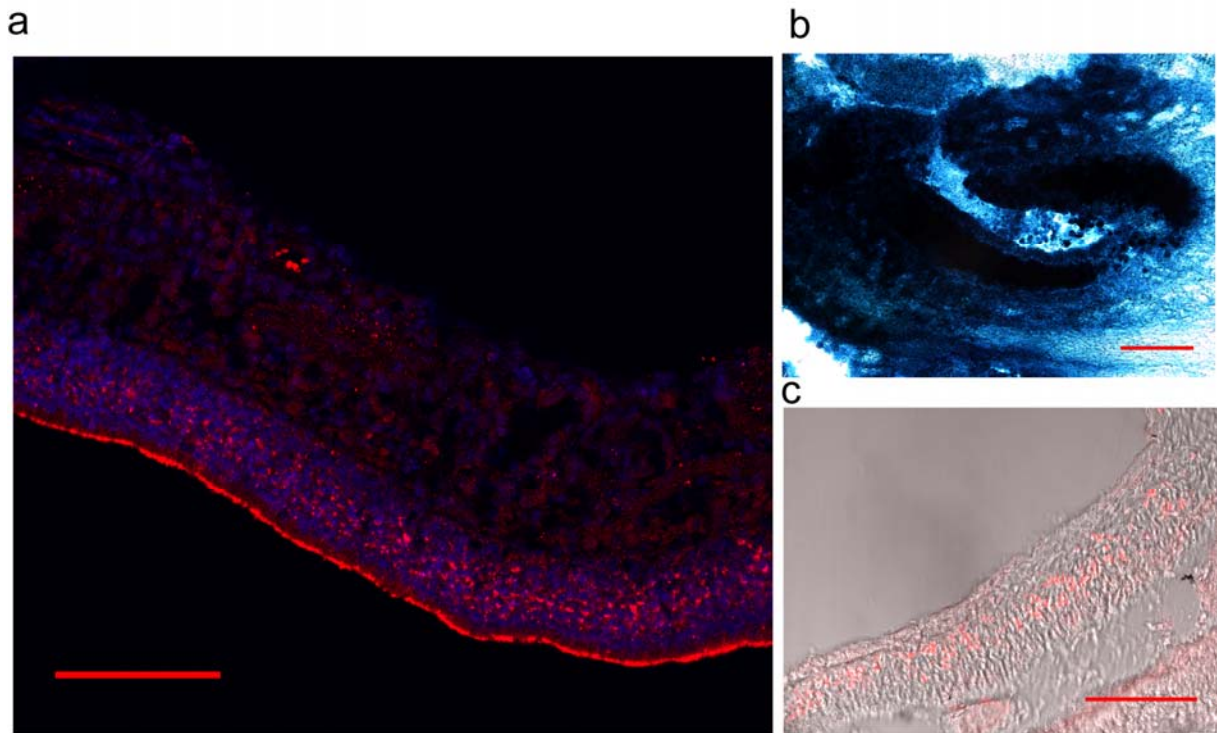
Figure 38. Expression of stoml-3 in the main olfactory epithelium of the mouse.

(a) OneSTrEP antibody staining of the olfactory epithelium isolated from a *Stoml-3^OneSTrEP* mouse revealed a robust staining of olfactory neurone cilia (anti-mouse AF633); **(b)** X-gal staining of the olfactory epithelium from a *Stoml-3^LacZ* mouse; **(c)** antibody staining of prokaryotic β-galactosidase confirms the results of x-gal staining (anti-chicken Cy3). Control mouse tissues had no staining and are not shown here. Bars – 100μm.
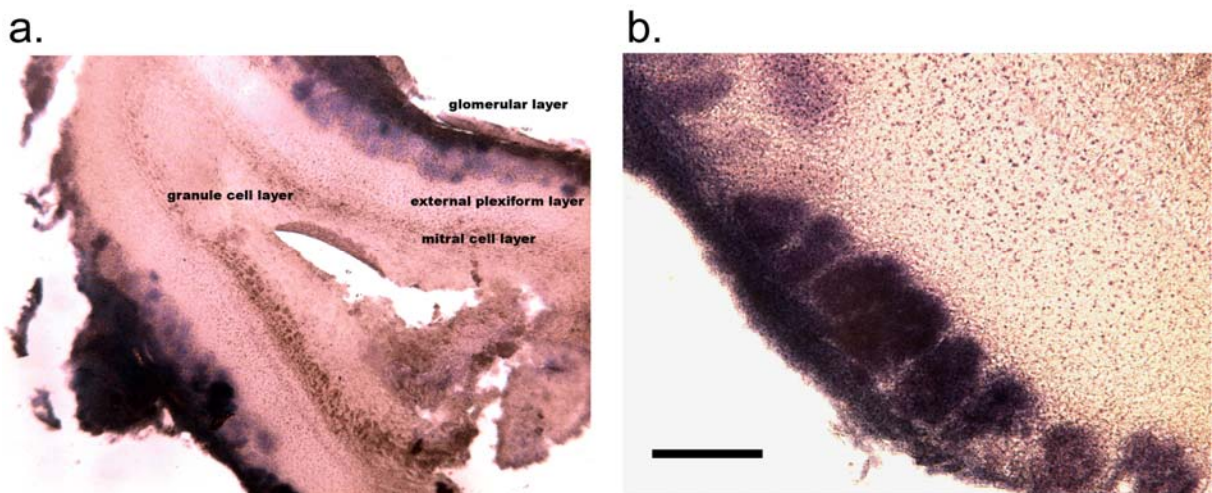
Figure 39. X-gal staining revealed an expression of the stoml-3 gene within the glomerular layer in olfactory bulbs of the adult mouse (transverse plane).

(a) transverse section of an olfactory bulb; **(b)** magnified region of the glomerular layer, separate glomeruli develop pronounces X-gal coloration. Bar – 100μm.

To determine the type of cells expressing STOML-3, a series of markers for different cell populations were used (**Figure 40**). Prominent co-staining of STOML-3 with OMP1, the marker for mature olfactory neurones, confirms the predominant neuronal nature of STOML-3 expression in the olfactory epithelium of the mouse (**Figure 40b**). Additionally, obvious staining of maturing neurones can also be observed (epithelium slises from 4 animals were analysed).
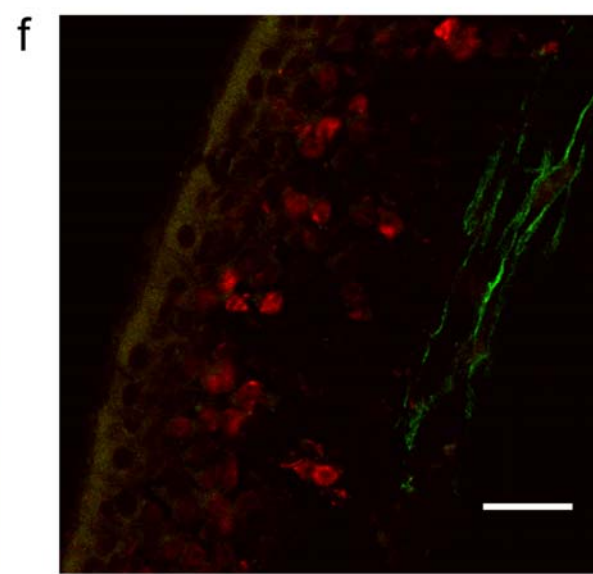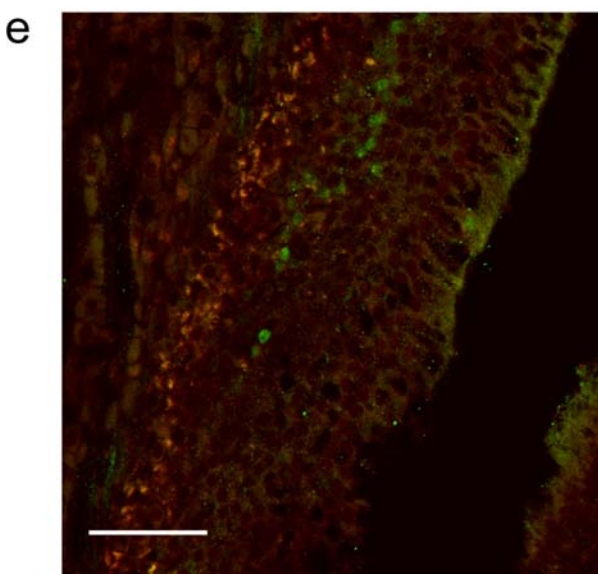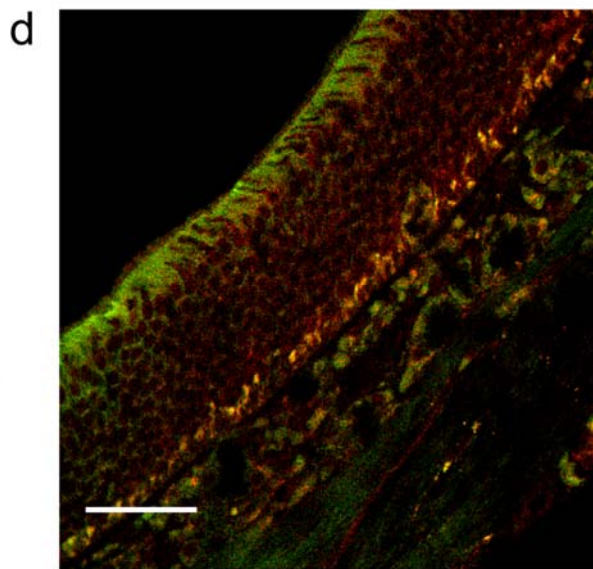
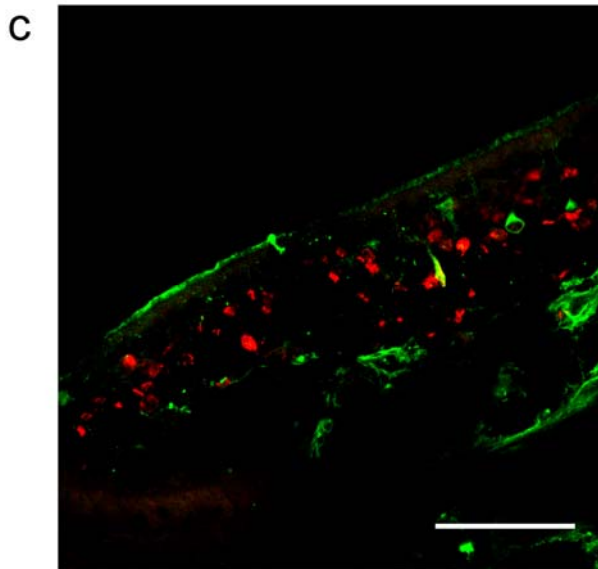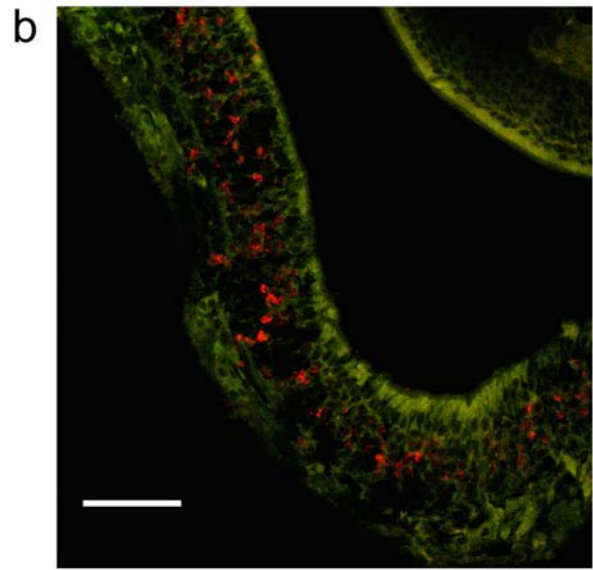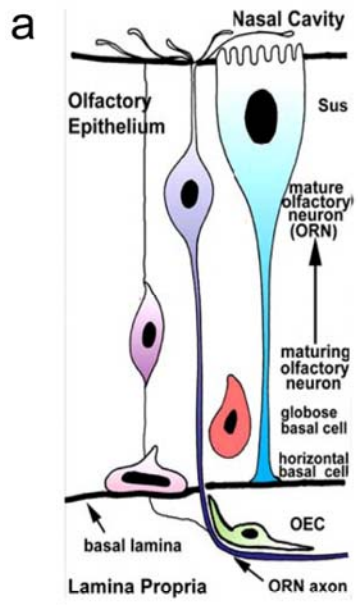**Figure 40. Expression of stoml-3 in the olfactory epithelium of the mouse.**

For the expression analyses the *Stoml-3^LacZ* reporter mouse line was used. Expression of STOML-3 was visualised using antibody staining of β-galactosidase (AlexaFluor633, red channel), AlexaFluor488 (green channel) was used for marker proteins.

(a) structure of the adult mouse epithelium; **(b)** β-gal/OMP - olfactory marker protein , expressed almost exclusively in mature olfactory sensory neurones, bar – 50μm; **(c)** β-gal/Ph3 – phospho histone 3, marker of dividing cell population, bar – 50μm; **(d)** β-gal/NeuroD – one of the maker proteins of immature receptor neurones, bar – 50μm; **(e)** β-gal/Ia1 - , bar – 50μm; **(f)** β-gal/GFAP – glial marker and marker of ensheating cells in the olfactory epithelium, bar – 20μm.

3.2.2.4 Histochemical analyses of STOML-3 expression pattern in the dorsal root ganglia and spinal cord of the mouse.

Genetic ablation of STOML-3 leads to the loss of mechanosensitivity in about 35% of skin mechanoreceptors (Wetzel et al, 2007). The effect on the organismic level can be potentially explained by the restricted expression pattern of the protein, where STOML-3 is present only in a distinct neuronal subpopulation and is a prerequisite for that population's proper functioning, thus leading to the described phenotype upon gene ablation. Nevertheless, there is a possibility that the effect is indirect and is mediated by another protein that depends upon STOML-3 for its functionality. To verify the hypothesis about the restricted expression pattern of STOML-3 in DRG neurones, DRG from *Stoml-3^LacZ* and *Stoml-3^OneSTrEP* mice were used for a series of histochemical studies using X-gal and an antibody against the OneSTrEP-tag, respectively. From the analyses of X-gal and antibody stained DRG sections, it can be concluded, that STOML-3 is expressed in neurones of all diameters. However, not all neurones in DRGs develop enzymatic colour reaction, which must be explained by a different level of STOML-3 expression in different DRG neurones (**Figure 41**).
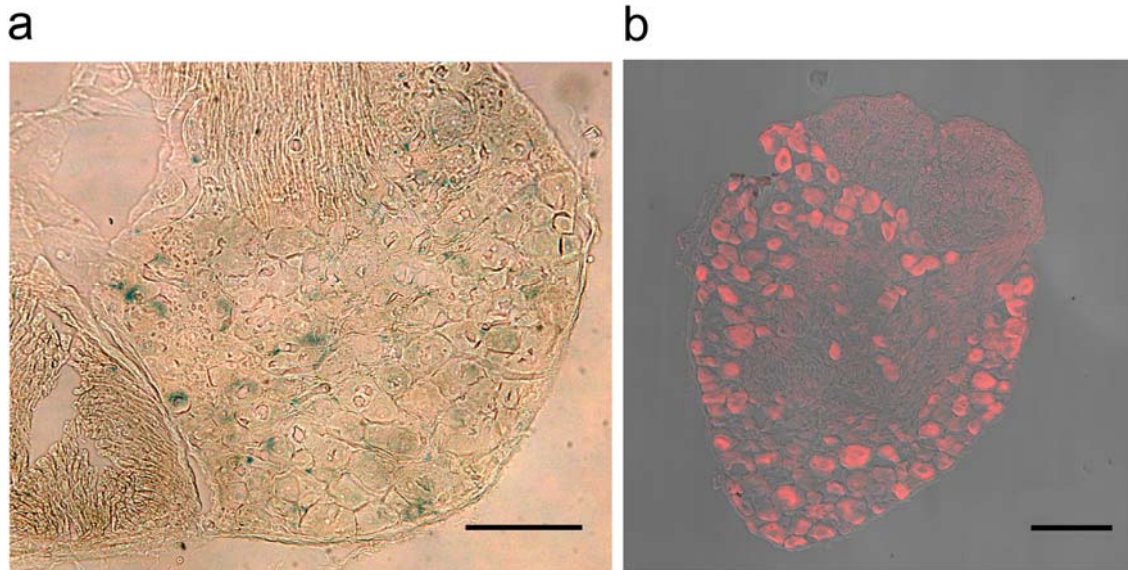
Figure 41. Expression of stoml-3 in DRG neurones.
(a) X-gal staining of dorsal root ganglia from *Stoml-3^{LacZ}* mice revealed rather weak coloration of majority of DRG neurones, bar-50μm ; **(b)** staining using an antibody directed against a prokaryotic β-galactosidase confirmed specificity of the enzymatic reaction and demonstrate coloration in all DRG neurones, bar – 100μm. Data from 4 mice.

In addition, expression of the *stoml-3* gene in the spinal cord was analysed. Histological sections from *Stoml-3^{LacZ}* mice were used for X-gal detection. Interestingly, staining of the spinal cord revealed development of a strong signal in a cell layer surrounding the central channel (**Figure 42**).
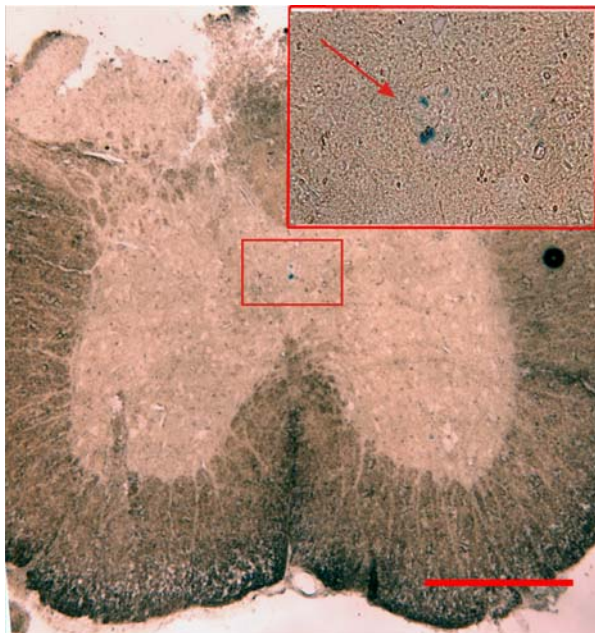
Figure 42. Spinal cord expression of STOML-3.
Stoml-3^{LacZ} mice where perfused with glutaraldehyde, transverse sections of the spinal cord were stained using X-gal and analysed in bright field. Expression of STOML-3 has a restricted pattern with a prominent staining in certain cell population in ependyma. **(inset)** scaled-up region labelled with a red box**.** In total three animals from different littets were analysed, at least 20 sections from different spinal cord regions each. Bar- 200μm.

3.2.2.5 Behavioural analyses of smell in *Stoml-3, stomatin and Stoml-3/Stomatin* knock-out mice.

STOML-3 is expressed at a high level in the olfactory epithelium of the mouse (Goldstein et al, 2003; Kobayakawa et al, 2002b). As it can be concluded from the histochemical analyses of Stoml-3^{LacZ} and Stoml-3^{OneSTrEP} olfactory system (**Figure 38 and 40**), the protein is predominantly expressed in mature olfactory neurones. This raised the question of what the functional role of STOML-3 in olfaction.

Stoml3 and *stomatin* knock-outs, as well as *Stoml-3/Stomatin* double knock-out animals, were tested in a behavioral assay for smell. In this experiment four animal cohorts, six animals in each, were used: *Stoml3-/-, Stomatin-/-, Stomatin+/- / Stoml3+/-* and C57BL/6j. To test smell ability the so-called „cookie test" was exploited, where a hidden piece of food serves as an olfactory stimulus. To increase interest in food-stimulus animals were left without food, the day before the planned experiment. The next day all animals were transferred into new empty cages and left to habituate for 10 to 15 minutes. Following this, a small piece of cookie was hidden in bedding in the cage and the time mice spend searching for the bait was recorded. Interestingly, despite the lack of STOML-3, all the animals revealed normal smell aptitude (**Figure 43**), indicating that STOML-3 is not necessary for normal smell ability, as assessed with this paradigm. Stomatin mutant animals, as well as, double heterozygotes (*stomatin+/- / Stoml3+/-*) also were normal in their smell aptitude (**Figure 43**).
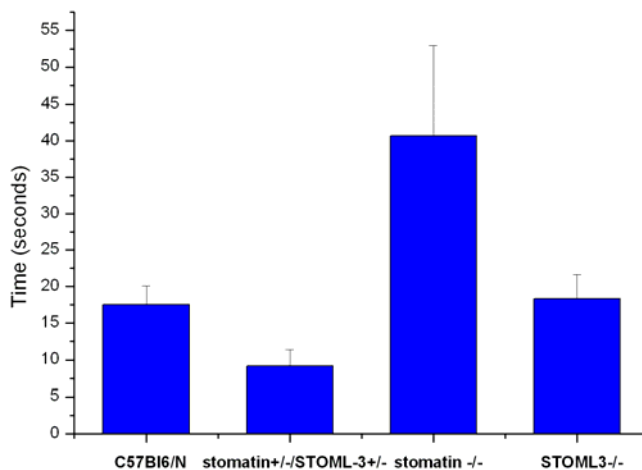
Figure 43. STOML-3 null animals display normal smell ability.
Stoml-3 and *stomatin* knock-out, as well as Stoml-3/Stomatin double heterozygote animals, were tested for the ability to smell. In the experiment four animal groups of different genotype, six animals in each, were tested. No statistically significant difference in ability to smell between mutant and control wild type mice was found.

4. Discussion.

In spite of quite extensive knowledge about the components and functioning of the somatosensory system at the organism level, our understanding of the molecular mechanisms underlying its functioning are still incomplete. With this work I tried to widen our knowledge about the molecular mechanisms of mechanosensation in mammals by characterising STOML-3, the only known component of mammalian mechanotransducer to date (Wetzel et al, 2007). I have exploited cell biological, genetic and proteomic approaches to identify anatomical structures and cell populations expressing STOML-3, sub-cellular components and cellular dynamics of the protein and most importantly – endogenous proteins that interact with STOML-3, which could be considered to be putative components of the mammalian neuroneal mechanotransducing machinery.

I have found that apart from the plasma membrane that STOML-3 is localised in a dynamic intracellular vesicular compartment. Part of this vesicular compartment was identified as a clathrin-independent, Rab11-positive recycling pool, while the major part of it did not show any obvious co-localisation with markers for different intracellular compartments and in all likelihood corresponds to transport vesicles. In support of this, several known interacting partners of STOML-3, such as stomatin and different ASIC subunits, were found to be co-transported within the same vesicle sub-population. The fact that STOML-3 interacts with ASICs and modulates their function allows us to speculate about possible preassembling of functional multiprotein complexes within the vesicles and their subsequent transportation in a "ready-to-function" state.

I managed to demonstrate that the predominant expression of STOML-3 is in the peripheral nervous system of the mouse as early as 14.5 day of development (dpc). At the same time, additional expression of STOML-3 in cell types known to be able to detect mechanical forces (e.g. osteocytes) (Lanyon, 1993) was found, supporting the idea that STOML-3 may be a more universal component of mechanotransduction machinery in cell types other than sensory neurons.

I have also generated and tested a mouse $Stoml-3^{STrEP}$ knock-in model, which can be used for affinity purification of endogenous binding partners of STOML-3 and thus represents a novel and very useful tool to discover the protein composition of the mammalian mechanosensitive complex.

4.1 STOML-3 defines a distinct, highly mobile vesicular population.

The vesicular compartment of the cell is diverse and serves different purposes, from delivery of protein cargo to recycling and subsequent degradation in the lysosomal compartment of single molecules or whole multiprotein complexes. Vesicles can be roughly divided into four major types according to their role in the cell: transport vesicles, endosomes, exosomes and lysosomes. As a rule, these vesicular types can not be distinguished on basis of their morphology alone and instead require the classification on the basis of the proteins associated with them in order to be discriminated from one another. I found that cell membrane-associated protein STOML-3 is localised to a highly mobile heterogeneous vesicular pool. Two major types of STOML-3 positive vesicles can be readily distinguished based on their shape: round vesicles that are ~500nm in diameter and a second rare population of elongated vesicles, whose length was ~1μm or larger (**Figure 12**)

The presence of STOML-3 in the vesicular compartment can be explained either by a role in vesicle formation/functioning or by passive involvement as vesicular cargo. Several of my findings support the first hypothesis, which is discussed below. In all likelihood, STOML-3 is a palmitoylated membrane protein with the hairpin structure that can form oligomers (Snyers et al, 1999a, 1999b). This predicted structure of the protein is reminiscent of caveolin and flotillins, known scaffolding proteins involved in plasma membrane organisation and vesicle formation (Solis et al, 2007; Browman et al, 2007; Langhorst et al, 2008a, 2008b; Schneider et al, 2008; Vassilieva et al, 2009; Stuermer, 2011a, 2011b; Bauer & Pelkmans, 2006). However, I found no sign of co-localisation between STOML-3 and caveolin or flotillins in DRG neurones, which may indicate the existence of a pathway distinct from caveolin and flotillin-mediated organization of the plasma membrane, which is defined by STOML-3. The hairpin structure, oligomerisation and evidence of cytoskeleton association for stomatin, which is the closest stomatin-family member to STOML-3 (Stewart et al, 1993; Snyers et al, 1999b, 1999a, 1998; Martinez-Salgado et al, 2007), suggest that STOML-3 may form membrane microdomains that are necessary for the assembly of cell-surface proteins into functional complexes and possibly also molecular platforms, which recruit material from a vesicle compartment, as well as participate in cytoskeleton dynamics. Nevertheless, further analysis of STOML-3 interacting partners and associated proteins is necessary to confirm the role in protein recruitment via organization of membrane microdomains.

In favour of the second hypothesis, that STOML-3 is simply a vesicle cargo, is the immediate physiological effect of STOML-3 on ASICs, which are plasma membrane proteins (Wetzel et

al, 2007). Electrophysiological recordings of acid-evoked currents indicate that the functional interaction between STOML-3 and ASIC subunits takes place on the membrane. Thus, presence of these both proteins within the same vesicle can be explained by co-trafficking of preassembled components of the same protein complex.

4.1.1 STOML-3 dynamics and assembly with the cytoskeleton.

Using live-cell imaging, together with pharmacological tools, I was able to demonstrate, that the high motility of the STOML-3 positive vesicular compartment is a microtubule dependent process. Data from the literature confirm that the speed and character of STOML-3 positive vesicle movement is similar to that of signalling endosomes in sensory axons and is in the range of kinesin-based movement (Cai et al, 2007; Cui et al, 2007; Gagliano et al, 2010; Shtridelman et al, 2009). Pharmacological manipulation of microtubules confirmed immediate interaction of the STOML-3 vesicles and microtubules. Interestingly, we observed vesicle fusion with the plasma membrane upon destabilising of microtubules with nocodazole. At the same time we observed progressive bending of the membrane during the course of the experiment, a phenomenon only observed in cases of STOML-3 overexpression, but not in experiments where neurones were transfected with EGFP. In all likelihood, destabilisation of the "tracks" formed by microtubules leads to dissociation of the vesicles from the cytoskeletal component and promotes plasma membrane fusion. It is known that proteins from the stomatin family oligomerise and can potentially form homo-multimeric "platforms" (Snyers et al, 1998). Robust insertion of such structures could potentially explain the membrane bending observed when STOML-3 transfected cells are treated with nocodazole. According to our data, the expression level of STOML-3 in DRG neurones is rather low and thus, it is difficult to expect, that such a robust change in membrane curvature, as it was observed *in vitro*, can take place *in vivo*. However, this does not exclude the possibility, that by association with components of mechanotransducing machinery and homo- or hetero-oligomerisation with other members of stomatin family, for instance stomatin, STOML-3 can produce a local bending of the plasma membrane around a mechanosensitive channel and thus, regulate the mechanosensitive properties of this channel.

4.1.2 Heterogeneity of the STOML-3 vesicular pool.

I found that the STOML-3 positive vesicular pool is heterogeneous and consists of abundant, ~500nm diameter vesicles and rare ~1μm long vesicles rather distinctive in shape.

Tubulation of the membrane and formation of tubular-vesicular compartments was previously described for BAR-domain proteins (Ferguson et al, 2009; Varkey et al, 2010; Yoon et al, 2001; Meunier et al, 2009; Wu et al, 2010), nevertheless morphological characteristics and dynamics of these structures are distinct from what was observed for STOML-3 positive vesicles. A relatively small number of the long vesicles per cell, even under overexpression conditions, a lack of co-localisation with known sub-cellular compartment markers and a significantly higher speed of movement may indicate a unique functional role of these vesicles in nervous system, which is currently unknown.

I have identified, that part of the $\sim 0.5\mu m$ STOML-3 positive vesicle population belongs to the Rab11-positive recycling endosomal compartment. DRG sensory neurones are highly polarised cells with very long processes. Maintenance and fine tuning of the plasma membrane protein composition involved in transduction, path finding, signalling, adhesion etc. requires constant influx and removal of proteins from the plasma membrane. The very long distance between the cell body and nerve endings makes it crucial to have a local mechanism regulating homeostasis and functionality of neuronal termini. Involvement of recycling endosomes in trafficking and regulation of membrane protein content in neurones has been extensively discussed (Brown et al, 2007; Correia et al, 2008; Lisé et al, 2006; Park et al, 2004; Wang et al, 2008; Ascaño et al, 2009; Eva et al, 2010). The recycling endosomal compartment is implicated in the trafficking of receptors, integrins and some adhesion molecules (Park et al, 2004; Brown et al, 2007; Correia et al, 2008; Lisé et al, 2006; Ascaño et al, 2009; Wang et al, 2008; Kamiguchi & Lemmon, 2000). Thus, the presence of STOML-3, an essential component of the mechanotransduction machinery, in recycling endosomes can be explained by the targeting and regulation of its expression on the cell surface. Due to the distinct morphology and extreme polarisation of neurones, the Rab11-positive compartment in these cells may assume a cell-specific function in addition to a local recycling of plasma membrane components. It was shown for sympathetic, as well as for sensory DRG neurones, that Rab11 vesicles move predominantly in anterograde direction and are involved in trafficking and re-targeting via transcytosis of proteins like Trk receptors (Ascaño et al, 2009), norepinephrine transporter (Matthies et al, 2010) and integrins (Eva et al, 2010). Nevertheless, the nature of Rab11-STOML-3 positive vesicles movement and the relevance of this mechanism *in vivo* needs to be investigated further. To investigate STOML-3 positive compartment further, experiments using compartmentalised cell cultures, as well as proteomic analyses of ligated sensory nerves are planned.

4.1.3 Involvement of STOML-3 positive vesicles in trafficking of mechanotransducer components in DRG sensory neurones.

We found that STOML-3 physically interacts with ASIC subunits, mammalian members of the Deg/ENaC family of ion channels, and regulates pH-gated ASIC currents (Lapatsina et al., in preparation). Microscopy analyses of STOML-3/ASIC2a and STOML-3/ASIC3 revealed co-localisation of the proteins in the same vesicular compartment. Stomatins and separate ASICs play an essential role in the transduction of mechanical stimuli by sensory neurones (Wetzel et al, 2007; Brown et al, 2008; Goodman et al, 2002; Price et al, 2001; Price et al, 2000; Martinez-Salgado et al, 2007; Huang et al, 1995; O'Hagan et al, 2005). A current model of the mammalian mechanotransduction complex is based on findings in *C.elegans* mechanotransduction. It was proposed that the mechanosensitive ion channels from the Deg/ENaC family (MEC-4 and MEC-10), are anchored between components of the extracellular matrix and the microtubular cytoskeleton. Shifting of these components against each other during mechanical stimulation leads to channel gating. MEC-2, a close homolog of STOML-3 protein, is proposed to tether a mechanosensitive ion channel to the cytoskeleton, providing a physical link between the mechanotransducer and microtubules (Ernstrom & Chalfie, 2002). More recently, analysis of the *C. elegans* mechanotransduction complex has revealed, that both, extracellular matrix components and microtubule are located to distinct compartments to MEC-2 protein (Cueva et al, 2007). This finding suggests that the earlier proposed model of a rigid complex is unlikely to exist and that a role of stomatins in mechanosensitive complex is more dynamic. Our finding, that a part of STOML-3 positive vesicular pool overlap with Rab11 compartment, supports the idea about distinct role of these vesicles in formation of mechanotrasduction mechinery. Thus, we propose that STOML-3 may define a novel vesicular population, involved in the trafficking of preassembled components of the mammalian mechanotransducer. We propose to term this novel vesicle population the *transducosome*.

4.2 Expression pattern of STOML-3 protein.

Despite the fact that STOML-3 was discovered as a protein specific to the olfactory epithelium, the subsequent studies carried out in our laboratory were supportive of the idea that it is also expressed in other neuronal types. Quantitative PCR allowed us to identify expression of STOML-3 in DRG, spinal cord, olfactory bulbs, brain and stomach. The expression level in DRG is more than 4000 times lower than in the olfactory epithelium

(Wetzel et al, 2007). More detailed characterisation of the protein expression profile was, until this study, hindered due to lack of truly specific STOML-3 antibodies. Thus, to study STOML-3 protein further, I have created a reporter *Stoml-3^{LacZ}* and *Stoml-3^{OneSTrEP}* mouse line. Using these animals, I was able to demonstrate that STOML-3 is indeed preferentially expressed in the olfactory epithelium and DRG neurones as early as 14.5 dpc. *Stoml-3^{OneSTrEP}* mouse allows a sub-cellular analysis of the *in vivo* distribution of STOML-3 in these tissues. The previously discribed hippocampal expression of STOML-3 was not confirmed by anti-OneSTrEP antibody staining.

4.2.1 Expression of STOML-3 in the main olfactory epithelium of the mouse.

The expression level of STOML-3 in the olfactory epithelium is already very high during development, which can be concluded from the very rapid and robust development of X-gal reaction at the first 30 minutes of incubation, thus, the results of histochemistry correspond to the previously reported real-time PCR data (Wetzel et al, 2007). Immunohistochemical analyses of the olfactory epithelium demonstrated olfactory neurone-specific localisation of STOML-3 in both maturating and mature olfactory neurones. Antibody staining of the olfactory epithelium from *Stoml-3^{OneSTrEP}* knock-in mice revealed a robust signal in olfactory neurone cilia, the structures that are directly involved in olfactory receptor transduction. Based on this, one can speculate that STOML-3 could be involved in the organisation of olfactory receptor complexes and thus, *stoml-3* null animals may have impaired olfaction. Nevertheless, behavioural analyses of olfaction ability in adult STOML-3 knock-out animals showed no difference compared to wild type control mice. Thus, we can assume that in spite of very robust expression in olfactory neurones, STOML-3 seems to play no crucial role in smell transduction. Olfactory neurone cilia are the primary cilia, the major function of which is cell signalling, based upon the expression of a variety of receptors, ion channels and effector molecules being localized to the cilium or basal body (Satir et al, 2010). Primary cilia are known to respond to mechanical stimulation and different chemicals including hormones and growth factors. In some cases primary cillia demonstrate light (Insinna & Besharse, 2008), temperature (Kuhara et al, 2008) and osmosensitivity (Christensen et al, 2005). In the kidney, two polycystin proteins (PC1 and PC2) form a mechanosensory complex that detects epithelium primary cilia deflection and translates this into signals associated with growth and differentiation (Low et al, 2006). Based on knowledge about the sensory role of primary cilia,

one can speculate, that STOML-3 could be involved in the formation of mechanosensory machinery in olfactory cilia (Grosmaitre et al, 2007).

One very distinctive characteristic of the olfactory neurones is their constant renewal, which is also connected with the formation of new processes and synapses within the olfactory bulb. As mentioned before, there is evidence of interaction between members of the stomatin family of proteins and components of the cytoskeleton (Ernstrom & Chalfie, 2002). Thus, another possible role of STOML-3 in the olfactory epithelium is the regulation of cytoskeleton dynamics and, possibly, involvement in enabling correct wiring of olfactory neurones. As it is not possible to carry out behavioural experiments on mice to verify their ability to discriminate between different odours, the most direct experiments need to be done, in order to verify a connectivity pattern in wild type versus conditional knock-out mice, are retrograde labelling and co-labelling with known olfactory neurone markers.

4.2.2. STOML-3 expression in the developing embryonic bones.

An unexpected finding for us was robust X-gal staining in forming mouse bones during embryonic development (E15). The cell type, which expresses STOML-3 in bones most probably corresponds to mesenchymal osteoblast precursors that move into developing bones between E14 and E16 (Lefebvre & Bhattaram, 2010). These precursors subsequently give rise to trabecular osteoblasts, osteocytes and stromal cells inside the bone; nevertheless, additional follow-up experiments will be necessary to confirm this hypothesis.

Bone is a dynamic tissue that adapts to environmental mechanical stimuli. Detection of changes in mechanical loading is important for both bone formation and homeostasis. Osteocytes are thought to be the main bone mechanosensors due to their location within the bone matrix and specialised cell organisation (Nowlan et al, 2010; Lefebvre & Bhattaram, 2010). Osteocytes are terminally differentiated cells that are housed in bone lacunae, which are connected by a network of channels (Lanyon, 1993) and make up the majority of cells in bone. Osteocytes extend primary cilia projections through the surrounding channels and communicate with each other, as well as with cells on the bone surface. The main mechanisms by which bone cells are thought to detect and respond to mechanical stimulation are: detection of fluid flow shear stress, mechanical deformation of cilia and pressure gradients induced by fluid flow. The molecular basis through which osteocytes sense these stimuli are not known (Papachroni et al, 2009; Guoliang et al, 2007). This raises the intriguing

possibility that signalling via mechanosensitive ion channels regulated by STOML-3 is involved in mechanotransduction in osteocytes.

4.2.3 STOML-3 expression in the peripheral nervous system of the mouse.

Histochemical and immunohistochemical analyses of DRGs from the *Stoml-3^{OneSTrEP}* and *Stoml-3^{LacZ}* mice demonstrated that expression of STOML-3 in DRG neurones is not restricted to large diameter neurones that are most likely Aβ fibres, but rather is present in all neurones regardless of size but with variations in the level of expression. Thus, my data suggest that larger neurons, which are A-β fibers, may have higher levels of STOML-3 expression than smaller neurons that are not low threshold mechanoreceptors. Thus, we can assume that the previously reported lack of mechanosensitivity in 40% of Aβ fibres is not due to the expression of STOML-3 in the restricted subpopulation of the sensory neurones, but rather due to other proteins that functionally interact with STOML-3. These data correspond with the results of *in-situ* hybridisation for *stoml-3* RNA in DRGs (Wetzel et al, 2007). Presence of STOML-3 in all DRG neurones supports the idea that the protein could participate in assembling of a basic platform in neurons, which connects different molecular components with each other in a cell-specific manner and directly or indirectly modulates their function. Whole-mount staining of *Stoml-3^{LacZ}* embryos older than E13 showed development of coloration in nerves innervating limbs, as well as the optic nerves. Thus, the time point at which expression of *stoml-3* can be detected using the *Stoml-3^{LacZ}* reporter mouse corresponds to the developmental stage at which neurogenesis of different sensory neurone population is finished and end organs are innervated (**Figure 43**) (Lechner et al, 2009b) .
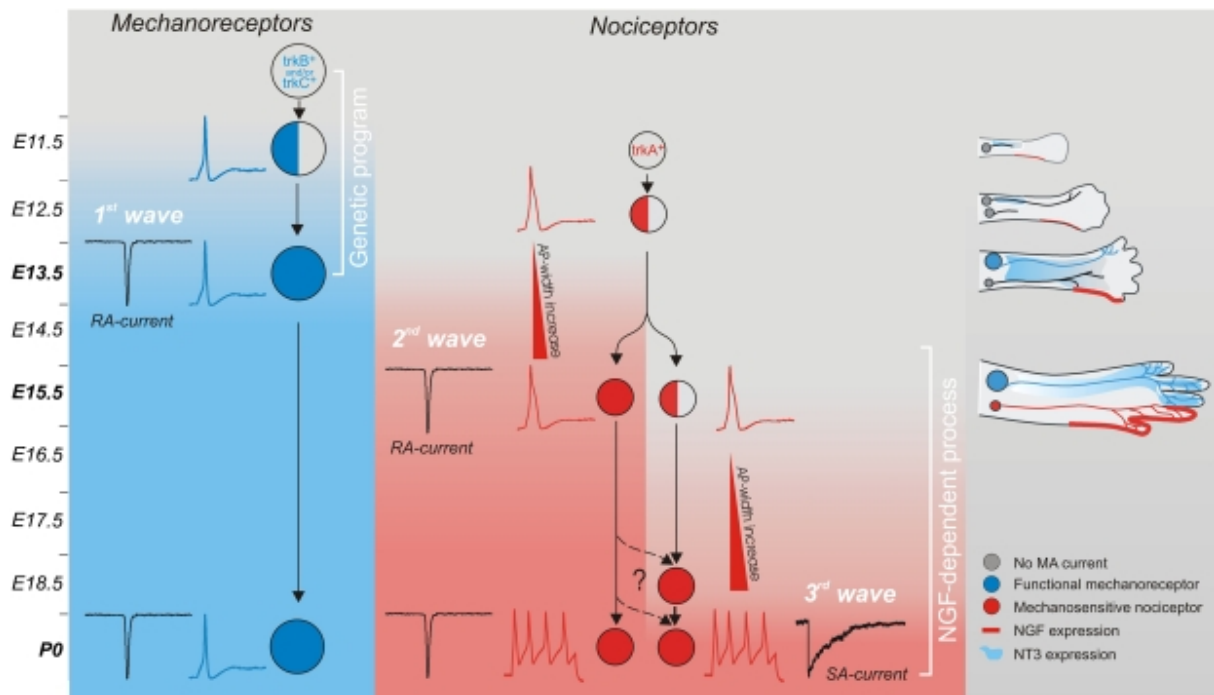
Stefan G Lechner et al. EMBO J. 2009

Figure 44. Waves of mechanosensitivity acquisition in different sensory neurone subtypes.
Model summarizing the three waves of mechanosensitivity acquisition in different sensory neuron subtypes. Developmental stage is depicted from top to bottom for mechanoreceptors (blue) and nociceptors (red). Cartoons (right) depict the innervation of the limb.

According to our real-time PCR data, STOML-3 is also expressed in the central nervous system, namely in the brain. Thus, to characterise the effect of STOML-3 ablation on mechanosensation further, I plan to use a conditional STOML-3 mouse line that I have created. *Stoml-3^{Tm}* mice, which have their first exon of *Stoml-3* gene floxed, were bred with a DRG neurone-specific Cre-deliter line *Islet*, which was generously provided by Prof. Carmen Birchmeier-Kohler. I have now established mice, in which the *Stoml-3* gene was specifically disrupted in tissues expressing *Islet* gene, namely in DRGs and motoneurones (Srinivas et al) . The advantage of this mouse, which is *Stoml-3* null in DRG neurones and wild type in the central nervous system, is that it allows separation of central and peripheral components on deficitis in mechanosensation demonstrated in behavioural experiments (Wetzel et al, 2007). Breeding *Stoml-3^{Tm}* mice with different Cre-lines, in order to create tissue or time-specific knock-outs of *Stoml-3* gene, will provide a useful tool for further characterisation of the protein at the organismal level.

4.2.4 Spinal cord expression of STOML-3 protein.

According to the previous real-time data (Wetzel et al, 2007), STOML-3 should be expressed in the spinal cord, however a histochemical analysis of spinal cord sections produced rather unexpected results. Virtually no obvious staining was detected apart from three to four cells surrounding the central channel. The central channel in mature animals is a cerebrospinal fluid (CSF) -filled space that runs through the length of entire spinal cord and joins to the fourth ventricle through the obex. The central channel is derived from the neural tube and preserves a certain degree of plasticity in comparison with the rest of central nervous system. The cavity of the central channel is lined with the ependyma, a neuroglia cell type involved in CSF production. Ependymal cells are ciliated at their apical surface and beating of these cilia provides circulation of CSF around the central nervous system. It has also been reported about potential stem cell activity of ependyma and direct involvement in regeneration (Meletis et al, 2008; Mothe & Tator, 2005). The restricted staining pattern to several cells of STOML-3 in an otherwise uniform population of ependymal cells indicates the presence of a certain cell type within the ependyma that expresses STOML-3. In a number of relatively recent publications it was demonstrated, that the central channel ependyma contains cells with characteristics similar to immature neurones in adult neurogenic niches (Hamilton et al, 2009; Marichal et al, 2009). The localisation of these cellular populations is also restricted to particular parts of the central channel. Considering the preferential neuronal expression pattern of STOML-3, staining with such markers like doublecortin (DCX) and poly-sialylated neural cell adhesion molecule (PSA-NCAM) typical of migrating neuroblasts, should be done in order to verify the true nature of STOML-3 positive cells in the spinal cord.

It also should be mentioned that another discrete population of neurones, surrounding the central canal of the spinal cord, has been reported by (Huang et al, 2006). These neurones were shown to express PKD2L1 receptor (transient receptor potential polycystic 2) and respond to acid stimulation. (Huang et al, 2006). Further co-staining of STOML-3 with PKD2L1 is necessary to verify if there is any connection between STOML-3 positive cells and acid-sensing PKD2L1 expressing neurones in the publication.

# 4.3 Potential mechanisms of stomatin-like protein 3 function.

Stomatin-like protein 3 is a member of the stomatin family, which in comparison with other members of the family has a restricted expression pattern. The only known function of this protein so far is a direct involvement in mechanosensory transduction in the mouse (Wetzel et al, 2007). The molecular mechanism, how ablation of this membrane-associated protein can make a group of mechanoreceptors mechanically insensitive, is however, not clear. Based on literature sources and data collected during this work, I can propose two working models explaining the regulation of a mechanosensitive channel or channels by STOML-3.

Direct regulation of channel properties.

The initial idea, which is based on the *C.elegans* transduction model, is supported mainly by the fact that STOML-3, as well as other family members, physically interacts with different ASIC subunits and regulates their properties. Nevertheless, in comparison with *C.elegans,* where a role for both MEC-4 and MEC-10 in mechanosensation has been clearly demonstrated (Chelur et al, 2002; Goodman et al, 2002; O'Hagan et al, 2005), the role of ASICs in mammalian mechanotransduction is contradictory. Two novel candidate proteins (Piezo1 and Piezo2) on a role of mechanosensitive channel have been recently reported by (Coste et al, 2010). In their paper they demonstrate, that overexpression of either of these two proteins in non-mechanosensitive cell lines results in the acquisition of mechanosensitive currents upon mechanical stimulation of the cell (Coste et al, 2010). It has not yet been proven that Piezo1 and Piezo2 are the mechanosensitive channels by themselves, and not activating or recruiting another channel, that is non-mechanosensitive under basal conditions. However it will be interesting to test whether STOML-3 can modify properties of Piezo-dependent mechanosensitive currents and whether STOML-3 physically interacts with Piezos.

Our group have previously found that a large extracellular filament or "tether" that attaches to the extracellular matrix appears to be required for mechanosensitive ion channel function in the mouse (Hu et al, 2010). A molecular mechanism by which the "tether" regulates activity of a mechanosensitive channel and whether it directly interacts with the channel, or rather with another component of mechanotransducing machinery, are not known. To verify a hypothesis about direct ion channel gating through physical interactions within a multiprotein complex identification and validation of mechanosensitive channel or channels as well as other interaction partners of STOML-3 is necessary. Thus, as the next step in characterisation of STOML-3 function, affinity purification of the protein interaction partners using the new Stoml-$3^{OneSTrEP}$ mice is planned. Another promising approach for identification of STOML-3

interaction partners is the purification of STOML3-containing vesicles using N-terminal OneSTrEP-tag, which, according to STOML-3 topology should be facing the cytoplasm of the cell (**Figure 44**). It is known for a number of plasma membrane protein complexes, that their protein components are transported together within the same vesicles. An advantage of this approach is that bulky extracellular proteins like "tether" and difficult to solubilise membrane proteins with multiple transmembrane domains like Piezos will not be missed during protein preparation and purification. Indeed the population of vesciles that we can potentially isolate that are STOML3/rab11 postive "transducosomes" may indeed contain many interesting novel proteins that are directly involved in the transduction. Once such vesicles are isolated it is relatively straightforward to identify all proteins present in the fraction using unbiased mass spectrometry techniques (Cox & Thompson, 2008; McPherson, 2010; Raimondo et al, 2011).
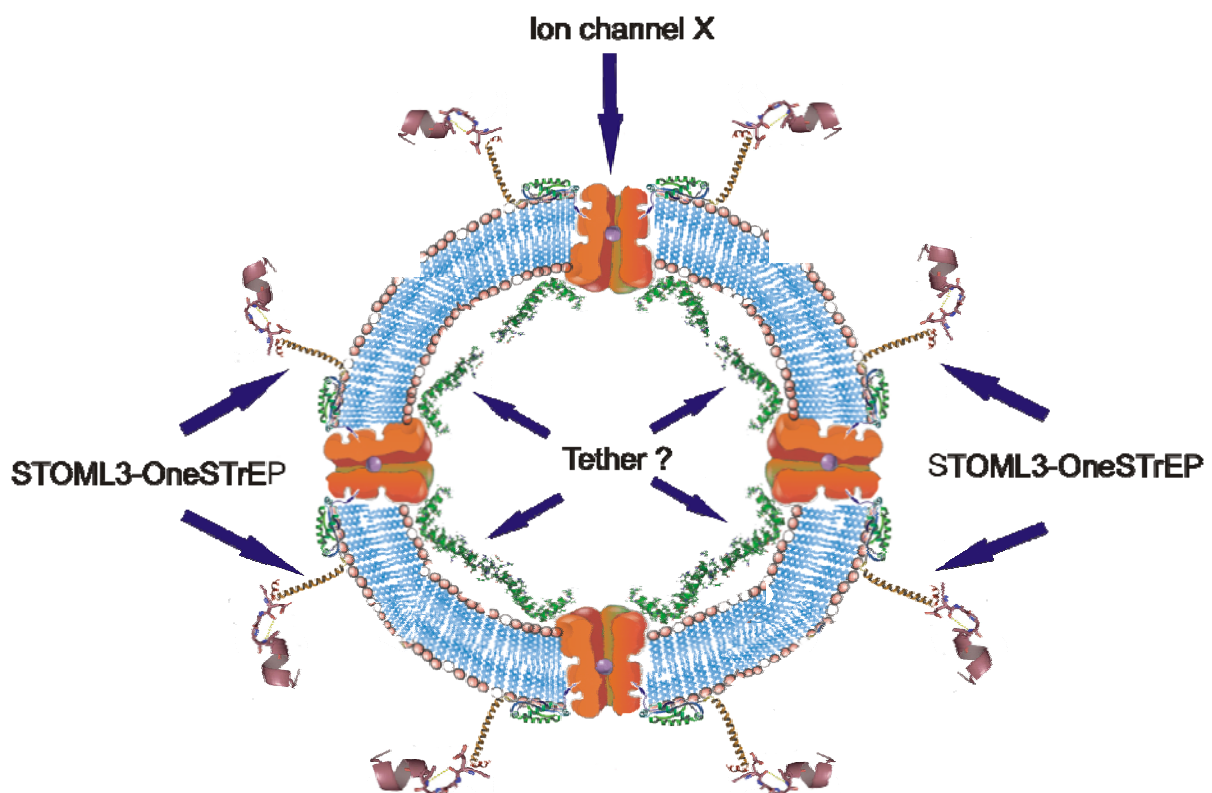
Figure 45. A scheme of STOML3-containing vesicle.

A number of plasma membrane proteins is transported together with their interaction partners within the same vesicle. According to STOML-3 topology N-terminal OneSTrEP-tag should face cytoplasm of the cell thus, can be used for the purification of STOML-3 positive vesicles in order to determine their content.

Indirect regulation of channel gating via changes in plasma membrane properties.

The hairpin structure of stomatins (Hiebl-Dirschmied et al, 1991a, 1991b), oligomerisation (Boute et al, 2000b; Huber et al, 2003), palmitoylation (Snyers et al, 1999a) and lipid-raft association (Huber et al, 2006; Salzer & Prohaska, 2001; Snyers et al, 1999b) indirectly support the idea that STOML-3 could modulate gating of a mechanosensitive ion channel by changing the physical characteristics of the plasma membrane environment. Our finding that STOML-3 can be the cause of significant membrane bending upon its incorporation into the plasma membrane is in accordance with this hypothesis, demonstrating that presence of STOML-3, most probably, changes mechanical properties of the membrane. Nevertheless, this model cannot explain the loss of mechanosensitivity in only a distinct neuronal population, when considering the widespread expression of STOML-3.

Finaly, I found that *stoml-3* expression is not restricted to neuronal tissues, but can also be detected at least within the olfactory epithelium and bone tissues. The cells from these tissues are reported to be able to detect and react on mechanical stimulation. Thereby, the role of STOML-3 in mechanotransduction, may be more general in character, than previously appreciated.

5.Appendix.

5.1 Abbreviations

Amp	Ampicillin
ASIC	Acid sensing ion channel
BAC	Bacterial artificial chromosome
BSA	Bovine serum albumin
b-gal	β-galactosidase
Cko mouse	Conditional knock-out mouse
CSF	Cerebrospinal fluid
Deg/ENaC	Degerin/ Epithelial Na+ channel
cDNA	Complementary DNA
Dpc	days post coitum
CNS	Central nervous system
DAPI	4′,6-Diamidino-2-phenylindol
DCX	Doublecortin
DMEM	Dulbecco's modified Eagle's medium
DMSO	Dimethyl sulfoxide
DNA	Deoxyribonucleic acid
dNTP	Deoxynucleotidetriphosphate
DTT	Dithiothreitol
DRG	Dorsal root ganglion
EDTA	Ethylenediaminetetraacetic acid
EGFP	Enhanced green fluorescent protein
ER	Endoplasmic reticulum
ES cells	Embryonic stem cells
FBS	Fetal bovine serum
FRT	Flippase Recognition Target
G418	Geneticin
GDP	Guanosine diphosphate
GTP	Guanosine-$5'$-triphosphate
HCl	Hydrochloric acid
HRP	horseradish peroxidase
i.p.	intraperitoneal
Kan	Kanamycin
Kd	Dissociation constant
KOH	Potassium hydroxide
LC/MS/MS	Liquid chromatography–mass spectrometry, tandem
LoxP	locus of X-over P1
MDCK	Madin Darby canine kidney
MEF	Mouse Embryonic Fibroblasts
MQ	Type-I ultrapure water (from Barnstead E-pure system)
mRNA	Messenger ribonucleic acid
NA	Numerical aperture
NaCl	Sodium chloride
NaOH	Sodium hydroxide
Neo	Neomycin
OD	Optical density
ORN	olfactory receptor neurone
PBS	Phosphate-buffered saline

PBT	PBS-Tween-20
PCR	Polymerase chain reaction
PFA	Paraformaldehyde
pH	Potentium hydrogenii
PNS	Peripheral nervous system
Pro	Prolin
RIPA buffer	Radioimmunoprecipitation assay buffer
RNase	Ribonuclease
rpm	Revolutions per minute
RT	Room temperature
SDS	Sodium dodecyl sulphate
s.e.m	Standard error of the mean
SD	Standard deviation
SSC	Sodiumchloride-sodiumcitrate
STOML	Stomatim-like
TAE	Tris-acetate EDTA
TE	Tris-EDTA
TCF	Transgenic core facility
TGN	Trans-Golgi network
TIRF	total internal reflection fluorescence
Tris	Tris-(hydroxymethyl-) aminoethane
WGA	Wheat Germ Agglutinin
WT	Wild type

5.2 MEF cell culture.

Mitomycin C treated dish		Plate type/number	Resuspension volume	Suspension volume per well
15cm dish		3 X 10cm dishes	30 ml	10 ml
15cm dish		9 X 6cm dishes	45 ml	5 ml
15cm dish		3 X 6 well plates	54 ml	3 ml
15cm dish	**For**	4 X 12 well plates	96 ml	2 ml
15cm dish		4 X 24 well plates	144 ml	1.5 ml
15cm dish		4 X 48 well plates	200 ml	1 ml
15cm dish		3 X 96 well plates	66 ml	0.2 ml

5.3 Primers for targeting vectors construction.

Name	Sequence 5'- 3'	Usage
MegLS	GGCTGCAGGAATTCGATATCAAGCTCTGAACCTCTGAATCTGTAAGCCA	Upstream sense and antisense mega-primers for retrieval *stoml-3* sequence to be targeted
MegLA	TAGACCAAGGTTTAATCTTTTAACCAGCCAG	
MegRS	GGAGAGTAAACACTGTCTGCAATAGACACCAC	Downstream sense and antisense mega-primers for retrieval *stoml-3* sequence to be targeted
MegRA	CCTCTTGAAAACCACACTGCTCGACGAGATGTTAGATGTTTGTATGCTCGAAG	
sLoxP-LS	GATGGAGGCTGACTTCCCTCCTCTTC	Upstream sense and antisense mega-primers for the single LoxP site insertion
sLoxP-LA	GGAACCGATGGAGAAATTGGCAAGCTTGATATCGCTCAGTGGTAGCCTGAGCTACAAG (EcoRV site introduced)	
sLoxP-RS	GACCCGAGTGACCCACTGCTCTAGTTCACTAGTGATTGCAGGCACGCAAGCAC (SpeI site introduced)	Downstream sense and antisense mega-primers for the single LoxP site insertion
sLoxP-RA	GCAGCCTTAAGGGCTGTCCTGAAG	
NeoMeg-LS	CATTTATTTGTGTAAGAGCTGTGGCTG	Upstream sense and antisense primes for FRT-Neo-FRT-LoxP cassette introduction
NeoMeg-LA	ACTTCGGAGCATTAGATAGATGCAGCTGAGCAAGCCTCTGAAAGCAAGCC	
NeoMeg-RS	GACCCGAGTGACCCACTGCTCTAGTGATATCAGCCTTCTCTCAAATACAACCAG (EcoRV site introduced)	Downstream sense and antisense primes for FRT-Neo-FRT-LoxP cassette introduction
NeoMeg-RA	GAAACGGCATGCTGGGTGGTG	
KI_MegSTrEP-LS	ATGGCTAGCTGGAGCCACCCGCAAACTTTGCGTGGGACACCTATGAC	Upstream sense and antisense primes for OneSTrEP-Stoml3-Ex1 construct introduction (*Stoml-3^{OneSTrEP} mouse line*)
KI_MegSTrEP-LA	CATCTCATTCTTGAGGTGCCTTTCAAATC	
KI_MegSTrEP-RS	GTAGGTTCCTTCCTCCTCTCTGAATGC	Downstream sense and antisense primes for OneSTrEP-Stoml3-Ex1 construct introduction (*Stoml-3^{OneSTrEP} mouse line*)
KI_MegSTrEP-RA	CCACTAAATTGTTCTTCTCCAGTTTCTCGTCATTAAAACTAAGCATAGTACTTGGTACTTACGGACT	
LacZ/Cre-LS	CATGGTACCCGTACTTTCAAACTTTGCGTGGG	Upstream sense and antisense primes for

|		
LacZ/Cre-LA	CAGTCATGGCTCATTCTTGAGGTGCCTTTCAAATCT TG	LacZ-Cre construct introduction (*Stoml-3^{LacZ} mouse line*)
LacZ/Cre-RS	CATCTAGAGAATTCCAGTTGTGACCAAAGAG	Downstream sense and antisense primes for LacZ-Cre construct introduction (*Stoml-3^{LacZ} mouse line*)
LacZ/Cre-RA	CAGGCGCCCAGTACTGACATGCCTACTTGCGGAG	
G-S	GCCCGATTGCAGTATTAACATGTGCTTG	Primers for Southern Blot probes amplification (probe G and probe J respectively)
G-A	CCACACCTCCTAATAGTGCCACTCCCCAG	
J-S	GAAGATAACTTCTCCCATGAAGTCTGAAACAATC	
J-A	CTAGTTGTATTTGGTAGATACCACCACCCTG	

5.4 Plasmid maps.
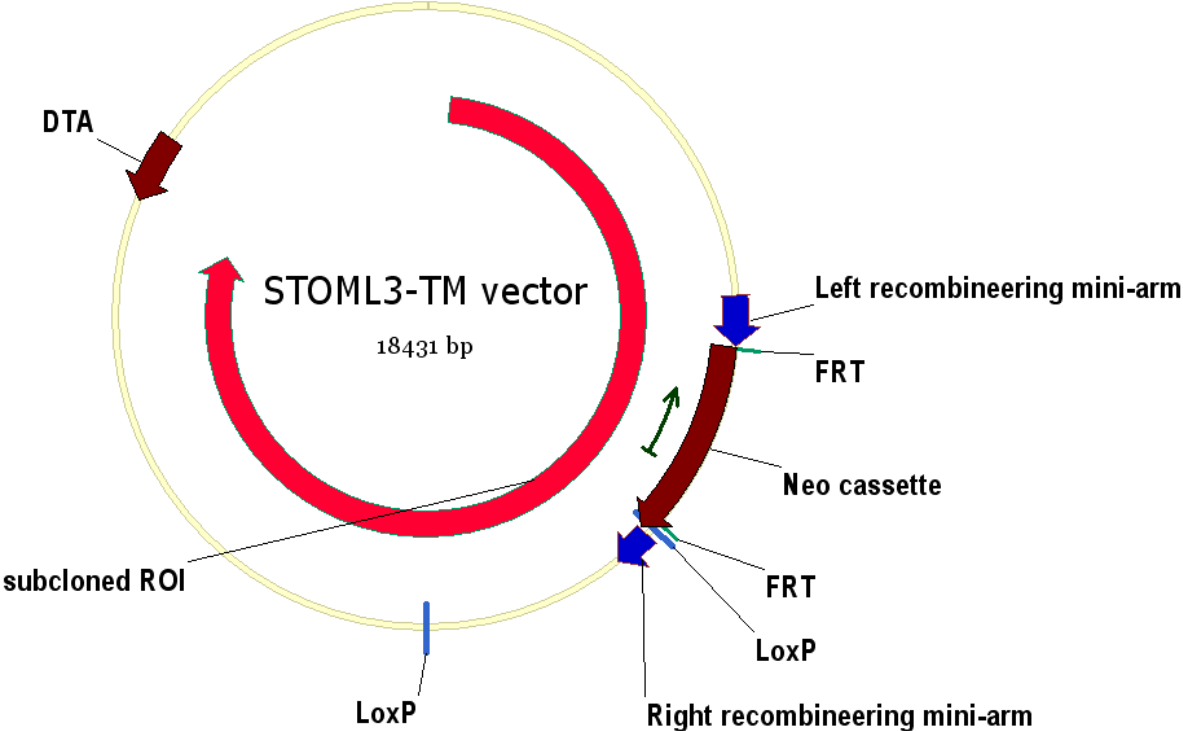
Figure 46. Targeting vector map of a conditional Stoml-3 knock-out (Stoml-3^{Tm})
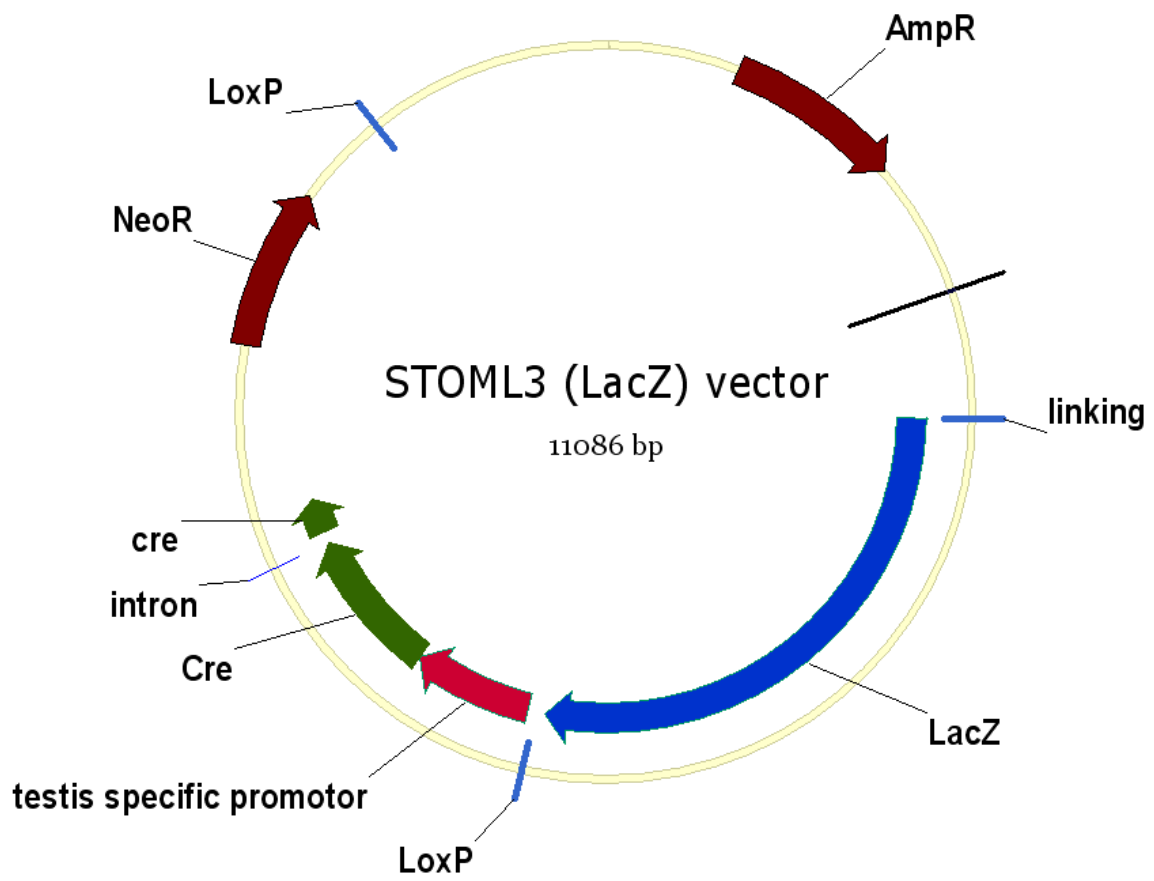
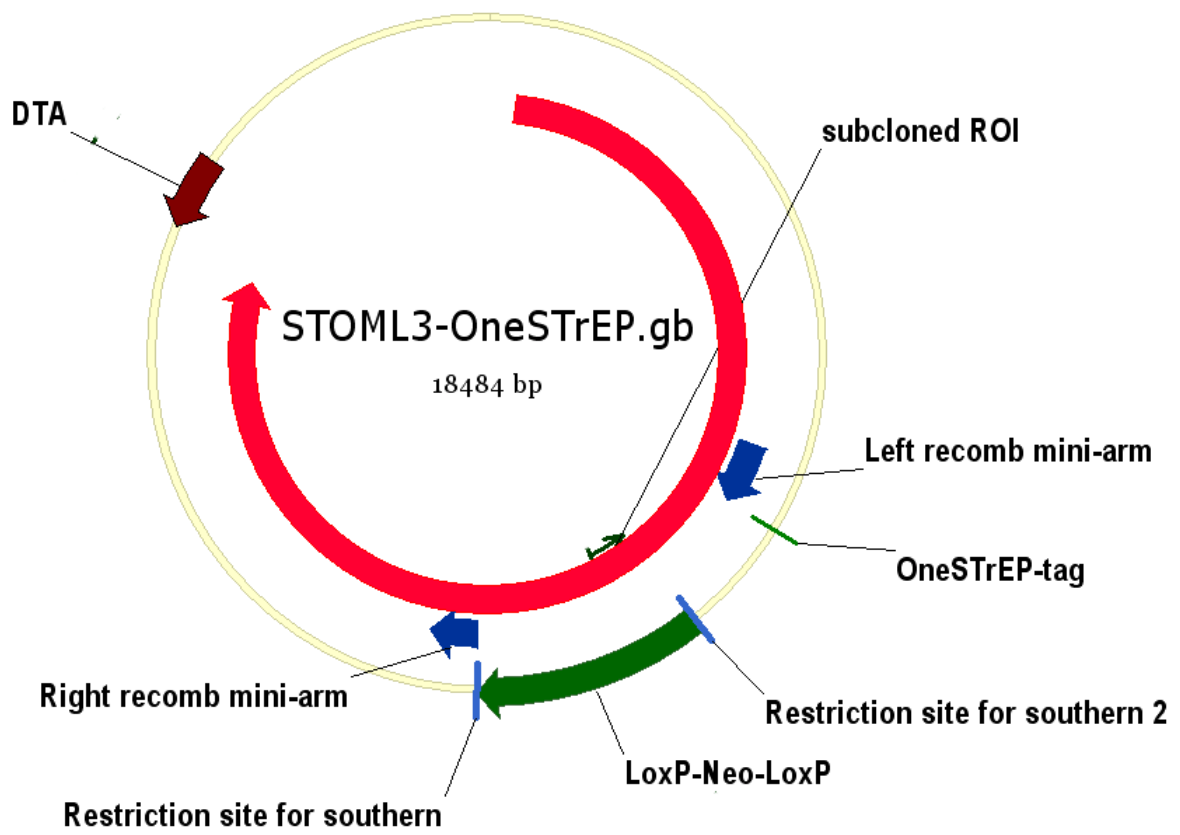**Figure 47. Targeting vector map of a Stoml-3-reporter line construct (Stoml-3^{LacZ}).**

Figure 48. Targeting vector map of a Stoml-3$^{\text{STrEP}}$ knock-in construct.

5.5 List of LC/MS identified proteins.

4F2_HUMAN 4F2 cell-surface antigen heavy chain (4F2hc) (Lymphocyte activation antigen 4F2 large subunit) (4F2 heavy chain antigen) (CD98 antigen) - Homo sapiens (Human)

ACTA_HUMAN Actin, aortic smooth muscle (Alpha-actin-2) - Homo sapiens (Human)

ACTB_HUMAN Actin, cytoplasmic 1 (Beta-actin) - Homo sapiens (Human)

ACTC_HUMAN Actin, alpha cardiac muscle 1 (Alpha-cardiac actin) - Homo sapiens (Human)

ACTG_HUMAN Actin, cytoplasmic 2 (Gamma-actin) - Homo sapiens (Human)

ACTN4_HUMAN Alpha-actinin-4 (Non-muscle alpha-actinin 4) (F-actin cross-linking protein) - Homo sapiens (Human)

ADT1_HUMAN ADP/ATP translocase 1 (Adenine nucleotide translocator 1) (ANT 1) (ADP,ATP carrier protein 1) (Solute carrier family 25 member 4) (ADP,ATP carrier protein, heart/skeletal muscle isoform T1) - Homo sapiens (Human)

ADT2_MOUSE ADP/ATP translocase 2 (Adenine nucleotide translocator 2) (ANT 2) (ADP,ATP carrier protein 2) (Solute carrier family 25 member 5) - Mus musculus (Mouse)

AFG32_HUMAN AFG3-like protein 2 (EC 3.4.24.-) (Paraplegin-like protein) - Homo sapiens (Human)

AIFM1_HUMAN Apoptosis-inducing factor 1, mitochondrial precursor (EC 1.-.-.-) (Programmed cell death protein 8) - Homo sapiens (Human)

AP3D1_HUMAN AP-3 complex subunit delta-1 (Adapter-related protein complex 3 subunit delta-1) (Delta-adapter) - Homo sapiens (Human)

ARF4_HUMAN ADP-ribosylation factor 4 - Homo sapiens (Human)

ARF6_HUMAN ADP-ribosylation factor 6 - Homo sapiens (Human)

ARL2_HUMAN ADP-ribosylation factor-like protein 2 - Homo sapiens (Human)

AT1A1_HUMAN Sodium/potassium-transporting ATPase alpha-1 chain precursor (EC 3.6.3.9) (Sodium pump 1) (Na(+)/K(+) ATPase 1) - Homo sapiens (Human)

AT1A2_HUMAN Sodium/potassium-transporting ATPase alpha-2 chain precursor (EC 3.6.3.9) (Sodium pump 2) (Na(+)/K(+) ATPase 2) - Homo sapiens (Human)

AT1B3_HUMAN Sodium/potassium-transporting ATPase subunit beta-3 (Sodium/potassium-dependent ATPase beta-3 subunit) (ATPB-3) (CD298 antigen) - Homo sapiens (Human)

AT2A2_HUMAN Sarcoplasmic/endoplasmic reticulum calcium ATPase 2 (EC 3.6.3.8) (Calcium pump 2) (SERCA2) (SR Ca(2+)-ATPase 2) (Calcium-transporting ATPase

sarcoplasmic reticulum type, slow twitch skeletal muscle isoform) (Endoplasmic reticulum class 1/2 Ca(2+) AT

ATD3A_HUMAN ATPase family AAA domain-containing protein 3A - Homo sapiens (Human)

ATPA_HUMAN ATP synthase subunit alpha, mitochondrial precursor (EC 3.6.3.14) - Homo sapiens (Human)

ATPB_HUMAN ATP synthase subunit beta, mitochondrial precursor (EC 3.6.3.14) - Homo sapiens (Human)

ATX1_HUMAN Ataxin-1 (Spinocerebellar ataxia type 1 protein) - Homo sapiens (Human)

ATX2L_HUMAN Ataxin-2-like protein (Ataxin-2 domain protein) (Ataxin-2-related protein) - Homo sapiens (Human)

BAP31_HUMAN B-cell receptor-associated protein 31 (BCR-associated protein Bap31) (p28 Bap31) (Protein CDM) - Homo sapiens (Human)

CALX_HUMAN Calnexin precursor (Major histocompatibility complex class I antigen-binding protein p88) (p90) (IP90) - Homo sapiens (Human)

CAZA1_HUMAN F-actin capping protein subunit alpha-1 (CapZ alpha-1) - Homo sapiens (Human)

CDC2_MOUSE Cell division control protein 2 homolog (EC 2.7.11.22) (EC 2.7.11.23) (p34 protein kinase) (Cyclin-dependent kinase 1) (CDK1) - Mus musculus (Mouse)

CH60_HUMAN 60 kDa heat shock protein, mitochondrial precursor (Hsp60) (60 kDa chaperonin) (CPN60) (Heat shock protein 60) (HSP-60) (Mitochondrial matrix protein P1) (P60 lymphocyte protein) (HuCHA60) - Homo sapiens (Human)

CHP1_HUMAN Calcium-binding protein p22 (Calcium-binding protein CHP) (Calcineurin homologous protein)

COF1_HUMAN Cofilin-1 (Cofilin, non-muscle isoform) (18 kDa phosphoprotein) (p18) - Homo sapiens (Human)

COR1C_MOUSE Coronin-1C (Coronin-3) - Mus musculus (Mouse)

DDX39_HUMAN ATP-dependent RNA helicase DDX39 (EC 3.6.1.-) (DEAD box protein 39) (Nuclear RNA helicase URH49) - Homo sapiens (Human)

DLDH_HUMAN Dihydrolipoyl dehydrogenase, mitochondrial precursor (EC 1.8.1.4) (Dihydrolipoamide dehydrogenase) (Glycine cleavage system L protein) - Homo sapiens (Human)

DNJBB_HUMAN DnaJ homolog subfamily B member 11 precursor (ER-associated dnaJ protein 3) (ErJ3) (ER-associated Hsp40 co-chaperone) (hDj9) (PWP1-interacting protein 4) - Homo sapiens (Human)

DODO2_HUMAN Dihydrolipoyllysine-residue succinyltransferase component of 2-oxoglutarate dehydrogenase complex, mitochondrial precursor (EC 2.3.1.61) (Dihydrolipoamide succinyltransferase component of 2-oxoglutarate dehydrogenase complex) (E2) (E2K) - Homo sapiens

DPM1_HUMAN Dolichol-phosphate mannosyltransferase (EC 2.4.1.83) (Dolichol-phosphate mannose synthase) (Dolichyl-phosphate beta-D-mannosyltransferase) (Mannose-P-dolichol synthase) (MPD synthase) (DPM synthase) - Homo sapiens (Human)

EF1A1_HUMAN Elongation factor 1-alpha 1 (EF-1-alpha-1) (Elongation factor 1 A-1) (eEF1A-1) (Elongation factor Tu) (EF-Tu) (Leukocyte receptor cluster member 7) - Homo sapiens (Human)

EFTU_HUMAN Elongation factor Tu, mitochondrial precursor (EF-Tu) (P43) - Homo sapiens (Human)

EMD_HUMAN Emerin - Homo sapiens (Human)

ENPL_HUMAN Endoplasmin precursor (Heat shock protein 90 kDa beta member 1) (94 kDa glucose-regulated protein) (GRP94) (gp96 homolog) (Tumor rejection antigen 1) - Homo sapiens (Human)

EXOC4_HUMAN Exocyst complex component 4 (Exocyst complex component Sec8) - Homo sapiens (Human)

GBLP_HUMAN Guanine nucleotide-binding protein subunit beta 2-like 1 (Guanine nucleotide-binding protein subunit beta-like protein 12.3) (Receptor of activated protein kinase C 1) (RACK1) (Receptor for activated C kinase) - Homo sapiens (Human)

GHC1_MOUSE Mitochondrial glutamate carrier 1 (GC-1) (Glutamate/H(+) symporter 1) (Solute carrier family 25 member 22) - Mus musculus (Mouse)

GOGB1_HUMAN Golgin subfamily B member 1 (Giantin) (Macrogolgin) - Homo sapiens (Human)

GPSN2_HUMAN Synaptic glycoprotein SC2 - Homo sapiens (Human)

GRP75_HUMAN Stress-70 protein, mitochondrial precursor (75 kDa glucose-regulated protein) (GRP 75) (Peptide-binding protein 74) (PBP74) (Mortalin) (MOT) - Homo sapiens (Human)

GRP78_HUMAN 78 kDa glucose-regulated protein precursor (GRP 78) (Heat shock 70 kDa protein 5) (Immunoglobulin heavy chain-binding protein) (BiP) (Endoplasmic reticulum lumenal Ca(2+)-binding protein grp78) - Homo sapiens (Human)

GSLG1_HUMAN Golgi apparatus protein 1 precursor (Golgi sialoglycoprotein MG-160) (E-selectin ligand 1) (ESL-1) Homo sapiens (Human)

HS70A_MOUSE Heat shock 70 kDa protein 1A (Heat shock 70 kDa protein 3) (HSP70.3) (Hsp68) - Mus musculus (Mouse)

HS70L_HUMAN Heat shock 70 kDa protein 1L (Heat shock 70 kDa protein 1-like) (Heat shock 70 kDa protein 1-Hom) (HSP70-Hom) - Homo sapiens (Human)

HSP71_HUMAN Heat shock 70 kDa protein 1 (HSP70.1) (HSP70-1/HSP70-2) - Homo sapiens (Human)

HSP76_HUMAN Heat shock 70 kDa protein 6 (Heat shock 70 kDa protein B') - Homo sapiens (Human)

HSP7C_HUMAN Heat shock cognate 71 kDa protein (Heat shock 70 kDa protein 8) - Homo sapiens (Human)

IBA2_HUMAN Ionized calcium-binding adapter molecule 2 - Homo sapiens (Human)

ILKAP_HUMAN Integrin-linked kinase-associated serine/threonine phosphatase 2C (EC 3.1.3.16) (ILKAP) - Homo sapiens (Human)

IMMT_HUMAN Mitochondrial inner membrane protein (Mitofilin) (p87/89) (Proliferation-inducing gene 4 protein) - Homo sapiens (Human)

JPH1_HUMAN Junctophilin-1 (Junctophilin type 1) (JP-1) - Homo sapiens (Human)

LMNA_HUMAN Lamin-A/C (70 kDa lamin) (Renal carcinoma antigen NY-REN-32) - Homo sapiens (Human)

LMNB1_HUMAN Lamin-B1 - Homo sapiens (Human)

LYSC_HUMAN Lysozyme C precursor (EC 3.2.1.17) (1,4-beta-N-acetylmuramidase C) - Homo sapiens (Human)

M2OM_MOUSE Mitochondrial 2-oxoglutarate/malate carrier protein (OGCP) (Solute carrier family 25 member 11) - Mus musculus (Mouse)

MDHM_HUMAN Malate dehydrogenase, mitochondrial precursor (EC 1.1.1.37) - Homo sapiens (Human)

MLRM_HUMAN Myosin regulatory light chain 2, nonsarcomeric (Myosin RLC) - Homo sapiens (Human)

MPCP_HUMAN Phosphate carrier protein, mitochondrial precursor (PTP) (Solute carrier family 25 member 3) - Homo sapiens (Human)

MYO15_HUMAN Myosin-XV (Unconventional myosin-15) - Homo sapiens (Human)

NFL_HUMAN Neurofilament triplet L protein (68 kDa neurofilament protein) (Neurofilament light polypeptide) (NF-L) - Homo sapiens (Human)

NPM_HUMAN Nucleophosmin (NPM) (Nucleolar phosphoprotein B23) (Numatrin) (Nucleolar protein NO38) - Homo sapiens (Human)

OR9Q2_HUMAN Olfactory receptor 9Q2 - Homo sapiens (Human)

P5CS_HUMAN Delta1-pyrroline-5-carboxylate synthetase (P5CS) (Aldehyde dehydrogenase 18 family member A1) [Includes: Glutamate 5-kinase (EC 2.7.2.11) (Gamma-glutamyl kinase) (GK); Gamma-glutamyl phosphate reductase (GPR) (EC 1.2.1.41) (Glutamate-5-semialdehydehydrogenase) - Homo sapiens (Human)

PCAT1_HUMAN 1-acylglycerophosphocholine O-acyltransferase 1 (EC 2.3.1.23) (Lung-type acyl-coa:lysophosphatidylcholine acyltransferase 1) (Acyltransferase-like 2) (Phosphonoformate immuno-associated protein 3) - Homo sapiens (Human)

PCCA_HUMAN Propionyl-CoA carboxylase alpha chain, mitochondrial precursor (EC 6.4.1.3) (PCCase subunit alpha) (Propanoyl-CoA:carbon dioxide ligase subunit alpha) - Homo sapiens (Human)

PCCB_HUMAN Propionyl-CoA carboxylase beta chain, mitochondrial precursor (EC 6.4.1.3) (PCCase subunit beta) (Propanoyl-CoA:carbon dioxide ligase subunit beta) - Homo sapiens (Human)

PHB2_HUMAN Prohibitin-2 (B-cell receptor-associated protein BAP37) (Repressor of estrogen receptor activity) (D-prohibitin) - Homo sapiens (Human)

PKHA6_HUMAN Pleckstrin homology domain-containing family A member 6 (Phosphoinositol 3-phosphate-binding protein 3) - Homo sapiens (Human)

PON2_HUMAN Serum paraoxonase/arylesterase 2 (EC 3.1.1.2) (EC 3.1.8.1) (PON 2) (Serum aryldialkylphosp) Homo sapiens (Human)

PRAF2_HUMAN PRA1 family protein 2 - Homo sapiens (Human)

PRKDC_HUMAN DNA-dependent protein kinase catalytic subunit (EC 2.7.11.1) (DNA-PK catalytic subunit) (DNA-PKcs) (DNPK1) (p460) - Homo sapiens (Human)

RAB14_HUMAN Ras-related protein Rab-14 - Homo sapiens (Human)

RAB1A_HUMAN Ras-related protein Rab-1A (YPT1-related protein) - Homo sapiens (Human)

RAB32_HUMAN Ras-related protein Rab-32 - Homo sapiens (Human)

RAB5C_HUMAN Ras-related protein Rab-5C (RAB5L) (L1880) - Homo sapiens (Human)

RAB6A_HUMAN Ras-related protein Rab-6A (Rab-6) - Homo sapiens (Human)

RAB7L_HUMAN Ras-related protein Rab-7L1 (Rab-7-like protein 1) - Homo sapiens (Human)

RADI_HUMAN Radixin - Homo sapiens (Human)

RHEB_HUMAN GTP-binding protein Rheb (Ras homolog enriched in brain) - Homo sapiens (Human)

RL7A_MOUSE 60S ribosomal protein L7a (Surfeit locus protein 3) - Mus musculus (Mouse)

RS2_MOUSE 40S ribosomal protein S2 (S4) (LLRep3 protein) - Mus musculus (Mouse)

RS3_HUMAN 40S ribosomal protein S3 - Homo sapiens (Human)

RS6_MOUSE 40S ribosomal protein S6 (Phosphoprotein NP33) - Mus musculus (Mouse)

S61A1_HUMAN Protein transport protein Sec61 subunit alpha isoform 1 (Sec61 alpha-1) - Homo sapiens (Human)

SC22B_HUMAN Vesicle-trafficking protein SEC22b (SEC22 vesicle-trafficking protein homolog B) (SEC22 vesicle-trafficking protein-like 1) (ERS24) (ERS-24) - Homo sapiens (Human)

SHOC2_HUMAN Leucine-rich repeat protein SHOC-2 (Ras-binding protein Sur-8) - Homo sapiens (Human)

SPTA2_HUMAN Spectrin alpha chain, brain (Spectrin, non-erythroid alpha chain) (Alpha-II spectrin) (Fodrin alpha chain) - Homo sapiens (Human)

SPTB2_HUMAN Spectrin beta chain, brain 1 (Spectrin, non-erythroid beta chain 1) (Beta-II spectrin) (Fodrin beta chain) - Homo sapiens (Human)

STOM_HUMAN Erythrocyte band 7 integral membrane protein (Stomatin) (Protein 7.2b) - Homo sapiens (Human)

SYIM_HUMAN Isoleucyl-tRNA synthetase, mitochondrial precursor (EC 6.1.1.5) (Isoleucine--tRNA ligase) (IleRS) - Homo sapiens (Human)

TBA1_MOUSE Tubulin alpha-1 chain (Alpha-tubulin 1) (Alpha-tubulin isotype M-alpha-1) - Mus musculus (Mouse)

TBAK_HUMAN Tubulin alpha-ubiquitous chain (Alpha-tubulin ubiquitous) (Tubulin K-alpha-1) - Homo sapiens (Human)

TBB1_HUMAN Tubulin beta-1 chain - Homo sapiens (Human)

TBB2A_HUMAN Tubulin beta-2A chain - Homo sapiens (Human)

TBB2C_HUMAN Tubulin beta-2C chain (Tubulin beta-2 chain) - Homo sapiens (Human)

TBB5_HUMAN Tubulin beta chain (Tubulin beta-5 chain) - Homo sapiens (Human)

TM109_HUMAN Transmembrane protein 109 precursor (Mitsugumin-23) (Mg23) - Homo sapiens (Human)

UBIQ_HUMAN Ubiquitin - Homo sapiens (Human)

VAPB_HUMAN Vesicle-associated membrane protein-associated protein B/C (VAMP-associated protein B/C) (VAMP-B/VAMP-C) (VAP-B/VAP-C) - Homo sapiens (Human)

VDAC1_MOUSE Voltage-dependent anion-selective channel protein 1 (VDAC-1) (mVDAC1) (mVDAC5) (Outer mitochondrial membrane protein porin 1) (Plasmalemmal porin) - Mus musculus (Mouse)

VDAC2_MOUSE Voltage-dependent anion-selective channel protein 2 (VDAC-2) (mVDAC2) (mVDAC6) (Outer mitochondrial membrane protein porin 2) - Mus musculus (Mouse)

VDAC3_MOUSE Voltage-dependent anion-selective channel protein 3 (VDAC-3) (mVDAC3) (Outer mitochondrial membrane protein porin 3) - Mus musculus (Mouse)

VIME_HUMAN Vimentin - Homo sapiens (Human)

5.6 Index of figures.

6. Bibliography.

Ahn J, Mundigl O, Muth TR, Rudnick G & Caplan MJ (1996) Polarized expression of GABA transporters in Madin-Darby canine kidney cells and cultured hippocampal neurons. *J. Biol. Chem* **271:** 6917-6924 Available at: [Accessed May 21, 2011]

Alías M, Ayuso-Tejedor S, Fernández-Recio J, Cativiela C & Sancho J (2010) Helix propensities of conformationally restricted amino acids. Non-natural substitutes for helix breaking proline and helix forming alanine. *Org. Biomol. Chem.* **8:** 788 Available at: [Accessed May 20, 2011]

Apodaca G, Katz LA & Mostov KE (1994) Receptor-mediated transcytosis of IgA in MDCK cells is via apical recycling endosomes. *J. Cell Biol* **125:** 67-86 Available at: [Accessed May 5, 2011]

Ascaño M, Richmond A, Borden P & Kuruvilla R (2009) Axonal targeting of Trk receptors via transcytosis regulates sensitivity to neurotrophin responses. *J. Neurosci* **29:** 11674-11685 Available at: [Accessed May 5, 2011]

Averill S, Delcroix JD, Michael GJ, Tomlinson DR, Fernyhough P & Priestley JV (2001) Nerve growth factor modulates the activation status and fast axonal transport of ERK 1/2 in adult nociceptive neurones. *Mol. Cell. Neurosci* **18:** 183-196 Available at: [Accessed May 5, 2011]

Barbieri MA, Roberts RL, Mukhopadhyay A & Stahl PD (1996a) Rab5 regulates the dynamics of early endosome fusion. *Biocell* **20:** 331-338 Available at: [Accessed May 4, 2011]

Barbieri MA, Li G, Mayorga LS & Stahl PD (1996b) Characterization of Rab5:Q79L-Stimulated Endosome Fusion. *Archives of Biochemistry and Biophysics* **326:** 64-72 Available at: [Accessed May 4, 2011]

Bargmann CI, Thomas JH & Horvitz HR (1990) Chemosensory Cell Function in the Behavior and Development of Caenorhabditis elegans. *Cold Spring Harbor Symposia on Quantitative Biology* **55:** 529 -538 Available at: [Accessed March 5, 2011]

Bauer M & Pelkmans L (2006) A new paradigm for membrane-organizing and -shaping scaffolds. *FEBS Lett* **580:** 5559-5564 Available at: [Accessed May 6, 2011]

Beattie EC, Carroll RC, Yu X, Morishita W, Yasuda H, von Zastrow M & Malenka RC (2000) Regulation of AMPA receptor endocytosis by a signaling mechanism shared with LTD. *Nat Neurosci* **3:** 1291-1300 Available at: [Accessed April 27, 2011]

Boute N, Gribouval O, Roselli S, Benessy F, Lee H, Fuchshuber A, Dahan K, Gubler MC, Niaudet P & Antignac C (2000) NPHS2, encoding the glomerular protein podocin, is mutated in autosomal recessive steroid-resistant nephrotic syndrome. *Nat. Genet* **24:** 349-354 Available at: [Accessed December 23, 2010]

Bradford MM (1976) A rapid and sensitive method for the quantitation of microgram quantities of protein utilizing the principle of protein-dye binding. *Analytical Biochemistry* **72:** 248-254 Available at: [Accessed May 23, 2011]

Brodsky FM, Chen CY, Knuehl C, Towler MC & Wakeham DE (2001) Biological basket weaving: formation and function of clathrin-coated vesicles. *Annu. Rev. Cell Dev. Biol* **17:** 517-568 Available at: [Accessed April 27, 2011]

Browman DT, Hoegg MB & Robbins SM (2007) The SPFH domain-containing proteins: more than lipid raft markers. *Trends Cell Biol* **17:** 394-402 Available at: [Accessed May 6, 2011]

Brown AG & Iggo A (1967) A quantitative study of cutaneous receptors and afferent fibres in the cat and rabbit. *J. Physiol. (Lond.)* **193:** 707-733 Available at: [Accessed May 23, 2011]

Brown AL, Liao Z & Goodman MB (2008) MEC-2 and MEC-6 in the Caenorhabditis elegans sensory mechanotransduction complex: auxiliary subunits that enable channel activity. *J. Gen. Physiol* **131:** 605-616 Available at: [Accessed December 23, 2010]

Brown TC, Correia SS, Petrok CN & Esteban JA (2007) Functional compartmentalization of endosomal trafficking for the synaptic delivery of AMPA receptors during long-term potentiation. *J. Neurosci* **27:** 13311-13315 Available at: [Accessed May 5, 2011]

Burack MA, Silverman MA & Banker G (2000) The role of selective transport in neuronal protein sorting. *Neuron* **26:** 465-472 Available at: [Accessed May 21, 2011]

Cai D, Verhey KJ & Meyhöfer E (2007) Tracking single Kinesin molecules in the cytoplasm of mammalian cells. *Biophys. J* **92:** 4137-4144 Available at: [Accessed April 19, 2011]

Campenot RB & MacInnis BL (2004) Retrograde transport of neurotrophins: fact and function. *J. Neurobiol* **58:** 217-229 Available at: [Accessed May 5, 2011]

Cayouette S, Bousquet SM, Francoeur N, Dupré É, Monet M, Gagnon H, Guedri YB, Lavoie C & Boulay G (2010) Involvement of Rab9 and Rab11 in the intracellular trafficking of TRPC6. *Biochimica et Biophysica Acta (BBA) - Molecular Cell Research* **1803:** 805-812 Available at: [Accessed May 6, 2011]

Chalfie M & Au M (1989) Genetic control of differentiation of the Caenorhabditis elegans touch receptor neurons. *Science* **243:** 1027-1033 Available at: [Accessed May 18, 2011]

Chalfie M & Sulston J (1981) Developmental genetics of the mechanosensory neurons of Caenorhabditis elegans. *Dev. Biol* **82:** 358-370 Available at: [Accessed May 18, 2011]

Chelur DS, Ernstrom GG, Goodman MB, Yao CA, Chen L, O' Hagan R & Chalfie M (2002) The mechanosensory protein MEC-6 is a subunit of the C. elegans touch-cell degenerin channel. *Nature* **420:** 669-673 Available at: [Accessed May 18, 2011]

Christensen ST, Voss JW, Teilmann SC & Lambert IH (2005) High expression of the taurine transporter TauT in primary cilia of NIH3T3 fibroblasts. *Cell Biology International* **29:** 347-351 Available at: [Accessed April 19, 2011]

Conner SD & Schmid SL (2003) Regulated portals of entry into the cell. *Nature* **422:** 37-44 Available at: [Accessed April 27, 2011]

Copeland NG, Jenkins NA & Court DL (2001) Recombineering: a powerful new tool for mouse functional genomics. *Nat Rev Genet* **2:** 769-779 Available at: [Accessed January 17, 2011]

Correia SS, Bassani S, Brown TC, Lise M-F, Backos DS, El-Husseini A, Passafaro M & Esteban JA (2008) Motor protein-dependent transport of AMPA receptors into spines during long-term potentiation. *Nat Neurosci* **11:** 457-466 Available at: [Accessed May 5, 2011]

Coste B, Mathur J, Schmidt M, Earley TJ, Ranade S, Petrus MJ, Dubin AE & Patapoutian A (2010) Piezo1 and Piezo2 are essential components of distinct mechanically activated cation channels. *Science* **330:** 55-60 Available at: [Accessed May 20, 2011]

Cox HD & Thompson CM (2008) Purification and proteomic analysis of synaptic vesicles. *Methods Mol. Biol* **432:** 259-274 Available at: [Accessed May 25, 2011]

Craig AM & Banker G (1994) Neuronal Polarity. *Annu. Rev. Neurosci.* **17:** 267-310 Available at: [Accessed May 21, 2011]

Cueva JG, Mulholland A & Goodman MB (2007) Nanoscale Organization of the MEC-4 DEG/ENaC Sensory Mechanotransduction Channel in Caenorhabditis elegans Touch Receptor Neurons. *The Journal of Neuroscience* **27:** 14089 -14098 Available at: [Accessed May 5, 2011]

Cui B, Wu C, Chen L, Ramirez A, Bearer EL, Li W-P, Mobley WC & Chu S (2007) One at a time, live tracking of NGF axonal transport using quantum dots. *Proceedings of the National Academy of Sciences* **104:** 13666 -13671 Available at: [Accessed April 19, 2011]

Da Cruz S, De Marchi U, Frieden M, Parone PA, Martinou J-C & Demaurex N (2010) SLP-2 negatively modulates mitochondrial sodium-calcium exchange. *Cell Calcium* **47:** 11-18 Available at: [Accessed December 25, 2010]

Da Cruz S, Parone PA, Gonzalo P, Bienvenut WV, Tondera D, Jourdain A, Quadroni M & Martinou J-C (2008) SLP-2 interacts with prohibitins in the mitochondrial inner membrane and contributes to their stability. *Biochim. Biophys. Acta* **1783:** 904-911 Available at: [Accessed December 25, 2010]

Danino D & Hinshaw JE (2001) Dynamin family of mechanoenzymes. *Curr. Opin. Cell Biol* **13:** 454-460 Available at: [Accessed May 18, 2011]

De Camilli P & Takei K (1996) Molecular mechanisms in synaptic vesicle endocytosis and recycling. *Neuron* **16:** 481-486 Available at: [Accessed April 27, 2011]

Delcroix JD, Averill S, Fernandes K, Tomlinson DR, Priestley JV & Fernyhough P (1999) Axonal transport of activating transcription factor-2 is modulated by nerve growth factor in nociceptive neurons. *J. Neurosci* **19:** RC24 Available at: [Accessed May 5, 2011]

Delcroix J-D, Valletta JS, Wu C, Hunt SJ, Kowal AS & Mobley WC (2003) NGF Signaling in Sensory NeuronsEvidence that Early Endosomes Carry NGF Retrograde Signals. *Neuron* **39:** 69-84 Available at: [Accessed May 5, 2011]

Delcroix J-D, Valletta J, Wu C, Howe CL, Lai C-F, Cooper JD, Belichenko PV, Salehi A & Mobley WC (2004) Trafficking the NGF signal: implications for normal and degenerating neurons. *Prog. Brain Res* **146:** 3-23 Available at: [Accessed May 5, 2011]

Delmas P, Hao J & Rodat-Despoix L (2011) Molecular mechanisms of mechanotransduction in mammalian sensory neurons. *Nat Rev Neurosci* **12:** 139-153 Available at: [Accessed May 21, 2011]

Di Fiore PP & De Camilli P (2001) Endocytosis and signaling. an inseparable partnership. *Cell* **106:** 1-4 Available at: [Accessed April 27, 2011]

Dillman JF 3rd, Dabney LP & Pfister KK (1996) Cytoplasmic dynein is associated with slow axonal transport. *Proc. Natl. Acad. Sci. U.S.A* **93:** 141-144 Available at: [Accessed May 21, 2011]

Doherty GJ & McMahon HT (2009) Mechanisms of Endocytosis. *Annu. Rev. Biochem.* **78:** 857-902 Available at: [Accessed April 12, 2011]

Ernstrom GG & Chalfie M (2002) Genetics of sensory mechanotransduction. *Annu. Rev. Genet* **36:** 411-453 Available at: [Accessed May 5, 2011]

Eva R, Dassie E, Caswell PT, Dick G, ffrench-Constant C, Norman JC & Fawcett JW (2010) Rab11 and Its Effector Rab Coupling Protein Contribute to the Trafficking of β1 Integrins during Axon Growth in Adult Dorsal Root Ganglion Neurons and PC12 Cells. *The Journal of Neuroscience* **30:** 11654 -11669 Available at: [Accessed May 5, 2011]

Ferguson SM, Ferguson S, Raimondi A, Paradise S, Shen H, Mesaki K, Ferguson A, Destaing O, Ko G, Takasaki J, Cremona O, O' Toole E & De Camilli P (2009) Coordinated actions of actin and BAR proteins upstream of dynamin at endocytic clathrin-coated pits. *Dev. Cell* **17:** 811-822 Available at: [Accessed May 6, 2011]

Gagliano J, Walb M, Blaker B, Macosko JC & Holzwarth G (2010) Kinesin velocity increases with the number of motors pulling against viscoelastic drag. *Eur. Biophys. J* **39:** 801-813 Available at: [Accessed April 19, 2011]

George J Siegel BWA (1999) Basic Neurochemistry. Available at: http://www.ncbi.nlm.nih.gov/books/NBK20385/ [Accessed May 21, 2011]

Gillespie PG & Walker RG (2001) Molecular basis of mechanosensory transduction. *Nature* **413:** 194-202 Available at: [Accessed May 21, 2011]

Goldenring JR, Aron LM, Lapierre LA, Navarre J & Casanova JE (2001) Expression and properties of Rab25 in polarized Madin-Darby canine kidney cells. *Meth. Enzymol* **329:** 225-234 Available at: [Accessed May 4, 2011]

Goldenring JR, Shen KR, Vaughan HD & Modlin IM (1993) Identification of a small GTP-binding protein, Rab25, expressed in the gastrointestinal mucosa, kidney, and lung. *J. Biol. Chem* **268:** 18419-18422 Available at: [Accessed May 4, 2011]

Goldstein BJ, Kulaga HM & Reed RR (2003) Cloning and characterization of SLP3: a novel member of the stomatin family expressed by olfactory receptor neurons. *J. Assoc. Res. Otolaryngol* **4:** 74-82 Available at: [Accessed May 3, 2011]

Goodman MB, Hall DH, Avery L & Lockery SR (1998) Active currents regulate sensitivity and dynamic range in C. elegans neurons. *Neuron* **20:** 763-772 Available at: [Accessed May 18, 2011]

Goodman MB, Ernstrom GG, Chelur DS, O'Hagan R, Yao CA & Chalfie M (2002) MEC-2 regulates C. elegans DEG/ENaC channels needed for mechanosensation. *Nature* **415:** 1039-1042 Available at: [Accessed December 23, 2010]

Górska-Andrzejak J, Stowers RS, Borycz J, Kostyleva R, Schwarz TL & Meinertzhagen IA (2003) Mitochondria are redistributed in Drosophila photoreceptors lacking milton, a kinesin-associated protein. *J. Comp. Neurol* **463:** 372-388 Available at: [Accessed March 20, 2011]

Gorvel JP, Chavrier P, Zerial M & Gruenberg J (1991) rab5 controls early endosome fusion in vitro. *Cell* **64:** 915-925 Available at: [Accessed May 4, 2011]

Green JB & Young JPW (2008) Slipins: ancient origin, duplication and diversification of the stomatin protein family. *BMC Evol. Biol* **8:** 44 Available at: [Accessed December 23, 2010]

Grosmaitre X, Santarelli LC, Tan J, Luo M & Ma M (2007) Dual functions of mammalian olfactory sensory neurons as odor detectors and mechanical sensors. *Nat Neurosci* **10:** 348-354 Available at: [Accessed May 25, 2011]

Guoliang GU, Kosaku K, Zhi C & H VK (2007) Osteocyte: a Cellular Basis for Mechanotransduction in Bone. *Journal of Biomechanical Science and Engineering* **2:** 150-165 Available at: [Accessed May 23, 2011]

Hájek P, Chomyn A & Attardi G (2007) Identification of a novel mitochondrial complex containing mitofusin 2 and stomatin-like protein 2. *J. Biol. Chem* **282:** 5670-5681 Available at: [Accessed December 23, 2010]

Hamilton LK, Truong MKV, Bednarczyk MR, Aumont A & Fernandes KJL (2009) Cellular organization of the central canal ependymal zone, a niche of latent neural stem cells in the adult mammalian spinal cord. *Neuroscience* **164:** 1044-1056 Available at: [Accessed April 19, 2011]

Hiebl-Dirschmied CM, Adolf GR & Prohaska R (1991a) Isolation and partial characterization of the human erythrocyte band 7 integral membrane protein. *Biochim. Biophys. Acta* **1065:** 195-202 Available at: [Accessed December 21, 2010]

Hiebl-Dirschmied CM, Entler B, Glotzmann C, Maurer-Fogy I, Stratowa C & Prohaska R (1991b) Cloning and nucleotide sequence of cDNA encoding human erythrocyte band 7 integral membrane protein. *Biochim. Biophys. Acta* **1090:** 123-124 Available at: [Accessed December 21, 2010]

Hirokawa N, Noda Y, Tanaka Y & Niwa S (2009) Kinesin superfamily motor proteins and intracellular transport. *Nat. Rev. Mol. Cell Biol* **10:** 682-696 Available at: [Accessed May 18, 2011]

Howe CL, Valletta JS, Rusnak AS & Mobley WC (2001) NGF signaling from clathrin-coated vesicles: evidence that signaling endosomes serve as a platform for the Ras-MAPK pathway. *Neuron* **32:** 801-814 Available at: [Accessed May 5, 2011]

Hu J, Chiang L-Y, Koch M & Lewin GR (2010) Evidence for a protein tether involved in somatic touch. *EMBO J* **29:** 855-867 Available at: [Accessed May 22, 2011]

Hu J & Lewin GR (2006) Mechanosensitive currents in the neurites of cultured mouse sensory neurones. *J. Physiol. (Lond.)* **577:** 815-828 Available at: [Accessed April 15, 2011]

Huang AL, Chen X, Hoon MA, Chandrashekar J, Guo W, Tränkner D, Ryba NJP & Zuker CS (2006) The cells and logic for mammalian sour taste detection. *Nature* **442:** 934-938 Available at: [Accessed May 23, 2011]

Huang M, Gu G, Ferguson EL & Chalfie M (1995) A stomatin-like protein necessary for mechanosensation in C. elegans. *Nature* **378:** 292-295 Available at: [Accessed May 5, 2011]

Huber TB, Schermer B, Müller RU, Höhne M, Bartram M, Calixto A, Hagmann H, Reinhardt C, Koos F, Kunzelmann K, Shirokova E, Krautwurst D, Harteneck C, Simons M, Pavenstädt H, Kerjaschki D, Thiele C, Walz G, Chalfie M & Benzing T (2006) Podocin and MEC-2 bind cholesterol to regulate the activity of associated ion channels. *Proc. Natl. Acad. Sci. U.S.A* **103:** 17079-17086 Available at: [Accessed May 6, 2011]

Huber TB, Simons M, Hartleben B, Sernetz L, Schmidts M, Gundlach E, Saleem MA, Walz G & Benzing T (2003) Molecular basis of the functional podocin–nephrin complex: mutations in the NPHS2 gene disrupt nephrin targeting to lipid raft microdomains. *Human Molecular Genetics* **12:** 3397 -3405 Available at: [Accessed May 6, 2011]

Insinna C & Besharse JC (2008) Intraflagellar transport and the sensory outer segment of vertebrate photoreceptors. *Dev. Dyn* **237:** 1982-1992 Available at: [Accessed April 19, 2011]

Junttila MR, Saarinen S, Schmidt T, Kast J & Westermarck J (2005) Single-stepStrep-tag purification for the isolation and identification of protein complexes from mammalian cells. *Proteomics* **5:** 1199-1203 Available at: [Accessed March 8, 2011]

Junutula JR, De Maziére AM, Peden AA, Ervin KE, Advani RJ, van Dijk SM, Klumperman J & Scheller RH (2004) Rab14 Is Involved in Membrane Trafficking between the Golgi Complex and Endosomes. *Mol Biol Cell* **15:** 2218-2229

Kadurin I, Huber S & Gründer S (2009) A single conserved proline residue determines the membrane topology of stomatin. *Biochem. J* **418:** 587-594 Available at: [Accessed May 6, 2011]

Kamiguchi H & Lemmon V (2000) Recycling of the cell adhesion molecule L1 in axonal growth cones. *J. Neurosci* **20:** 3676-3686 Available at: [Accessed May 5, 2011]

Kandel E, Schwartz J & Jessell T (2000) Principles of Neural Science 4th ed. McGraw-Hill Medical

Kang J-S, Tian J-H, Pan P-Y, Zald P, Li C, Deng C & Sheng Z-H (2008) Docking of axonal mitochondria by syntaphilin controls their mobility and affects short-term facilitation. *Cell* **132:** 137-148 Available at: [Accessed March 20, 2011]

Kaplan JM & Horvitz HR (1993) A dual mechanosensory and chemosensory neuron in Caenorhabditis elegans. *Proc. Natl. Acad. Sci. U.S.A* **90:** 2227-2231 Available at: [Accessed March 5, 2011]

Kitt KN, Hernández-Deviez D, Ballantyne SD, Spiliotis ET, Casanova JE & Wilson JM (2008) Rab14 Regulates Apical Targeting in Polarized Epithelial Cells. *Traffic* **9:** 1218-1231

Kobayakawa K, Hayashi R, Morita K, Miyamichi K, Oka Y, Tsuboi A & Sakano H (2002) Stomatin-related olfactory protein, SRO, specifically expressed in the murine olfactory sensory neurons. *J. Neurosci* **22:** 5931-5937 Available at: [Accessed December 23, 2010]

Korndörfer IP & Skerra A (2002) Improved affinity of engineered streptavidin for the Strep-tag II peptide is due to a fixed open conformation of the lid-like loop at the binding site. *Protein Sci* **11:** 883-893

Kuhara A, Okumura M, Kimata T, Tanizawa Y, Takano R, Kimura KD, Inada H, Matsumoto K & Mori I (2008) Temperature Sensing by an Olfactory Neuron in a Circuit Controlling Behavior of C. elegans. *Science* **320:** 803 -807 Available at: [Accessed April 19, 2011]

Langhorst MF, Jaeger FA, Mueller S, Sven Hartmann L, Luxenhofer G & Stuermer CAO (2008a) Reggies/flotillins regulate cytoskeletal remodeling during neuronal differentiation via CAP/ponsin and Rho GTPases. *Eur. J. Cell Biol* **87:** 921-931 Available at: [Accessed May 6, 2011]

Langhorst MF, Reuter A, Jaeger FA, Wippich FM, Luxenhofer G, Plattner H & Stuermer CAO (2008b) Trafficking of the microdomain scaffolding protein reggie-1/flotillin-2. *Eur. J. Cell Biol* **87:** 211-226 Available at: [Accessed May 6, 2011]

Lanyon LE (1993) Osteocytes, strain detection, bone modeling and remodeling. *Calcif. Tissue Int* **53 Suppl 1:** S102-106; discussion S106-107 Available at: [Accessed April 18, 2011]

Lapatsina L, Brand J, Poole K, Daumke O & Lewin GR (2011) Stomatin-domain proteins. *Eur J Cell Biol* Available at: http://www.ncbi.nlm.nih.gov/pubmed/21501885 [Accessed April 26, 2011]

Lechner SG, Frenzel H, Wang R & Lewin GR (2009) Developmental waves of mechanosensitivity acquisition in sensory neuron subtypes during embryonic development. *EMBO J* **28:** 1479-1491 Available at: [Accessed April 15, 2011]

Lee EC, Yu D, Martinez de Velasco J, Tessarollo L, Swing DA, Court DL, Jenkins NA & Copeland NG (2001) A highly efficient Escherichia coli-based chromosome engineering system adapted for recombinogenic targeting and subcloning of BAC DNA. *Genomics* **73:** 56-65 Available at: [Accessed April 24, 2011]

Lefebvre V & Bhattaram P (2010) Vertebrate skeletogenesis. *Curr. Top. Dev. Biol* **90:** 291-317 Available at: [Accessed May 18, 2011]

Lewin GR & Moshourab R (2004) Mechanosensation and pain. *J. Neurobiol* **61:** 30-44 Available at: [Accessed May 23, 2011]

Lisé M-F, Wong TP, Trinh A, Hines RM, Liu L, Kang R, Hines DJ, Lu J, Goldenring JR, Wang YT & El-Husseini A (2006) Involvement of myosin Vb in glutamate receptor trafficking. *J. Biol. Chem* **281:** 3669-3678 Available at: [Accessed May 5, 2011]

Liu P, Jenkins NA & Copeland NG (2003) A Highly Efficient Recombineering-Based Method for Generating Conditional Knockout Mutations. *Genome Research* **13:** 476 -484 Available at: [Accessed January 17, 2011]

Low SH, Vasanth S, Larson CH, Mukherjee S, Sharma N, Kinter MT, Kane ME, Obara T & Weimbs T (2006) Polycystin-1, STAT6, and P100 Function in a Pathway that Transduces Ciliary Mechanosensation and Is Activated in Polycystic Kidney Disease. *Developmental Cell* **10:** 57-69 Available at: [Accessed April 19, 2011]

Lumpkin EA & Caterina MJ (2007) Mechanisms of sensory transduction in the skin. *Nature* **445:** 858-865 Available at: [Accessed May 23, 2011]

Marichal N, García G, Radmilovich M, Trujillo-Cenóz O & Russo RE (2009) Enigmatic central canal contacting cells: immature neurons in "standby mode"? *J Neurosci* **29:** 10010-10024

Martinez-Salgado C, Benckendorff AG, Chiang L-Y, Wang R, Milenkovic N, Wetzel C, Hu J, Stucky CL, Parra MG, Mohandas N & Lewin GR (2007) Stomatin and sensory neuron mechanotransduction. *J. Neurophysiol* **98:** 3802-3808 Available at: [Accessed December 23, 2010]

Marzesco A (true graphic)]Marie & Zahraoui A (2005) Assay of Rab13 in Regulating Epithelial Tight Junction Assembly. In *GTPases Regulating Membrane Targeting and Fusion* pp 182-193. Academic Press Available at: http://www.sciencedirect.com/science/article/B7CV2-4J7BJVN-H/2/0486d81eb4c7032b64a09d20f0bd9b0d [Accessed April 27, 2011]

Marzesco A-M, Dunia I, Pandjaitan R, Recouvreur M, Dauzonne D, Benedetti EL, Louvard D & Zahraoui A (2002) The Small GTPase Rab13 Regulates Assembly of Functional Tight Junctions in Epithelial Cells. *Mol Biol Cell* **13:** 1819-1831

Matthies HJG, Moore JL, Saunders C, Matthies DS, Lapierre LA, Goldenring JR, Blakely RD & Galli A (2010) Rab11 supports amphetamine-stimulated norepinephrine transporter trafficking. *J. Neurosci* **30:** 7863-7877 Available at: [Accessed May 23, 2011]

McPherson PS (2010) Proteomic analysis of clathrin-coated vesicles. *Proteomics* **10:** 4025-4039 Available at: [Accessed May 25, 2011]

Meletis K, Barnabé-Heider F, Carlén M, Evergren E, Tomilin N, Shupliakov O & Frisén J (2008) Spinal cord injury reveals multilineage differentiation of ependymal cells. *PLoS Biol* **6:** e182 Available at: [Accessed April 19, 2011]

Meunier B, Quaranta M, Daviet L, Hatzoglou A & Leprince C (2009) The membrane-tubulating potential of amphiphysin 2/BIN1 is dependent on the microtubule-binding cytoplasmic linker protein 170 (CLIP-170). *European Journal of Cell Biology* **88:** 91-102 Available at: [Accessed May 6, 2011]

Morita E, Sandrin V, Alam SL, Eckert DM, Gygi SP & Sundquist WI (2007) Identification of Human MVB12 Proteins as ESCRT-I Subunits that Function in HIV Budding. *Cell Host Microbe* **2:** 41-53

Morris RL & Hollenbeck PJ (1993) The regulation of bidirectional mitochondrial transport is coordinated with axonal outgrowth. *J. Cell. Sci* **104 (Pt 3):** 917-927 Available at: [Accessed March 20, 2011]

Morrow IC & Parton RG (2005) Flotillins and the PHB domain protein family: rafts, worms and anaesthetics. *Traffic* **6:** 725-740 Available at: [Accessed December 27, 2010]

Mostov K (1993) Protein traffic in polarized epithelial cells: the polymeric immunoglobulin receptor as a model system. *J. Cell Sci. Suppl* **17:** 21-26 Available at: [Accessed May 21, 2011]

Mothe AJ & Tator CH (2005) Proliferation, migration, and differentiation of endogenous ependymal region stem/progenitor cells following minimal spinal cord injury in the adult rat. *Neuroscience* **131:** 177-187 Available at: [Accessed April 19, 2011]

Murdoch B & Roskams AJ (2007) Olfactory epithelium progenitors: insights from transgenic mice and in vitro biology. *J Mol Hist* **38:** 581-599 Available at: [Accessed March 20, 2011]

Nakata T & Hirokawa N (2003) Microtubules provide directional cues for polarized axonal transport through interaction with kinesin motor head. *J Cell Biol* **162:** 1045-1055

Nilsson I, Sääf A, Whitley P, Gafvelin G, Waller C & von Heijne G (1998) Proline-induced disruption of a transmembrane alpha-helix in its natural environment. *J. Mol. Biol* **284:** 1165-1175 Available at: [Accessed May 20, 2011]

Nokes RL, Fields IC, Collins RN & Fölsch H (2008) Rab13 regulates membrane trafficking between TGN and recycling endosomes in polarized epithelial cells. *J Cell Biol* **182:** 845-853

Nowlan NC, Sharpe J, Roddy KA, Prendergast PJ & Murphy P (2010) Mechanobiology of embryonic skeletal development: Insights from animal models. *Birth Defects Res. C Embryo Today* **90:** 203-213 Available at: [Accessed May 18, 2011]

O'Hagan R, Chalfie M & Goodman MB (2005) The MEC-4 DEG/ENaC channel of Caenorhabditis elegans touch receptor neurons transduces mechanical signals. *Nat Neurosci* **8:** 43-50 Available at: [Accessed May 5, 2011]

Oellerich T, Grønborg M, Neumann K, Hsiao H-H, Urlaub H & Wienands J (2009) SLP-65 Phosphorylation Dynamics Reveals a Functional Basis for Signal Integration by Receptor-proximal Adaptor Proteins. *Molecular & Cellular Proteomics* **8:** 1738 -1750 Available at: [Accessed April 15, 2011]

Owczarek CM, Treutlein HR, Portbury KJ, Gulluyan LM, Kola I & Hertzog PJ (2001) A novel member of the STOMATIN/EPB72/mec-2 family, stomatin-like 2 (STOML2), is ubiquitously expressed and localizes to HSA chromosome 9p13.1. *Cytogenet. Cell Genet* **92:** 196-203 Available at: [Accessed December 23, 2010]

Page AJ, Brierley SM, Martin CM, Martinez-Salgado C, Wemmie JA, Brennan TJ, Symonds E, Omari T, Lewin GR, Welsh MJ & Blackshaw LA (2004) The ion channel ASIC1 contributes to visceral but not cutaneous mechanoreceptor function. *Gastroenterology* **127:** 1739-1747 Available at: [Accessed May 16, 2011]

Papachroni KK, Karatzas DN, Papavassiliou KA, Basdra EK & Papavassiliou AG (2009) Mechanotransduction in osteoblast regulation and bone disease. *Trends Mol Med* **15:** 208-216 Available at: [Accessed May 23, 2011]

Park M, Penick EC, Edwards JG, Kauer JA & Ehlers MD (2004) Recycling Endosomes Supply AMPA Receptors for LTP. *Science* **305:** 1972 -1975 Available at: [Accessed May 5, 2011]

Pereira-Leal JB & Seabra MC (2001) Evolution of the Rab family of small GTP-binding proteins. *J. Mol. Biol* **313:** 889-901 Available at: [Accessed March 13, 2011]

Pfeffer S & Aivazian D (2004) Targeting Rab GTPases to distinct membrane compartments. *Nat. Rev. Mol. Cell Biol* **5:** 886-896 Available at: [Accessed January 16, 2011]

Price MP, McIlwrath SL, Xie J, Cheng C, Qiao J, Tarr DE, Sluka KA, Brennan TJ, Lewin GR & Welsh MJ (2001) The DRASIC Cation Channel Contributes to the Detection of Cutaneous Touch and Acid Stimuli in Mice. *Neuron* **32:** 1071-1083 Available at: [Accessed May 5, 2011]

Price MP, Lewin GR, McIlwrath SL, Cheng C, Xie J, Heppenstall PA, Stucky CL, Mannsfeldt AG, Brennan TJ, Drummond HA, Qiao J, Benson CJ, Tarr DE, Hrstka RF, Yang B,

Williamson RA & Welsh MJ (2000) The mammalian sodium channel BNC1 is required for normal touch sensation. *Nature* **407:** 1007-1011 Available at: [Accessed May 5, 2011]

Price MP, Thompson RJ, Eshcol JO, Wemmie JA & Benson CJ (2004) Stomatin Modulates Gating of Acid-sensing Ion Channels. *Journal of Biological Chemistry* **279:** 53886 -53891 Available at: [Accessed May 6, 2011]

Proikas-Cezanne T, Gaugel A, Frickey T & Nordheim A (2006) Rab14 is part of the early endosomal clathrin-coated TGN microdomain. *FEBS Letters* **580:** 5241-5246 Available at: [Accessed April 27, 2011]

Raimondo F, Morosi L, Chinello C, Magni F & Pitto M (2011) Advances in membranous vesicle and exosome proteomics improving biological understanding and biomarker discovery. *Proteomics* **11:** 709-720 Available at: [Accessed May 25, 2011]

Raub TJ, Koroly MJ & Roberts RM (1990) Endocytosis of wheat germ agglutinin binding sites from the cell surface into a tubular endosomal network. *J. Cell. Physiol* **143:** 1-12 Available at: [Accessed March 20, 2011]

Ren M, Xu G, Zeng J, De Lemos-Chiarandini C, Adesnik M & Sabatini DD (1998) Hydrolysis of GTP on rab11 is required for the direct delivery of transferrin from the pericentriolar recycling compartment to the cell surface but not from sorting endosomes. *Proc. Natl. Acad. Sci. U.S.A* **95:** 6187-6192 Available at: [Accessed May 6, 2011]

Reynolds AJ, Hendry IA & Bartlett SE (2001) Anterograde and retrograde transport of active extracellular signal-related kinase 1 (ERK1) in the ligated rat sciatic nerve. *Neuroscience* **105:** 761-771 Available at: [Accessed May 5, 2011]

Rivera-Milla E, Stuermer CAO & Málaga-Trillo E (2006) Ancient origin of reggie (flotillin), reggie-like, and other lipid-raft proteins: convergent evolution of the SPFH domain. *Cell. Mol. Life Sci* **63:** 343-357 Available at: [Accessed December 27, 2010]

Roza C, Puel J-L, Kress M, Baron A, Diochot S, Lazdunski M & Waldmann R (2004) Knockout of the ASIC2 channel in mice does not impair cutaneous mechanosensation, visceral mechanonociception and hearing. *J. Physiol. (Lond.)* **558:** 659-669 Available at: [Accessed May 16, 2011]

Sakane A, Honda K & Sasaki T (2010) Rab13 Regulates Neurite Outgrowth in PC12 Cells through Its Effector Protein, JRAB/MICAL-L2. *Mol Cell Biol* **30:** 1077-1087

Salzer U, Ahorn H & Prohaska R (1993) Identification of the phosphorylation site on human erythrocyte band 7 integral membrane protein: implications for a monotopic protein structure. *Biochimica et Biophysica Acta (BBA) - Biomembranes* **1151:** 149-152 Available at: [Accessed December 26, 2010]

Salzer U & Prohaska R (2001) Stomatin, flotillin-1, and flotillin-2 are major integral proteins of erythrocyte lipid rafts. *Blood* **97:** 1141 -1143 Available at: [Accessed May 6, 2011]

Sampo B, Kaech S, Kunz S & Banker G (2003) Two distinct mechanisms target membrane proteins to the axonal surface. *Neuron* **37:** 611-624 Available at: [Accessed May 21, 2011]

Satir P, Pedersen LB & Christensen ST (2010) The primary cilium at a glance. *J Cell Sci* **123:** 499-503 Available at: [Accessed April 19, 2011]

Saxena S, Howe CL, Cosgaya JM, Steiner P, Hirling H, Chan JR, Weis J & Krüttgen A (2005) Differential endocytic sorting of p75NTR and TrkA in response to NGF: a role for late endosomes in TrkA trafficking. *Molecular and Cellular Neuroscience* **28:** 571-587 Available at: [Accessed May 5, 2011]

Schlierf B, Fey GH, Hauber J, Hocke GM & Rosorius O (2000) Rab11b is essential for recycling of transferrin to the plasma membrane. *Exp. Cell Res* **259:** 257-265 Available at: [Accessed May 6, 2011]

Schmid SL (1997) Clathrin-coated vesicle formation and protein sorting: an integrated process. *Annu. Rev. Biochem* **66:** 511-548 Available at: [Accessed April 27, 2011]

Schmidt TG, Koepke J, Frank R & Skerra A (1996) Molecular interaction between the Strep-tag affinity peptide and its cognate target, streptavidin. *J. Mol. Biol* **255:** 753-766 Available at: [Accessed March 8, 2011]

Schneider A, Rajendran L, Honsho M, Gralle M, Donnert G, Wouters F, Hell SW & Simons M (2008) Flotillin-dependent clustering of the amyloid precursor protein regulates its endocytosis and amyloidogenic processing in neurons. *J. Neurosci* **28:** 2874-2882 Available at: [Accessed May 6, 2011]

Schwartz SL, Cao C, Pylypenko O, Rak A & Wandinger-Ness A (2007) Rab GTPases at a glance. *J Cell Sci* **120:** 3905-3910 Available at: [Accessed March 13, 2011]

Seidel G & Prohaska R (1998) Molecular cloning of hSLP-1, a novel human brain-specific member of the band 7/MEC-2 family similar to Caenorhabditis elegans UNC-24. *Gene* **225:** 23-29 Available at: [Accessed December 23, 2010]

Semprini S, Troup TJ, Kotelevtseva N, King K, Davis JRE, Mullins LJ, Chapman KE, Dunbar DR & Mullins JJ (2007) Cryptic loxP sites in mammalian genomes: genome-wide distribution and relevance for the efficiency of BAC/PAC recombineering techniques. *Nucleic Acids Res* **35:** 1402-1410 Available at: [Accessed May 16, 2011]

Shtridelman Y, Holzwarth GM, Bauer CT, Gassman NR, DeWitt DA & Macosko JC (2009) In vivo Multimotor Force–Velocity Curves by Tracking and Sizing Sub-Diffraction Limited Vesicles. *Cel. Mol. Bioeng.* **2:** 190-199 Available at: [Accessed April 19, 2011]

Smith ESJ & Lewin GR (2009) Nociceptors: a phylogenetic view. *J. Comp. Physiol. A Neuroethol. Sens. Neural. Behav. Physiol* **195:** 1089-1106 Available at: [Accessed May 23, 2011]

Smythe E (2002) Direct interactions between rab GTPases and cargo. *Mol. Cell* **9:** 205-206 Available at: [Accessed January 16, 2011]

Snyers L, Umlauf E & Prohaska R (1998) Oligomeric nature of the integral membrane protein stomatin. *J. Biol. Chem* **273:** 17221-17226 Available at: [Accessed December 23, 2010]

Snyers L, Umlauf E & Prohaska R (1999a) Cysteine 29 is the major palmitoylation site on stomatin. *FEBS Lett* **449:** 101-104 Available at: [Accessed December 23, 2010]

Snyers L, Umlauf E & Prohaska R (1999b) Association of stomatin with lipid-protein complexes in the plasma membrane and the endocytic compartment. *Eur. J. Cell Biol* **78:** 802-812 Available at: [Accessed December 23, 2010]

Solis GP, Hoegg M, Munderloh C, Schrock Y, Malaga-Trillo E, Rivera-Milla E & Stuermer CAO (2007) Reggie/flotillin proteins are organized into stable tetramers in membrane microdomains. *Biochem. J* **403:** 313-322 Available at: [Accessed May 6, 2011]

Somsel Rodman J & Wandinger-Ness A (2000) Rab GTPases coordinate endocytosis. *J. Cell. Sci* **113 Pt 2:** 183-192 Available at: [Accessed January 16, 2011]

Srinivas S, Watanabe T, Lin C-S, William CM, Tanabe Y, Jessell TM & Costantini F Cre reporter strains produced by targeted insertion of EYFP and ECFP into the ROSA26 locus. *BMC Dev Biol* **1:** 4-4

Stenmark H, Parton RG, Steele-Mortimer O, Lütcke A, Gruenberg J & Zerial M (1994) Inhibition of rab5 GTPase activity stimulates membrane fusion in endocytosis. *EMBO J* **13:** 1287-1296

Stewart GW, Argent AC & Dash BC (1993) Stomatin: a putative cation transport regulator in the red cell membrane. *Biochim. Biophys. Acta* **1225:** 15-25 Available at: [Accessed December 23, 2010]

Stowers RS, Megeath LJ, Górska-Andrzejak J, Meinertzhagen IA & Schwarz TL (2002) Axonal transport of mitochondria to synapses depends on milton, a novel Drosophila protein. *Neuron* **36:** 1063-1077 Available at: [Accessed March 20, 2011]

Stuermer CAO (2011a) Reggie/flotillin and the targeted delivery of cargo. *J. Neurochem* **116:** 708-713 Available at: [Accessed May 6, 2011]

Stuermer CAO (2011b) Microdomain-forming proteins and the role of the reggies/flotillins during axon regeneration in zebrafish. *Biochim. Biophys. Acta* **1812:** 415-422 Available at: [Accessed May 6, 2011]

Tavernarakis N, Driscoll M & Kyrpides NC (1999) The SPFH domain: implicated in regulating targeted protein turnover in stomatins and other membrane-associated proteins. *Trends Biochem. Sci* **24:** 425-427 Available at: [Accessed December 27, 2010]

Tondera D, Grandemange S, Jourdain A, Karbowski M, Mattenberger Y, Herzig S, Da Cruz S, Clerc P, Raschke I, Merkwirth C, Ehses S, Krause F, Chan DC, Alexander C, Bauer C, Youle R, Langer T & Martinou J-C (2009) SLP-2 is required for stress-induced mitochondrial hyperfusion. *EMBO J* **28:** 1589-1600 Available at: [Accessed January 12, 2011]

Tsunozaki M & Bautista DM (2009) Mammalian somatosensory mechanotransduction. *Curr. Opin. Neurobiol* **19:** 362-369 Available at: [Accessed May 23, 2011]

Ullrich O, Reinsch S, Urbé S, Zerial M & Parton RG (1996) Rab11 regulates recycling through the pericentriolar recycling endosome. *J. Cell Biol* **135:** 913-924 Available at: [Accessed May 6, 2011]

Vallee RB & Bloom GS (1991) Mechanisms of fast and slow axonal transport. *Annu. Rev. Neurosci* **14:** 59-92 Available at: [Accessed May 21, 2011]

Varkey J, Isas JM, Mizuno N, Jensen MB, Bhatia VK, Jao CC, Petrlova J, Voss JC, Stamou DG, Steven AC & Langen R (2010) Membrane curvature induction and tubulation are common features of synucleins and apolipoproteins. *J. Biol. Chem* **285:** 32486-32493 Available at: [Accessed May 6, 2011]

Vassilieva EV, Ivanov AI & Nusrat A (2009) Flotillin-1 stabilizes caveolin-1 in intestinal epithelial cells. *Biochem. Biophys. Res. Commun* **379:** 460-465 Available at: [Accessed May 6, 2011]

Verkhratsky A (2005) Physiology and Pathophysiology of the Calcium Store in the Endoplasmic Reticulum of Neurons. *Physiological Reviews* **85:** 201 -279 Available at: [Accessed May 23, 2011]

Voss S & Skerra A (1997) Mutagenesis of a flexible loop in streptavidin leads to higher affinity for the Strep-tag II peptide and improved performance in recombinant protein purification. *Protein Eng* **10:** 975-982 Available at: [Accessed March 8, 2011]

Wang D, Mentzer WC, Cameron T & Johnson RM (1991) Purification of band 7.2b, a 31-kDa integral phosphoprotein absent in hereditary stomatocytosis. *J. Biol. Chem* **266:** 17826-17831 Available at: [Accessed January 12, 2011]

Wang Z, Edwards JG, Riley N, Provance DW, Karcher R, Li X-dong, Davison IG, Ikebe M, Mercer JA, Kauer JA & Ehlers MD (2008) Myosin Vb Mobilizes Recycling Endosomes and AMPA Receptors for Postsynaptic Plasticity. *Cell* **135:** 535-548 Available at: [Accessed May 5, 2011]

Way JC & Chalfie M (1989) The mec-3 gene of Caenorhabditis elegans requires its own product for maintained expression and is expressed in three neuronal cell types. *Genes Dev* **3:** 1823-1833 Available at: [Accessed March 5, 2011]

Weber M, Wehling M & Lösel R (2008) Proteins interact with the cytosolic mineralocorticoid receptor depending on the ligand. *Am. J. Physiol. Heart Circ. Physiol* **295:** H361-365 Available at: [Accessed April 15, 2011]

Wetzel C, Hu J, Riethmacher D, Benckendorff A, Harder L, Eilers A, Moshourab R, Kozlenkov A, Labuz D, Caspani O, Erdmann B, Machelska H, Heppenstall PA & Lewin GR (2007) A stomatin-domain protein essential for touch sensation in the mouse. *Nature* **445:** 206-209 Available at: [Accessed December 23, 2010]

Witte C-P, No l L, Gielbert J, Parker J & Romeis T (2004) Rapid one-step protein purification from plant material using the eight-amino acid StrepII epitope. *Plant Mol Biol* **55:** 135-147 Available at: [Accessed March 8, 2011]

Wu M, Huang B, Graham M, Raimondi A, Heuser JE, Zhuang X & De Camilli P (2010) Coupling between clathrin-dependent endocytic budding and F-BAR-dependent tubulation in a cell-free system. *Nat. Cell Biol* **12:** 902-908 Available at: [Accessed May 6, 2011]

Yamamoto Y, Nishimura N, Morimoto S, Kitamura H, Manabe S, Kanayama H-omi, Kagawa S & Sasaki T (2003) Distinct roles of Rab3B and Rab13 in the polarized transport of apical, basolateral, and tight junctional membrane proteins to the plasma membrane. *Biochem. Biophys. Res. Commun* **308:** 270-275 Available at: [Accessed April 27, 2011]

Yokoyama H, Fujii S & Matsui I (2008) Crystal Structure of a Core Domain of Stomatin from Pyrococcus horikoshii Illustrates a Novel Trimeric and Coiled-Coil Fold. *Journal of Molecular Biology* **376:** 868-878 Available at: [Accessed December 23, 2010]

Yoon Y, Pitts KR & McNiven MA (2001) Mammalian Dynamin-like Protein DLP1 Tubulates Membranes. *Mol. Biol. Cell* **12:** 2894-2905 Available at: [Accessed May 6, 2011]

Yun RH, Anderson A & Hermans J (1991) Proline in alpha-helix: stability and conformation studied by dynamics simulation. *Proteins* **10:** 219-228 Available at: [Accessed May 20, 2011]

Zerial M & McBride H (2001) Rab proteins as membrane organizers. *Nat. Rev. Mol. Cell Biol* **2:** 107-117 Available at: [Accessed March 13, 2011]

Zhang CL, Ho PL, Kintner DB, Sun D & Chiu SY (2010) Activity-Dependent Regulation of Mitochondrial Motility by Calcium and Na/K-ATPase at Nodes of Ranvier of Myelinated Nerves. *The Journal of Neuroscience* **30:** 3555 -3566 Available at: [Accessed April 27, 2011]

Zhang S, Arnadottir J, Keller C, Caldwell GA, Yao CA & Chalfie M (2004) MEC-2 is recruited to the putative mechanosensory complex in C. elegans touch receptor neurons through its stomatin-like domain. *Curr. Biol* **14:** 1888-1896 Available at: [Accessed December 23, 2010]

Zhu Y, Paszty C, Turetsky T, Tsai S, Kuypers FA, Lee G, Cooper P, Gallagher PG, Stevens ME, Rubin E, Mohandas N & Mentzer WC (1999) Stomatocytosis is absent in "stomatin"-deficient murine red blood cells. *Blood* **93:** 2404-2410 Available at: [Accessed January 11, 2011]